

ONLINE FINGERPRINT VERIFICATION SYSTEM

by

Sharat S. Chikkerur

A thesis submitted to the
Faculty of the Graduate School
of the
State University of New York at Buffalo
in partial fulfillment of the requirements for the
degree of

Master of Science

June 2005

Department of Electrical Engineering

Contents

| | | |
|----------|---|-----------|
| 1 | Introduction | 2 |
| 1.1 | Biometrics | 2 |
| 1.1.1 | Biometrics and Pattern Recognition | 5 |
| 1.1.2 | The Verification Problem | 6 |
| 1.1.3 | Performance Evaluation | 7 |
| 1.1.4 | System Errors | 8 |
| 1.1.5 | Caveat | 10 |
| 1.2 | Fingerprint as a Biometric: Fingerprints 101 | 12 |
| 1.3 | Fingerprint Sensors | 15 |
| 1.4 | Fingerprint Representations and Matching Algorithms | 18 |
| 1.4.1 | Image | 18 |
| 1.4.2 | Minutiae Representation | 20 |
| 1.4.3 | Texture Descriptors | 25 |
| 1.5 | Thesis Outline | 27 |
| 2 | Fingerprint Image Enhancement Using STFT Analysis | 28 |
| 2.1 | Prior Related Work | 29 |
| 2.1.1 | Spatial Domain Filtering | 30 |
| 2.1.2 | Fourier Domain Filtering | 34 |
| 2.1.3 | Intrinsic Images | 36 |
| 2.2 | Proposed Algorithm: STFT Analysis | 39 |
| 2.2.1 | Overview | 39 |
| 2.2.2 | Ridge Orientation Image | 43 |
| 2.2.3 | Ridge Frequency Image | 44 |
| 2.2.4 | Region Mask | 45 |
| 2.2.5 | Enhancement | 46 |
| 2.3 | Experimental Evaluation | 47 |
| 2.4 | Summary | 48 |

| | | |
|----------|---|-----------|
| 3 | Feature Extraction Using Chain Code Contours | 54 |
| 3.1 | Prior Related Work | 57 |
| 3.1.1 | Binarization Approach | 57 |
| 3.1.2 | Direct Gray-Scale Approaches | 60 |
| 3.2 | Proposed Algorithm: Chain Code Representation | 62 |
| 3.3 | Experimental Evaluation | 68 |
| 3.4 | Summary | 69 |
| 4 | Fingerprint Matching | 73 |
| 4.1 | Prior Related Work | 77 |
| 4.1.1 | Global Matching | 77 |
| 4.1.2 | Local Matching | 80 |
| 4.2 | Proposed Approach: Graph Based Matching | 83 |
| 4.2.1 | Representation: K-plet | 83 |
| 4.2.2 | Graphical View | 85 |
| 4.2.3 | Local Matching: Dynamic Programming | 85 |
| 4.2.4 | Consolidation: Coupled Breadth First Search | 88 |
| 4.2.5 | Matching Algorithm | 92 |
| 4.3 | Experimental Evaluation | 92 |
| 4.4 | Summary | 92 |
| 5 | Conclusion | 95 |
| 5.1 | Software | 96 |

List of Figures

| | | |
|------|--|----|
| 1.1 | Various biometric modalities: Fingerprints, speech, handwriting, face, hand geometry and chemical biometrics | 4 |
| 1.2 | General architecture of a biometric system | 5 |
| 1.3 | An illustration showing the intra user variation present in biometric signals | 7 |
| 1.4 | Genuine and impostor distributions | 9 |
| 1.5 | (i)Typical FAR and FRR vs threshold (ii)Typical ROC curve | 10 |
| 1.6 | An illustration of a general biometric system with points of threats identified | 12 |
| 1.7 | (a) Local Features: Minutiae (b) Global Features: Core and Delta | 13 |
| 1.8 | Fingerprint Classes: (a)Tended Arch (b)Arch (c)Right Loop (d)Left Loop (e)Whorl | 14 |
| 1.9 | General architecture of a fingerprint verification system | 15 |
| 1.10 | Offline and on-line aquisition: (a)Acquired by rolling inked finger on paper (b) Latent fingerprint acquired from a crime scene, (c,d,f) Acquired from optical, (e) Acquired from a capacitive sensor. | 16 |
| 1.11 | (a) General schematic for an FTIR based optical sensor (b) Schematic of a capacitive sensor | 17 |
| 1.12 | Various commercial sensors available for <i>live capture</i> of fingerprints | 19 |
| 1.13 | The illustration shows the results of correlation between images of the same user(a) and different user(b). It can be seen the the peak output of the correlation is high in case of genuine match and low for an impostor match. | 21 |
| 1.14 | The figure shows the primary approach for matching minutiae. Each fingerprint is represented as a set of tuples each specifying the properties of minutiae(usually (x,y,θ)). The process of matching involves recovering the geometric transformation between the two sets. This may include rotation, scaling or non-linear distortion as illustrated. | 22 |
| 1.15 | The minutia are matched by transforming one set of minutiae and determining the number of minutiae that fall within a bounded region of another. | 24 |
| 1.16 | The illustration shows the response of the image to a gabor filter bank oriented at four different direction. The figure also illustrates the circular tessellation followed in [40]. The fingercode consists of the AAD (Average Absolute Deviation) within each sector. In practice 8 orientations are used. | 26 |

| | | |
|------|--|----|
| 2.1 | Fingerprint images of different quality. The quality decreases from left to right. (a) Good quality image with high contrast between the ridges and valleys (b) Insufficient distinction between ridges and valleys in the center of the image (c) Dry print | 29 |
| 2.2 | The anisotropic filtering kernel proposed by Greenberg et. al [80]. The filter shown has $S=-2, V=10, \sigma_1^2(x_0) = 4 \sigma_2^2(x_0) = 2$ | 31 |
| 2.3 | Gabor Filter Kernel: (a)Even symmetric part of the filter (b) The Fourier spectrum of the Gabor kernel showing the localization in the frequency domain | 33 |
| 2.4 | Block diagram of the filtering scheme proposed by Sherlock and Monro [11] | 35 |
| 2.5 | Projection sum obtained for a window oriented along the ridges (a) Sample fingerprint (b) Synthetic image (c)Radon Transform of the fingerprint region | 38 |
| 2.6 | Overview of the proposed approach | 40 |
| 2.7 | (a)Overlapping window parameters used in the STFT analysis (b) Illustration of how analysis windows are moved during analysis (b)Spectral window used during STFT analysis | 42 |
| 2.8 | Surface wave approximation: (a) Local region in a fingerprint image (b) Surface wave approximation (c,d) Fourier spectrum of the real fingerprint and the surface wave. The symmetric nature of the Fourier spectrum arrives from the properties of the Fourier transform for real signals [29] | 43 |
| 2.9 | Outline of the enhancement algorithm | 46 |
| 2.10 | Results of the proposed approach: (a)Original Image (b)Orientation Image (c)Energy Image (d)Ridge Frequency Image (e)Angular Coherence Image (f)Enhanced Image . | 49 |
| 2.11 | Results: (a,b) Original and enhanced image(sample taken from FVC2002 DB1 database) (c,d) Original and enhanced image(sample taken from FVC2002 DB2 database) . . . | 50 |
| 2.12 | Results: (a,b)Original and enhanced image(sample taken from FVC2002 DB3 database) (c,d) Original and enhanced image(sample taken from FVC2002 DB4database) . . . | 51 |
| 2.13 | Comparative Results: (a)Original image displaying poor contrast and ridge structure (b)Result of root filtering [92]. (c)Result of Gabor filter based enhancement (d) Result using proposed algorithm | 52 |
| 2.14 | Effect on accuracy : (a)ROC curves with and without enhancement (b)Some sample images from DB3 database | 53 |
| 3.1 | Different types of minutiae details present in a fingerprint image | 55 |
| 3.2 | Unreliability of minutiae type: The same minutiae extracted from two different impressions. In (a) it appears as a bifurcation but a ridge ending in (b) | 56 |
| 3.3 | Binarization approach: The figure shows the different stages in a typical feature extractor following the binarization approach | 58 |
| 3.4 | Binarization scheme proposed by Domeniconi et al [24]: (a)A section of a fingerprint image (b)Ridges and valleys visualized as a 3D surface (c)Surface gradients. Notice that the gradients are zero on the ridges and valleys | 61 |

| | | |
|------|--|----|
| 3.5 | Chain code contour representation: (a)An example of an object boundary (b) Direction convention used for chain code representation, (c) Resulting chain code representation | 62 |
| 3.6 | Adaptive binarization: (a)Original Image(b)Binary image obtained by MINDTCT(c) Binary image obtained by our approach | 64 |
| 3.7 | Chain code contour representation: (a)The contour is extracted by tracing the ridge boundaries in a counter clockwise direction. Each contour element along with its co-ordinates, curvature slope and other information is stored in a list (b) The slope convention | 65 |
| 3.8 | (a) Minutiae marked by significant turn in the contour (b) Left turn (b) Right turn | 67 |
| 3.9 | Minutiae Detection (a) Detection of turning points, (b) and (c) Vector cross product for determining the turning type, (d) Determining minutiae direction | 68 |
| 3.10 | Heuristic post processing rules: (a) Fingerprint image with locations of spurious minutiae marked (b) Types of spurious minutiae removed by applying heuristic rules (i-iv) | 69 |
| 3.11 | Examples of features extracted from FVC2002 database. | 70 |
| 3.12 | Summary results: (a)Sensitivity Distribution (b) Overall Statistics | 70 |
| 3.13 | Some results of feature extraction. Images a-d are taken from FVC2002 DB1-DB4 databases respectively. The minutiae missed by the algorithm are highlighted in green | 72 |
| 4.1 | An illustration of the large intra-class variation between images of the same user | 75 |
| 4.2 | An illustration of the non-linear distortion | 76 |
| 4.3 | Explicit alignment: An illustration of the relative alignment using ridges associated with minutiae m_i and m'_j. | 80 |
| 4.4 | Illustration of the local secondary features used by [45, 43] | 82 |
| 4.5 | Illustration of two fingerprints of the same user with marked minutiae and the corresponding adjacency graph based on the K-plet representation. In this particular example each minutia is connected to its K=4 nearest neighbors. It is also to be noted that the topologies of the graphs are different due to an extra unmatched minutiae in the left print | 86 |
| 4.6 | Illustration showing that greedy approaches of performing minutiae pairing is sub-optimal. Minutiae marked with O are from the reference fingerprint and those marked with X are from the test fingerprint. The figure illustrates wrong assignment of one minutia m_I^1 with m_T^2. | 86 |
| 4.7 | An overview of the CBFS algorithm | 89 |
| 4.8 | Steps I,II of the example | 90 |
| 4.9 | Steps III-VI of the example | 91 |
| 4.10 | A comparison of ROC curves for FVC2002 DB1 database | 93 |

Acknowledgments

I wish to thank Dr. Cartwright and Dr. Govindaraju for their continuing support during the last two years and extending me the greatest freedom in deciding the direction and scope of my research. It has been both a privilege and a rewarding experience working with them. I would also like to thank my other committee members, Dr. Titus and Dr. Kondi for their guidance. I also thank Dr. Sharath Pankanti, Dr. Nalini Ratha and other members of the Exploratory Computer Vision Group group at IBM T. J. Watson Research Center, Hawthorne, NY for providing me the opportunity to work with them over the summer of 2004 and 2005. My interaction with them has been very fruitful and to a large extent has shaped the nature of my research. My special thanks also goes to Srirangaraj Setlur for giving me an opportunity to work at CUBS right at the beginning of my graduate studies. I also wish to acknowledge Tsai-Yang-Jea(Alan) and Chaohang Wu for their extended co-operation during the last two years. The work on feature extraction was possible only due to the collaboration with Chaohang while the development of the matching algorithm was the result of my discussions with Alan. I also thank all student members of the CUBS research group for engaging me in productive discussions and debate. In particular I extend my thanks to Sergey Tulyakov, Faisal Farooq, Amit Mhatre, Karthik Sridharan and Sankalp Nayak among others.

Abstract

Existing security measures rely on knowledge-based approaches like passwords or token-based approaches such as swipe cards and passports to control access to physical and virtual spaces. Though ubiquitous, such methods are not very secure. Tokens such as badges and access cards may be shared or stolen. Furthermore, they cannot differentiate between authorized user and a person having access to the tokens or passwords.

Biometrics such as fingerprint, face and voice print offers means of reliable personal authentication that can address these problems and is gaining citizen and government acceptance. Fingerprints were one of the first forms of biometric authentication to be used for law enforcement and civilian applications. Contrary to popular belief and despite decades of research in fingerprints, reliable fingerprint recognition is still an open problem. In this thesis, we present three specific contributions to advance the state of the art in this field.

Reliable extraction of features from poor quality prints is the most challenging problem faced in the area of fingerprint recognition. In this thesis, we introduce a new approach for fingerprint image enhancement based on Short Time Fourier Transform(STFT) Analysis. STFT is a well known time-frequency analysis technique to analyze non-stationary signals. In this thesis, we extend its application to the analysis 2D fingerprint images. The proposed analysis and enhancement algorithm simultaneously estimates several intrinsic properties of the fingerprint such as the foreground region mask, local ridge orientation and local frequency. We also objectively measure the effectiveness of the enhancement algorithm and show that it can improve the sensitivity and recognition accuracy of existing feature extraction and matching algorithms.

We also present a new feature extraction algorithm based on chain code contour processing. Chain codes provide us with a loss-less representation of the fingerprint ridge contours along with providing us with a wide range of information about the contour such as curvature, direction, length etc. The algorithm has several advantages over the techniques proposed in literature such as increased computational efficiency, improved localization and higher sensitivity. We present an objective evaluation of the feature extraction algorithm and show that it performs better than the existing approaches such as NIST MINDTCT algorithm.

Finally we present a novel minutia based fingerprint recognition algorithm that incorporates three new ideas. Firstly, we define a new representation called K-plet to encode the local neighborhood of each minutia. Secondly, we also present a dynamic programming approach for matching each local neighborhood in an optimal fashion. Lastly, we present CBFS (Coupled Breadth First Search), a new dual graph traversal algorithm for consolidating all the local neighborhood matches. We present an experimental evaluation of the proposed approach and show that it performs better than the popular NIST BOZORTH3 matching algorithm.

Chapter 1

Introduction

In an increasingly digital world, reliable personal authentication has become an important human computer interface activity. National security, e-commerce, and access to computer networks are some examples where establishing a person's identity is vital. Existing security measures rely on knowledge-based approaches like passwords or token-based approaches such as swipe cards and passports to control access to physical and virtual spaces. Though ubiquitous, such methods are not very secure. Tokens such as badges and access cards may be shared or stolen. Passwords and PIN numbers may be stolen electronically. Furthermore, they cannot differentiate between authorized user and a person having access to the tokens or knowledge.

Biometrics such as fingerprint, face and voice print offers means of reliable personal authentication that can address these problems and is gaining citizen and government acceptance.

1.1 Biometrics

Biometrics is the science of verifying the identity of an individual through physiological measurements or behavioral traits. Since biometric identifiers are associated permanently with the user they are more reliable than token or knowledge based authentication methods. Biometrics offers several advantages over traditional security measures. These include

1. **Non-repudiation:** With token and password based approaches, the perpetrator can always deny committing the crime pleading that his/her password or ID was stolen or compromised even when confronted with an electronic audit trail. There is no way in which his claim can be verified effectively. This is known as the problem of deniability or of 'repudiation'. However, biometrics is indefinitely associated with a user and hence it cannot be lent or stolen making such repudiation infeasible.
2. **Accuracy and Security:** Password based systems are prone to dictionary and brute force attacks. Furthermore, such systems are as vulnerable as their weakest password. On the other hand, biometric authentication requires the physical presence of the user and therefore cannot be circumvented through a dictionary or brute force style attack. Biometrics have also been shown to possess a higher bit strength compared to password based systems [42] and are therefore inherently secure.
3. **Screening:** In screening applications, we are interested in preventing the users from assuming multiple identities (e.g. a terrorist using multiple passports to enter a foreign country). This requires that we ensure a person has not already enrolled under another assumed identity before adding his new record into the database. Such screening is not possible using traditional authentication mechanisms and biometrics provides the only available solution.

The various biometric modalities can be broadly categorized as

- **Physical biometrics:** These involve some form of physical measurement and includes modalities such as face, fingerprints, iris-scans, hand geometry etc.
- **Behavioral biometrics:** These are usually temporal in nature and involves measuring the *way* in which a user performs certain tasks. This includes modalities such as speech, signature, gait, keystroke dynamics etc.
- **Chemical biometrics:** This is still a nascent field and involves measuring chemical cues such as odor and the chemical composition of human perspiration.

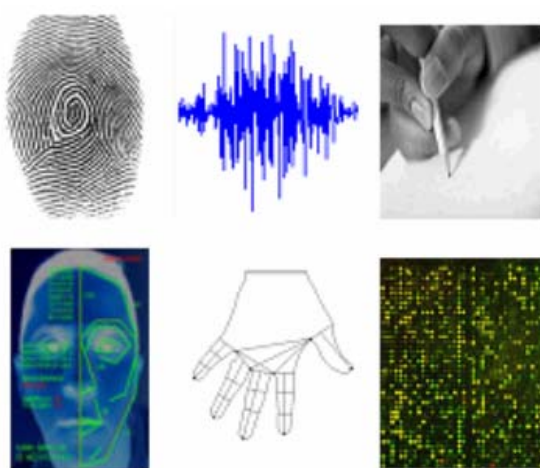


Figure 1.1: Various biometric modalities: Fingerprints, speech, handwriting, face, hand geometry and chemical biometrics

It is also instructive to compare the relative merits and de-merits of biometric and password/cryptographic key based systems. Table 1.1 provides a summary of them.

Depending on the application, biometrics can be used for identification or for verification. In verification, the biometric is used to validate the claim made by the individual. The biometric of the user is compared with the biometric of the claimed individual in the database. The claim is rejected or accepted based on the match. (In essence, the system tries to answer the question, "Am I whom I claim to be?"). In identification, the system recognizes an individual by comparing his biometrics with every record in the database. (In essence, the system tries to answer the question,

| Biometric Authentication | Password/Key based authentication |
|--|---|
| Based on physiological measurements or behavioral traits | Based on something that the user 'has' or 'knows' |
| Authenticates the user | Authenticates the password/key |
| Is permanently associated with the user | Can be lent, lost or stolen |
| Biometric templates have high uncertainty | Have zero uncertainty |
| Utilizes probabilistic matching | Requires exact match for authentication |

Table 1.1: Comparison of biometric and password/key based authentication

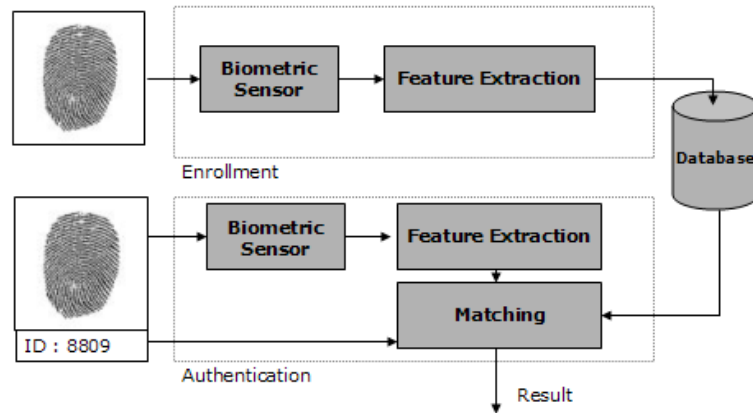


Figure 1.2: General architecture of a biometric system

”Who am I?”). In this thesis, we will be dealing mainly with the problem of verification using fingerprints. In general, biometric verification consists of two stages (Figure 1.2) (i) Enrollment and (ii) Authentication. During enrollment, the biometrics of the user is captured and the extracted features (template) are stored in the database. During authentication, the biometrics of the user is captured again and the extracted features are compared with the ones already existing in the database to determine a match. The specific record to fetch from the database is determined using the claimed identity of the user. The database itself may be central or distributed with each user carrying his template on a smart card.

1.1.1 Biometrics and Pattern Recognition

As recently as a decade ago, biometrics did not exist as a separate field. It has evolved through interaction and confluence of several fields. Fingerprint recognition emerged from the application of pattern recognition to forensics. Speaker verification evolved out of the signal processing community. Face detection and recognition was largely researched by the computer vision community. While biometrics is primarily considered as application of pattern recognition techniques, it has several outstanding differences from conventional classification problems as enumerated below

1. In a conventional pattern classification problem such as Optical Character Recognition(OCR)

recognition, the number of patterns to classify is small (A-Z) compared to the number of samples available for each class. However in case of biometric recognition, the number of classes is as large as the set of individuals in the database. Moreover, it is very common that only a single template is registered per user.

2. The primary task in biometric recognition is that of choosing a proper feature representation. Once the features are carefully chosen, the act of performing verification is fairly straightforward and commonly employs simple metrics such as Euclidean distance. Hence the most challenging aspects of biometric identification involves signal and image processing for feature extraction.
3. Since biometric templates represent personally identifiable information of individuals, security and privacy of the data is of particular importance unlike other applications of pattern recognition.
4. Modalities such as fingerprints, where the template is expressed as an unordered point set(minutiae) do not fall under the category of traditional multi-variate/vectorial features commonly used in pattern recognition.

1.1.2 The Verification Problem

Here we consider the problem of biometric verification in a more formal manner. In a verification problem, the biometric signal from the user is compared against a single enrolled template. This template is chosen based on the claimed identity of the user. Each user i is represented by a biometric B_i . It is assumed that there is a one-to-one correspondence between the biometric B_i and the identity i of the individual. The feature extraction phase results in a machine representation(template) T_i of the biometric.

During verification, the user claims an identity j and provides a biometric signal B_j . The feature extractor now derives the corresponding machine representation T_j . The recognition consists of computing a similarity score $S(T_i, T_j)$. The claimed identity is assumed to be true if the $S(T_i, T_j) >$



Figure 1.3: An illustration showing the intra user variation present in biometric signals

Th for some threshold Th . The choice of the threshold also determines the trade-off between user convenience and system security as will be seen in the ensuing section.

1.1.3 Performance Evaluation

Unlike passwords and cryptographic keys, biometric templates have high uncertainty. There is considerable variation between biometric samples of the same user taken at different instances of time (Figure 1.3). Therefore the match is always done probabilistically. This is in contrast to exact match required by password and token based approaches. The inexact matching leads to two forms of errors

- **False Accept** An impostor may sometime be accepted as a genuine user, if the similarity with his template falls within the intra-user variation of the genuine user.
- **False Reject** When the acquired biometric signal is of poor quality, even a genuine user may be rejected during authentication. This form of error is labeled as a 'false reject'.

The system may also have other less frequent forms of errors such as

- **Failure to enroll(FTE)** It is estimated that nearly 4% of the population have illegible fingerprints. This consists of senior population, laborers who use their hands a lot and injured individuals. Due to the poor ridge structure present in such individuals, such users cannot

be enrolled into the database and therefore cannot be subsequently authenticated. Such individuals are termed as 'goats' [12]. A biometric system should have exception handling mechanism in place to deal with such scenarios.

- **Failure to authenticate (FTA)** This error occurs when the system is unable to extract features during verification even though the biometric was legible during enrollment. In case of fingerprints this may be caused due to excessive sweating, recent injury etc. In case of speech, this may be caused due to cold, sore throat etc. It should be noted that this error is distinct from False Reject where the rejection occurs during the matching phase. In FTA, the rejection occurs in the feature extraction stage itself.

1.1.4 System Errors

A biometric matcher takes two templates T and T' and outputs a score

$$S = S(T, T')$$

which is a measure of similarity between the two templates. The two templates are identical if $S(T, T')=1$ and are completely different if $S(T, T')=0$. Therefore the similarity can be related to matching probability in some monotonic fashion. An alternative way to compute the match probability is to compute the matching distance $D(T, T')$. In this case, identical templates will have $D(T, T')=0$ and dissimilar templates should ideally have $D(T, T')=\infty$. Usually a matcher outputs the similarity score $S(T, T') \in [0, 1]$.

Given two biometric samples, we construct two hypothesis

- The null hypothesis H_0 : The two samples match.
- The alternate hypothesis H_1 : The two samples don't match.

The matching decides whether H_0 is true or H_1 is true. The decision of the matcher is based on

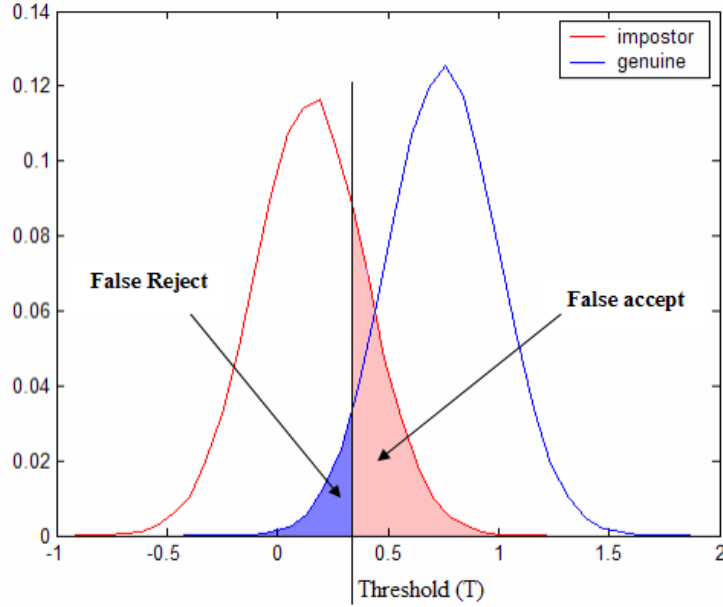


Figure 1.4: Genuine and impostor distributions

some fixed threshold Th :

$$\text{Decide } H_0 \text{ if } S(T, T') > Th \quad (1.1)$$

$$\text{Decide } H_1 \text{ if } S(T, T') \leq Th \quad (1.2)$$

Due to variability in the biometric signal, the scores $S(T, T')$ for the same person is not always unity and the score $S(T, T')$ for different person is not exactly zero. In general the scores from matching genuine pairs are usually 'high' and the results from matching impostor pairs are usually 'low' (Figure 1.4).

Given that p_g and p_i represent the distribution of genuine and impostor scores respectively, the FAR and FRR at threshold T is given by

$$FAR(T) = \int_T^1 p_i(x) dx \quad (1.3)$$

$$FRR(T) = \int_0^T p_g(x) dx \quad (1.4)$$

The corresponding ROC curve is obtained by plotting FAR(x-axis) vs 1-FRR(y axis). Figures 1.5 display a typical curve. The interpretation of these two will be covered in a later section.

1.1.5 Caveat

Although biometrics offers reliable means of authentication, they are also subject to their own set of unique security problems [66]. Similar to computer networks, a biometric system can be prone to denial of service attack, Trojan horse attack and other forms of vulnerabilities. While there are formal techniques to detect and handle intrusions into computer systems, such methods have not been developed to safeguard biometric systems. With biometric interfaces, implementations and representation being made public, it is no longer possible to maintain 'security by obscurity' and as such, it is considered to be a bad practice [81]. The security of biometric systems was mentioned as one of the pertinent issues of academic research in 'Biometrics Research Agenda', a NSF workshop attended by industry and academic experts. The recent X9.84 national standard (www.x9.org) was proposed to address these very concerns. While several theoretical solutions have been presented to these problems, practical solutions will require considerable research efforts.

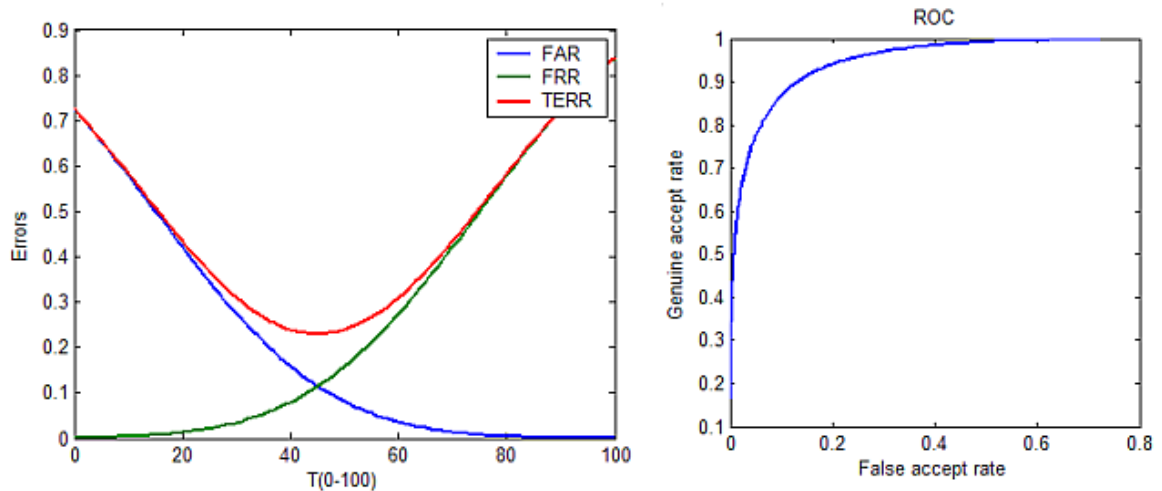


Figure 1.5: (i)Typical FAR and FRR vs threshold (ii)Typical ROC curve

The architecture of a general biometric system consists of several stages (Figure 1.6). An input device (A) is used to acquire and digitize the biometric signal such as face or fingerprint. A feature extraction module (B) extracts the distinguishing characteristics from the raw digital data (E.g. Minutiae extraction from a fingerprint image). These distinguishing features are used to construct an invariant representation or a template. During enrollment the template generated is stored in the database (D) and is retrieved by the matching module (C) during authentication. The matcher arrives at a decision based on similarity of the two templates and also taking into account the signal quality and other variables. Within this framework we can identify eight locations where security attacks may occur.

- (1) Fake biometric attack: In this mode of attack, a replica of a biometric feature is presented instead of the original. Examples include: gummy fingers, voice recordings, photograph of the face, etc.
- (2) Denial of service attack: The sensor may be tampered or destroyed completely in a bid to prevent others from authenticating themselves.
- (3) Electronic replay attack: A biometric signal may be captured from an insecure link during transmission and then resubmitted repeatedly thereby circumventing the sensor.
- (4,6) Trojan horse attack: The feature extraction process may be overridden so that it always reproduces the template and the score chosen by the attacker.
- (5,7) Snooping and tampering: The link between the feature extraction module and the matcher or the link between the matcher and the database may be intercepted and the genuine template may be replaced with a counterfeit template. This template may have been recorded earlier and may not correspond to the current biometric signal.
- (8) Back end attack: In this mode of attack, the security of the central database is compromised and the genuine templates are replaced with counterfeit ones.

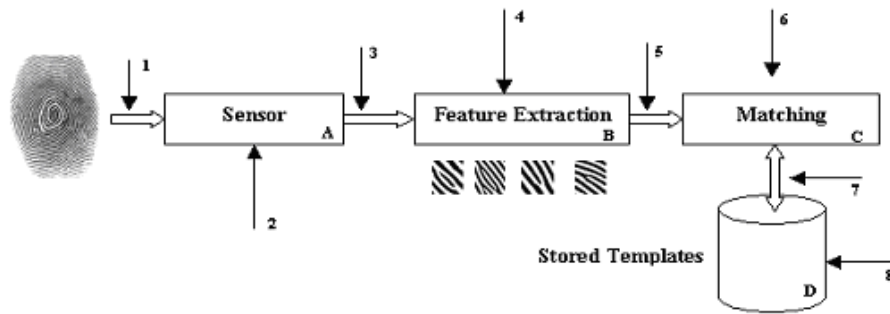


Figure 1.6: An illustration of a general biometric system with points of threats identified

1.2 Fingerprint as a Biometric: Fingerprints 101

Fingerprints were accepted formally as valid personal identifier in the early twentieth century and have since then become a de-facto authentication technique in law-enforcement agencies world wide. The FBI currently maintains more than 400 million fingerprint records on file. Fingerprints have several advantages over other biometrics, such as the following:

1. **High universality:** A large majority of the human population has legible fingerprints and can therefore be easily authenticated. This exceeds the extent of the population who possess passports, ID cards or any other form of tokens.
2. **High distinctiveness:** Even identical twins who share the same DNA have been shown to have different fingerprints, since the ridge structure on the finger is not encoded in the genes of an individual. Thus, fingerprints represent a stronger authentication mechanism than DNA. Furthermore, there has been no evidence of identical fingerprints in more than a century of forensic practice. There are also mathematical models [62] that justify the high distinctiveness of fingerprint patterns.
3. **High permanence:** The ridge patterns on the surface of the finger are formed in the womb and remain invariant until death except in the case of severe burns or deep physical injuries.

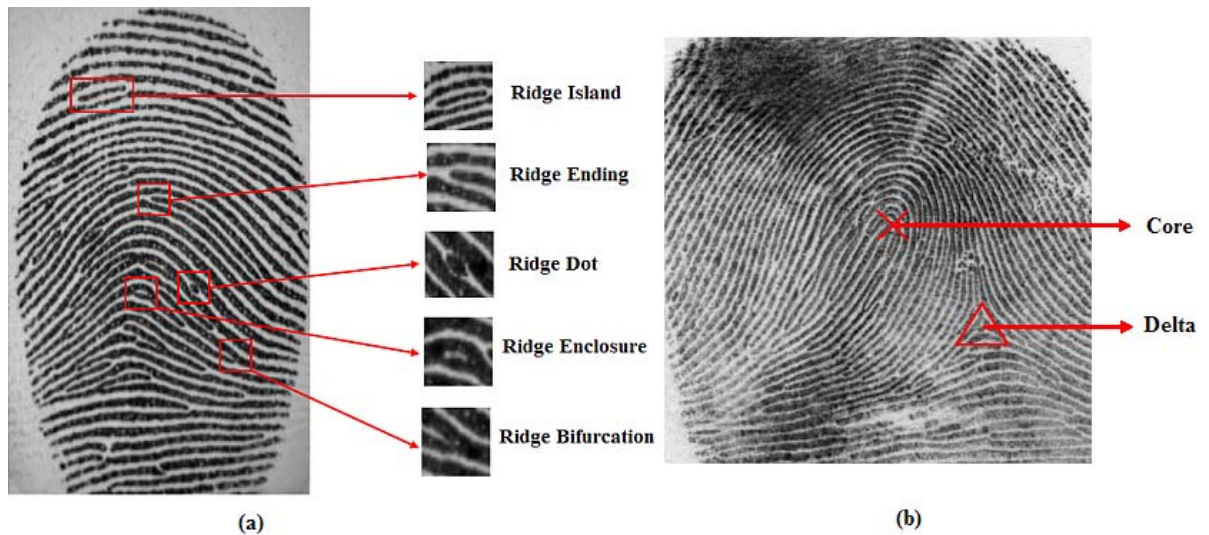


Figure 1.7: (a) Local Features: Minutiae (b) Global Features: Core and Delta

-
4. **Easy collectability:** The process of collecting fingerprints has become very easy with the advent of online sensors. These sensors are capable of capturing high resolution images of the finger surface within a matter of seconds [54]. This process requires minimal or no user training and can be collected easily from co-operative or non co-operative users. In contrast, other accurate modalities like iris recognition require very co-operative users and have considerable learning curve in using the identification system.
 5. **High performance:** Fingerprints remain one of the most accurate biometric modalities available to date with jointly optimal FAR (false accept rate) and FRR (false reject rate). Forensic systems are currently capable of achieving FAR of less than 10^{-4} [3].
 6. **Wide acceptability:** While a minority of the user population is reluctant to give their fingerprints due to the association with criminal and forensic fingerprint databases, it is by far the most widely used modality for biometric authentication.

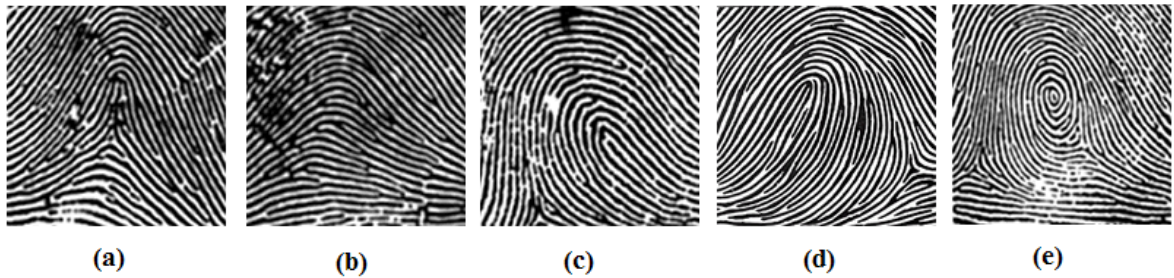


Figure 1.8: **Fingerprint Classes: (a)Tented Arch (b)Arch (c)Right Loop (d)Left Loop (e)Whorl**

The fingerprint surface is made up of a system of ridges and valleys that serve as friction surface when we are gripping the objects. The surface exhibits very rich structural information when examined as an image. The fingerprint images can be represented by both global as well as local features. The global features include the ridge orientation, ridge spacing and singular points such as core and delta. The singular points are very useful from the classification perspective (See Figure 1.8). However, verification usually relies exclusively on minutiae features. Minutiae are local features marked by ridge discontinuities. There are about 18 distinct types of minutiae features that include ridge endings, bifurcations, crossovers and islands. Among these, *ridge endings* and *bifurcation* are the commonly used features.(See Figure 1.7). A ridge ending occurs when the ridge flow abruptly terminates and a ridge bifurcation is marked by a fork in the ridge flow. Most matching algorithms do not even differentiate between these two types since they can easily get exchanged under different pressures during acquisition. Global features do not have sufficient discriminative power on their own and are therefore used for binning or classification before the extraction of the local minutiae features.

The various stages of a typical fingerprint recognition system is shown in Figure 1.9. The fingerprint image is acquired using off-line methods such as creating an inked impression on paper or through a live capture device consisting of an optical, capacitive, ultrasound or thermal sensor [54]. The first stage consists of standard image processing algorithms such as noise removal and

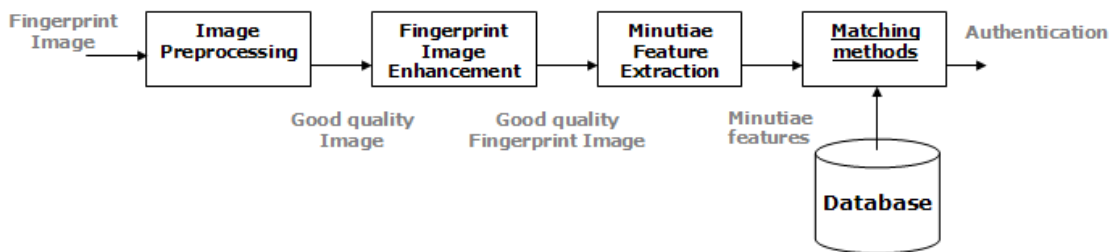


Figure 1.9: General architecture of a fingerprint verification system

smoothing. However, it is to be noted that unlike regular images, the fingerprint image represents a system of oriented texture and has very rich structural information within the image. Furthermore, the definition of noise and unwanted artifacts are also specific to fingerprints. The fingerprint image enhancement algorithms are specifically designed to exploit the periodic and directional nature of the ridges. Finally, the minutiae features are extracted from the image and are subsequently used for matching. Although research in fingerprint verification research has been pursued for several decades now, there are several open research challenges still remaining, some of which will be addressed in the ensuing sections of this thesis.

1.3 Fingerprint Sensors

Traditionally fingerprints were acquired by transferring the inked impression onto the paper. This process is termed as *off-line* acquisition. Existing authentication systems are based on *live-scan* devices that capture the fingerprint image in real time.

The live-scan devices may be based on one of the following sensing schemes

1. **Optical Sensors** These are the oldest and most widely used technology. In most devices, a charged coupled device (CCD) converts the image of the fingerprint, with dark ridges and light valleys, into a digital signal. They are fairly inexpensive and can provide resolutions up to 500 dpi. Most sensors are based on FTIR(Frustrated Total Internal Reflection) technique to acquire the image. In this scheme , a source illuminates the fingerprint through one side

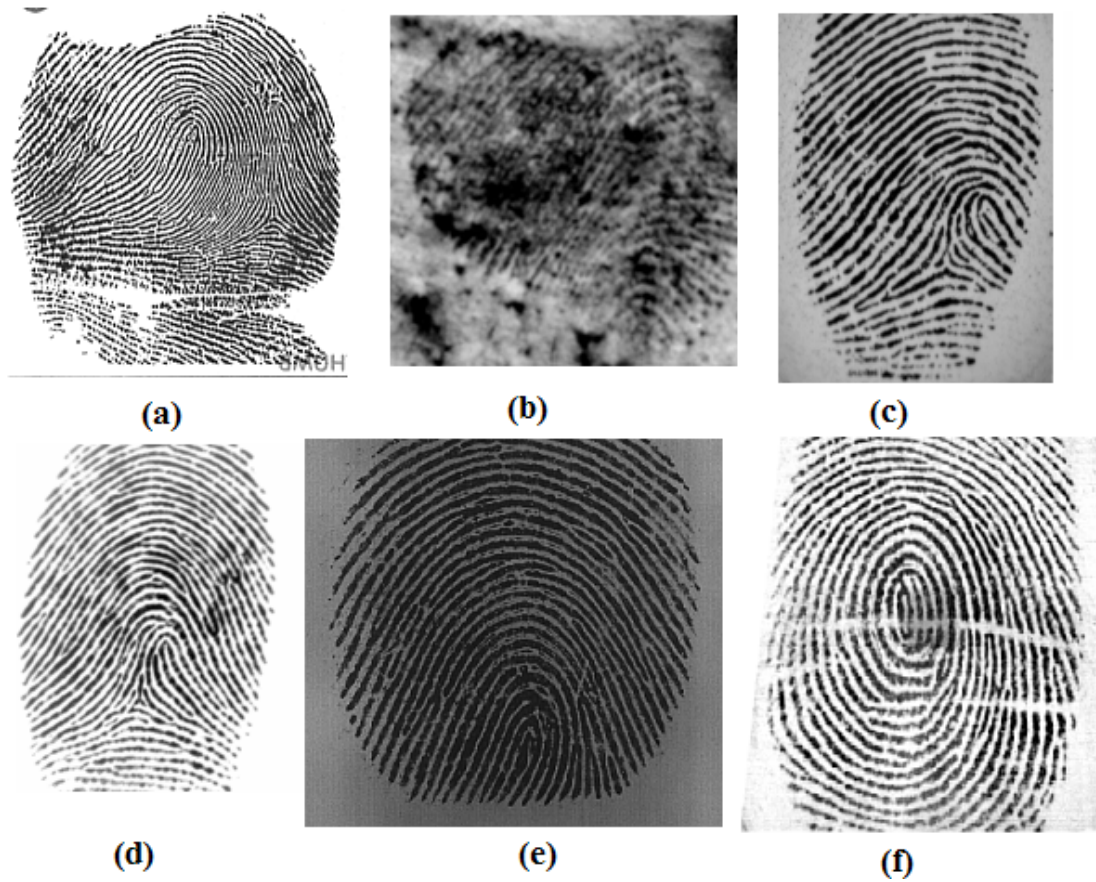


Figure 1.10: Offline and on-line acquisition: (a) Acquired by rolling inked finger on paper (b) Latent fingerprint acquired from a crime scene, (c,d,f) Acquired from optical, (e) Acquired from a capacitive sensor.

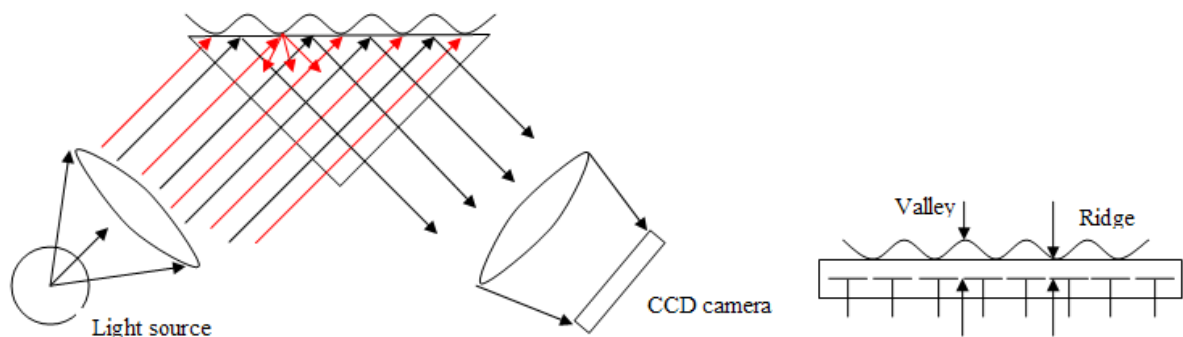


Figure 1.11: (a) General schematic for an FTIR based optical sensor (b) Schematic of a capacitive sensor

of the prism as shown (Figure 1.11). Due to internal reflection phenomenon, most of the light is reflected back to the other side where it is recorded by a CCD camera. However, in regions where the fingerprint surface comes in contact with the prism, the light is diffused in all directions and therefore does not reach the sensor resulting in dark regions. The quality of the image depends on whether the fingerprint is dry or wet. Another problem faced by optical sensors is the residual patterns left by the previous fingers. Furthermore it has been shown that fake fingers [56] are able to fool most commercial sensors. Optical sensors are also among the bulkiest sensor due to the optics involved.

2. **Capacitive Sensors** The silicon sensor acts as one plate of a capacitor, and the finger as another other. The capacitance between the sensing plate and the finger depends inversely as the distance between them . Since the ridges are closer, they correspond to increased capacitance and the valleys corresponds to smaller capacitance. This variation is converted into an 8-bit gray scale digital image. Most of the electronic devices featuring fingerprint authentication use this form of solid state sensors due to its compactness. However, sensors that are smaller than 0.5”x0.5” are not useful since it reduces the accuracy recognition [62].
3. **Ultra-sound Sensors** Ultrasound technology is perhaps the most accurate of the fingerprint sensing technologies. It uses ultrasound waves and measures the distance based on the

impedance of the finger, the plate, and air. These sensors are capable of very high resolution. Sensors with 1000dpi or more are already available (www.ultra-scan.com). However, these sensors tend to be very bulky and contain moving parts making them suitable only for law enforcement and access control applications.

4. **Thermal Sensors** These sensors are made up of pyro-electric materials whose properties change with temperature. These are usually manufactured in the form of strips (www.atmel.com). As the fingerprints is swiped across the sensor, there is differential conduction of heat between the ridges and valleys (since skin conducts heat better than the air in the valleys) that is measured by the sensor. Full size thermal sensors are not practical since skin reaches thermal equilibrium very quickly once placed on the sensor leading to loss of signal. This would require us to constantly keep the sensor at a higher or lower temperature making it very energy inefficient. The sweeping action prevents the finger from reaching thermal equilibrium leading to good contrast images. However, since the sensor can acquire only small strips at a time, a sophisticated image registration and reconstruction scheme is required to construct the whole image from the strips.

1.4 Fingerprint Representations and Matching Algorithms

Fingerprint matching may be broadly classified into the following categories based on their representation

1.4.1 Image

In this representation, the image itself is used as a template. Matching is performed by correlation [79, 7].



Figure 1.12: Various commercial sensors available for *live capture* of fingerprints

The correlation between two images $I_1(x, y), I_2(x, y)$ is given by

$$I_c(k, l) = \sum_x \sum_y I_1(x + k, y + l)I_1(x, y) \text{ in the spatial domain} \quad (1.5)$$

$$I_c(k, l) = FFT^{-1}\{FFT(I_1)FFT^*(I_2)\} \text{ in the Fourier domain} \quad (1.6)$$

The correlator matches by searching for the peak magnitude value in the correlation image (See Figure 1.13). The position of the peak indicates the translation between the images and the strength of the peak indicates the similarity between the images. This requires reasonably low resolution images and is very fast, since correlation may also be implemented through optical techniques [18, 51, 78]. However, the matching is global and requires an accurate registration of the fingerprint image, since correlation is not invariant to translation and rotation. Furthermore the accuracy of correlation based techniques also degrade with non-linear distortion of the fingerprint. The problem caused by distortion may be overcome by performing local correlation as proposed in [58] and [7]. Baze et al. select 'interesting' regions in the fingerprint image to perform this correlation since plain ridges do not carry any information except their orientation and ridge frequency. The 'interesting' regions include regions around the minutiae, regions of high curvature and regions around the singular points such as core and delta.

1.4.2 Minutiae Representation

The purpose of the matching algorithm is to compare two fingerprint images or templates and returns a similarity score that corresponds to the probability of match between the two prints. Except for the correlation based algorithms (See section 1.4.1), most of the algorithm extract *features* for the purpose of matching. Minutiae features are the most popular of all the existing representation and also form the basis of the visual matching process used by human experts.

Minutiae represent local discontinuities and mark position where the ridge comes to an end or bifurcates into two (See figure 1.7). These form the most frequent types of minutiae, although a total of 18 minutiae types have been identified so far [54]. Each minutiae may be described by a number of attributes such as its position (x,y) its orientation θ , its quality. However, most algorithms

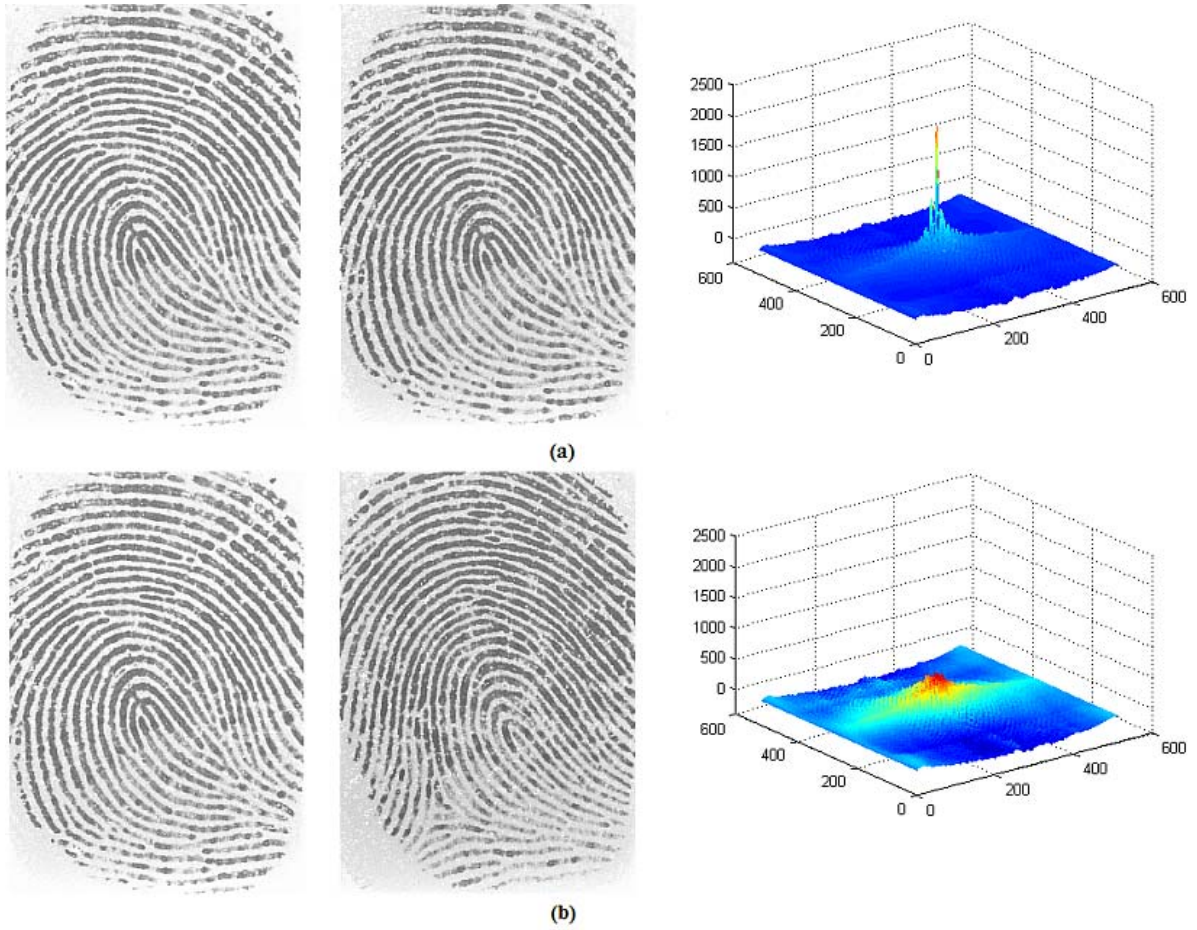


Figure 1.13: The illustration shows the results of correlation between images of the same user(a) and different user(b). It can be seen the the peak output of the correlation is high in case of genuine match and low for an impostor match.

consider only its position and orientation. Given a pair of fingerprints and their corresponding minutiae features to be matched, features may be represented as an unordered set given by

$$I_1 = \{m_1, m_2, \dots, m_M\} \text{ where } m_i = (x_i, y_i, \theta_i) \quad (1.7)$$

$$I_2 = \{m'_1, m'_2, \dots, m'_N\} \text{ where } m'_i = (x'_i, y'_i, \theta'_i) \quad (1.8)$$

It is to be noted that both the point sets are *unordered* and have different number of points (M and

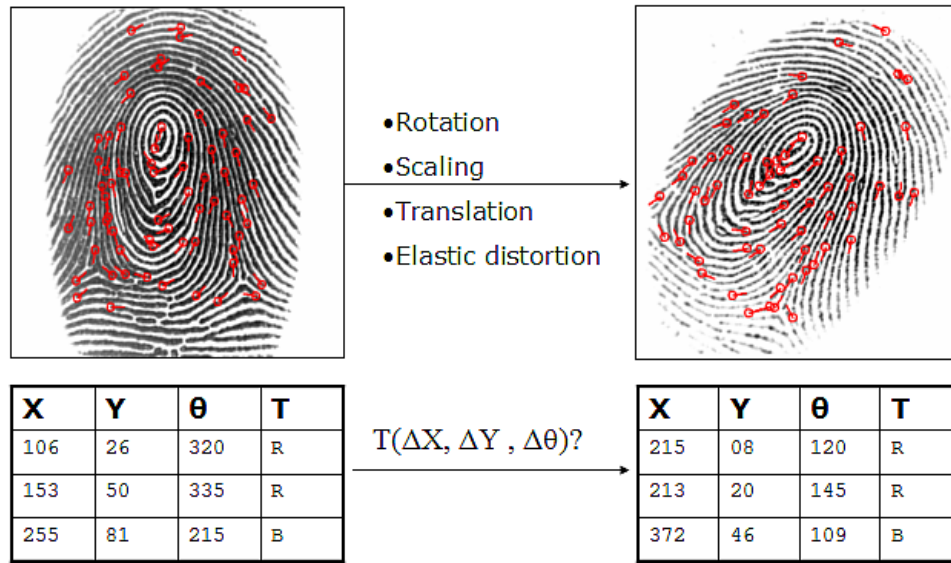


Figure 1.14: The figure shows the primary approach for matching minutiae. Each fingerprint is represented as a set of tuples each specifying the properties of minutiae(usually (x,y,θ)). The process of matching involves recovering the geometric transformation between the two sets. This may include rotation, scaling or non-linear distortion as illustrated.

N respectively). Furthermore, we do not know the correspondences between the point sets. This can be treated as a *point pattern matching* problem. Here the objective is to find a point m'_j in I_2 that exclusively corresponds to each point m_i in I_1 . However, we need to consider the following situations while obtaining the point correspondences.

1. The point m_i in I_1 may not have any point corresponding to it in I_2 . This may happen when m_i is a spurious minutia generated by the feature extractor.
2. Conversely, The point m'_j in I_2 may not be associated with any point in I_1 . This may happen when the point corresponding to m'_j was not captured by the sensor or was missed by the feature extractor.

Usually points in I_2 is related to points in I_1 through a geometric transformation $T()$. Therefore, the technique used by most minutiae matching algorithms is to recover the transformation function

T() that maps the two point sets as shown in (Figure 1.15). The resulting point set I'_2 is given by

$$I'_2 = T(I_1) = \{m''_1, m''_2, m''_3 \dots m''_N\} \quad (1.9)$$

$$m''_1 = T(m'_1) \quad (1.10)$$

$$\vdots \quad (1.11)$$

$$m''_N = T(m'_N) \quad (1.12)$$

$$(1.13)$$

The minutiae pair m_i and m''_j are considered to be a match only if

$$\sqrt{(x_i - x''_j)^2 + (y_i - y''_j)^2} \leq r_0 \quad (1.14)$$

$$\min(|\theta_i - \theta''_j|, 360 - |\theta_i - \theta''_j|) < \theta_0 \quad (1.15)$$

Here r_0 and θ_0 denote the tolerance window.

The matcher can make one of the following assumptions on the nature of the transformation T

1. **Rigid Transformation:** Here it is assumed that one point set is rotated and shifted version of the other. Optionally it may also be assumed that a scaling factor is also present. During rigid transformation, the shape of the objects is preserved intact [29]. Thus squares will be transformed to squares and circles will be transformed to circles. In case of point sets, the relative geometry of the points will remain the same. The transformation T is given by the relation

$$\begin{bmatrix} x' \\ y' \end{bmatrix} = \begin{bmatrix} \cos(\theta) & -\sin(\theta) \\ \sin(\theta) & \cos(\theta) \end{bmatrix} \begin{bmatrix} x \\ y \end{bmatrix} + \begin{bmatrix} \Delta x \\ \Delta y \end{bmatrix} \quad (1.16)$$

2. **Affine Transformation:** Affine transformations are generalization of Euclidean transform. Shape and angle are not preserved during transformation. Therefore a circle is transformed to a ellipse after transformation. Scaling, shearing and generalized affine transformation can be expressed by

$$\begin{bmatrix} x' \\ y' \end{bmatrix} = \begin{bmatrix} a_{11} & a_{12} \\ a_{21} & a_{22} \end{bmatrix} \begin{bmatrix} x \\ y \end{bmatrix} + \begin{bmatrix} \Delta x \\ \Delta y \end{bmatrix} \quad (1.17)$$

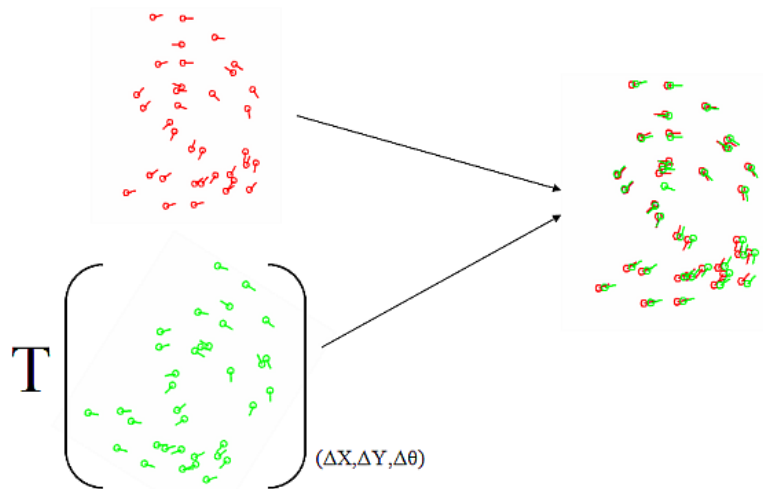


Figure 1.15: The minutiae are matched by transforming one set of minutiae and determining the number of minutiae that fall within a bounded region of another.

-
3. **Non-linear Transformation:** Here the transformation may be due to any arbitrary and complex transformation function $T(x,y)$. Recovering such a transformation is done by modeling it as a piece-wise linear transformation [30, 31] or through the use of thin plate spline deformation models [4, 9].

The following are the challenges faced when matching minutiae point sets

1. There is no inherent ordering in the collection of points.
2. The point set is of variable size and does not fall into the traditional scheme of pattern recognition where the data is assumed to be represented as multi-variate vector instances.
3. Furthermore the lack of knowledge about the point correspondences between the two point sets, make it a combinatorial problem requiring algorithm design rather than statistical pattern recognition solutions.
4. Missing and occluded features are common and further complicate the process of matching.

1.4.3 Texture Descriptors

Minutiae based matching algorithms do not perform well in case of small fingerprints that have very few minutiae. Furthermore the minutiae extraction process itself is error prone in such cases. Prabhakar et. al [40] propose a filter bank based approach to matching fingerprints to deal with such instances. The fingerprint can also be viewed as a system of oriented texture. Human experts routinely utilize the rich structural and texture cues present during the process of matching. However, minutiae based represents does not encode this information either explicitly or implicitly. They show that a combination of minutiae and texture features provide a substantial improvement in the matching performance.

Most textured images contain a limited range of spatial frequency and can be distinguished based on the dominant frequency content. Texture can be discriminated by decomposing it at different scales(frequency) and orientation. However, most of the fingerprints have same spatial frequency content, therefore reducing their discriminative capabilities. They describe a new texture descriptor scheme called 'finger code' that utilizes both global and local ridge descriptions. The features are extracted by tessellating the image around a reference point(the core). The feature consists of an ordered collection of texture descriptors from each of the individual cells. (Note: the algorithm assumes that the fingerprint is vertically oriented. Rotation is compensated by computing the features at various orientations). The texture descriptors are obtained by filtering each sector with 8 oriented Gabor filters and then computing the AAD (Average Absolute Deviation) of the pixel values in each cell. The features are concatenated to obtain the finger code (See Figure 1.16).

The matching is based on measuring the Euclidean distance between the feature vectors. Approximate rotation invariance is achieved by storing five templates per finger in the database each corresponding to the rotated versions of the original template. Furthermore five more templates are generated by rotating the image by 11.25 degrees. Therefore each finger has 10 associated templates stored in the database. The score is taken as the minimum score obtained after matching with each of the stored template. Note that the generation of 10 templates is an off line process. While verification only one template is generated.

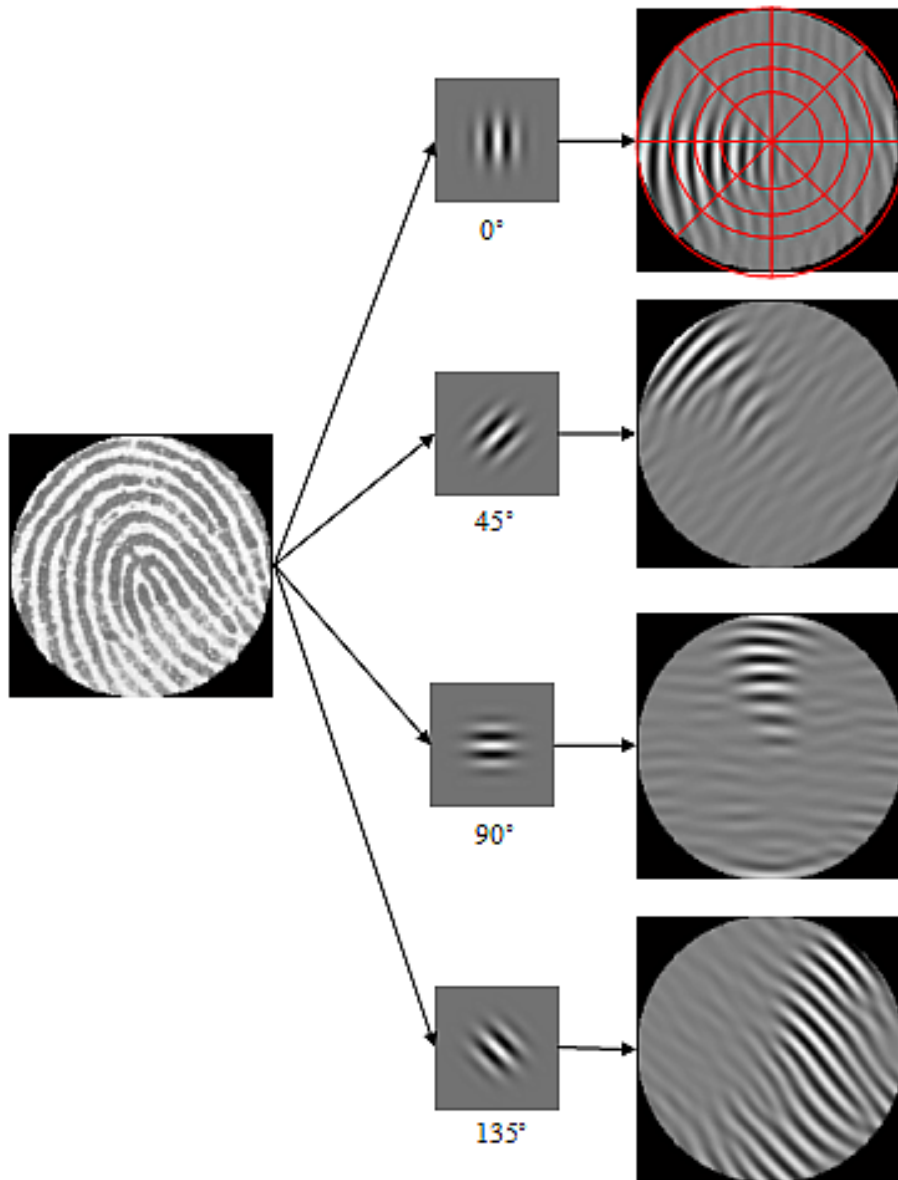


Figure 1.16: The illustration shows the response of the image to a gabor filter bank oriented at four different direction. The figure also illustrates the circular tessellation followed in [40]. The fingercodes consists of the AAD (Average Absolute Deviation) within each sector. In practice 8 orientations are used.

The disadvantage of this approach is that it requires that the core be accurately located. This is not possible in case of bad prints. Also, the performance is inferior compared to minutiae based matcher. However, since the representation differs significantly and is statistically independent from minutiae based approaches, the decision can be combined with minutiae based matcher to yield higher accuracy.

Jain et. al [41] proposed an approach for combining the texture information with minutiae features to improve recognition performance. The algorithm used is a variant of the 'fingercodex'. The difference lies in the method of tessellation. While fingercodex uses circular tessellation (relies on central location of the core), the current algorithm uses rectangular tessellation. Instead of relying on the core location as in the previous approach, here the two fingerprints are aligned using the extracted minutiae features. The texture features are derived based on the response of the 30x30 block to a bank of 8 directionally selective Gabor filters. The extracted features are compared using Euclidean distance and the final score is weighed based on the amount of overlap between the two fingers.

1.5 Thesis Outline

I have tried to make the thesis as self contained as possible by including the relevant background and literature at the beginning of each chapter. I have allowed redundancy only where the clarity of material mandates it. The rest of the thesis is organized as follows. Chapter 2 introduces a new fingerprint enhancement algorithm based on STFT analysis. Chapter 3 presents a novel feature extraction algorithm based on chain code based contour processing. We present a novel graph based matching algorithm for matching fingerprints in Chapter 4. Finally Chapter 5 summarizes the important contributions of this thesis.

Chapter 2

Fingerprint Image Enhancement Using STFT Analysis

The performance of a fingerprint feature extraction and matching algorithm depend heavily upon the quality of the input fingerprint image. While the 'quality' of a fingerprint image cannot be objectively measured, it roughly corresponds to the the clarity of the ridge structure in the fingerprint image. A 'good' quality fingerprint image has high contrast and well defined ridges and valleys. A 'poor' quality fingerprint is marked by low contrast and ill-defined boundaries between the ridges and valleys. There are several reasons that may degrade the quality of the fingerprint image.

1. The ridges are broken by presence of creases, bruises or wounds on the fingerprint surface
2. Excessively dry fingers lead to fragmented ridges
3. Sweaty fingerprints lead to bridging between successive ridges

The quality of fingerprint encountered during verification varies over a wide range (See Figure 2.1). It is estimated that roughly 10% of the fingerprint encountered during verification can be classified as 'poor' [54]. Poor quality fingerprints lead to generation of spurious minutiae. In smudgy regions, genuine minutiae may also be lost, the net effect of both leading to loss in accuracy of the matcher.



Figure 2.1: Fingerprint images of different quality. The quality decreases from left to right. (a) Good quality image with high contrast between the ridges and valleys (b) Insufficient distinction between ridges and valleys in the center of the image (c) Dry print

The robustness of the recognition system can be improved by incorporating an enhancement stage prior to feature extraction. Due to the non-stationary nature of the fingerprint image, general-purpose image processing algorithms are not very useful in this regard but serve as a preprocessing step in the overall enhancement scheme. Furthermore pixel oriented enhancement schemes like histogram equalization [29], mean and variance normalization [35], weiner filtering [80] improve the legibility of the fingerprint but do not alter the ridge structure. Also, the definition of noise in a generic image and a finger print are widely different. The *noise* in a fingerprint image consists of breaks in the directional flow of ridges. In the next section, we will discuss some filtering approaches that were specifically designed to enhance the ridge structure.

2.1 Prior Related Work

Due to the non-stationary nature of the fingerprint image, using a single filter that operates on the entire image is not effective. Instead, the filter parameters have to be adapted to enhance the local ridge structure. A majority of the existing techniques are based on the use of *contextual* filters

whose parameters depend on the local ridge frequency and orientation. Human experts routinely use *context* when identifying . The context information includes

1. *Ridge continuity*: The underlying morphogenetic process that produced the ridges does not allow for irregular breaks in the ridges except at ridge endings.
2. *Regularity*: Although the fingerprint represents a non-stationary image, the intrinsic properties such as instantaneous orientation and ridge frequency varies very slowly and gradually across the fingerprint surface.

Due to the regularity and continuity properties of the fingerprint image, occluded and corrupted regions can be recovered using the contextual information from the surrounding neighborhood. Hong et al [35] label such regions as '*recoverable*' regions. The efficiency of an automated enhancement algorithm depends on the extent to which they utilize contextual information. The filters themselves may be defined in spatial or in the Fourier domain.

2.1.1 Spatial Domain Filtering

O’Gorman et al. [60] proposed the use of contextual filters for fingerprint image enhancement for the first time. They used an anisotropic smoothing kernel whose major axis is oriented parallel to the ridges. For efficiency, they precompute the filter in 16 directions. The net result of the filter is that it increases contrast in a direction perpendicular to the ridges while performing smoothing in the direction of the ridges. Recently, Greenberg et al. [80] proposed the use of an anisotropic filter that is based on structure adaptive filtering [95]. The filter kernel is adapted at each point in the image and is given by

$$f(x, x_0) = S + V\rho(x - x_0)\exp\left\{-\left(\frac{((x - x_0).n)^2}{\sigma_1^2(x_0)} + \frac{((x - x_0).n_\perp)^2}{\sigma_2^2(x_0)}\right)\right\} \quad (2.1)$$

Here n and n_\perp represents unit vectors parallel and perpendicular to the ridges respectively. σ_1 and σ_2 control the eccentricity of the filter. $\rho(x - x_0)$ determines the support of the filter and chosen such that $\rho(x) = 0$ when $|x - x_0| > r$.

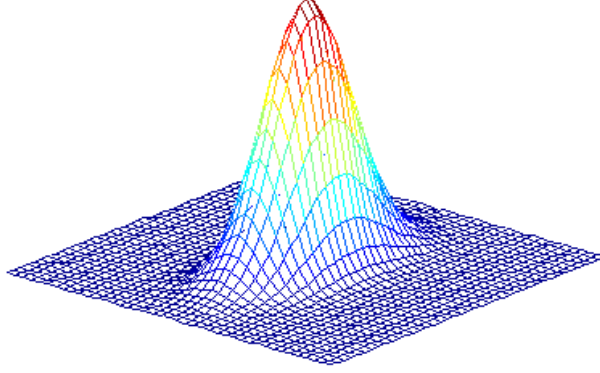


Figure 2.2: The anisotropic filtering kernel proposed by Greenberg et. al [80]. The filter shown has $\mathbf{S}=-\mathbf{2}$, $\mathbf{V}=\mathbf{10}$, $\sigma_1^2(x_0) = 4$ $\sigma_2^2(x_0) = 2$

Another approach based on directional filtering kernel is by Hong et al. [35]. The main stages of their algorithm are as follows

1. *Normalization*: This procedure normalizes the global statistics of the image, by reducing each image to a fixed mean and variance. Although this pixel wise operation does not change the ridge structure, the contrast and brightness of the image are normalized as a result. The normalized image is defined as

$$G(i, j) = \left\{ \begin{array}{l} M_0 + \sqrt{\frac{VAR_0((I-M)^2)}{VAR}}, \text{ if } I(i, j) > M \\ M_0 - \sqrt{\frac{VAR_0((I-M)^2)}{VAR}}, \text{ otherwise} \end{array} \right\} \quad (2.2)$$

2. *Orientation Estimation*: This step determines the dominant direction of the ridges in different parts of the fingerprint image . This is a critical process and errors occurring at this stage is propagated into the frequency estimation and filtering stages. More details are discussed w.r.t intrinsic images (see Section 2.1.3)
3. *Frequency Estimation*: This step is used to estimate the inter-ridge separation in different regions of the fingerprint image. More techniques for frequency estimation are discussed w.r.t intrinsic images (see Section 2.1.3).

4. *Segmentation*: In this step, a region mask is derived that distinguishes between 'recoverable', 'unrecoverable' and 'background' portions of the fingerprint image.
5. *Filtering*: Finally using the context information consisting of the dominant ridge orientation and ridge separation, a band pass filter is used to enhance the ridge structure.

The algorithm uses a properly oriented Gabor kernel for performing the enhancement. Gabor filters have important signal properties such as optimal joint space frequency resolution [69]. Daugman [23] and Lee [52] have used Gabor elementary functions as wavelet basis functions to represent generic 2D images. Daugman gives the following form for the 2D Gabor elementary function

$$G(x, y) = \exp(-\pi[(x - x_0)^2\alpha^2 + (y - y_0)^2\beta^2]).\exp(-2\pi i[u_0(x - x_0) + v_0(y - y_0)]) \quad (2.3)$$

x_0 and y_0 represent the center of the elementary function in the spatial domain. u_0 and v_0 represent the modulation frequencies. α^2 and β^2 represent the variance along the major and minor axes respectively and therefore the extent of support in the spatial domain.

The even symmetric form that is oriented at an angle ϕ is given by

$$G(x, y) = \exp\left\{-\frac{1}{2}\left[\frac{(x \cos(\phi))^2}{\delta_x^2} + \frac{(y \sin(\phi))^2}{\delta_y^2}\right]\right\} \cos(2\pi f x \cos(\phi)) \quad (2.4)$$

Here f represents the ridge frequency, ϕ represents the dominant ridge direction and the choice of δ_x^2 and δ_y^2 determines the shape of the envelope and also the trade of between enhancement and spurious artifacts. If $\delta_x^2 \gg \delta_y^2$ results in excessive smoothing in the direction of the ridges causing discontinuities and artifacts at the boundaries. The determination of the ridge orientation and ridge frequencies are discussed in detail in section 2.1.3. This is by far, the most popular approach for fingerprint verification.

Gabor elementary functions form a very intuitive representation of fingerprint images since they capture the periodic,yet non-stationary nature of the fingerprint regions. However, unlike fourier bases or discrete cosine bases, using Gabor elementary functions have the following problems.

1. From a signal processing point of view, they do not form a tight frame. This means that the image cannot be represented as a linear superposition of the Gabor elementary functions with

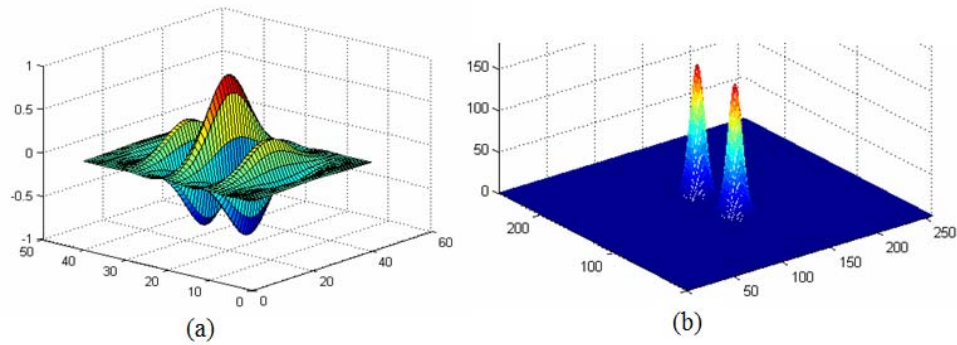


Figure 2.3: Gabor Filter Kernel: (a) Even symmetric part of the filter (b) The Fourier spectrum of the Gabor kernel showing the localization in the frequency domain

coefficients derived by projecting the image onto the same set of basis functions. However, Lee [52] has derived conditions under which a set of self similar Gabor basis functions form a complete and approximately orthonormal set of basis functions.

2. They are biorthogonal bases. This means that the basis functions used to derive the coefficients (analysis functions) and the basis functions used to reconstruct the image (synthesis functions) are not identical or orthogonal to each other. However, Daugman proposes a simple optimization approach to obtain the coefficients.
3. From the point of enhancing fingerprint images also, there is no rigorously justifiable reason for choosing the Gabor kernel over other directionally selective filters such as directional derivatives of gaussians or steerable wedge filters [26, 84]. While the compact support of the Gabor kernel is beneficial from a time-frequency analysis perspective, it does not necessarily translate to an efficient means for enhancement. Our algorithm is based on a filter that has separable radial and angular components and is tuned specifically to the distribution of orientation and frequencies in the local region of the fingerprint image.

Other approaches based on spatial domain techniques can be found in [83]. More recent work based on reaction diffusion techniques can be found in [14, 93].

2.1.2 Fourier Domain Filtering

Although spatial convolution using anisotropic or gabor filters is easily accomplished in the Fourier domain, this section deals with filters that are defined explicitly in the Fourier domain. Sherlock and Monro [11] perform contextual filtering completely in the Fourier Domain. Each image is convolved with precomputed filters of the same size as the image. The precomputed filter bank (labeled PF0,PF1..PFN in Figure 2.4) are oriented in eight different direction in intervals of 45° . However, the algorithm assumes that the ridge frequency is constant through out the image in order to prevent having a large number of precomputed filters. Therefore the algorithm does not utilize the full contextual information provided by the fingerprint image. The filter used is separable in radial and angular domain and is given by

$$H(\rho, \phi) = H_\rho(\rho)H_\phi(\phi) \quad (2.5)$$

$$H_\rho(\rho) = \sqrt{\left[\frac{(\rho\rho_{BW})^{2n}}{(\rho\rho_{BW})^{2n} + (\rho^2 - \rho_0^2)^{2n}} \right]} \quad (2.6)$$

$$H_\phi(\phi) = \begin{cases} \cos^2 \frac{\pi}{2} \frac{(\phi - \phi_c)}{\phi_{BW}} & \text{if } |\phi| < \phi_{BW} \\ 0 & \text{otherwise} \end{cases} \quad (2.7)$$

Here $H_\rho(\rho)$ is a band-pass butterworth filter with center defined by ρ_0 and bandwidth ρ_{BW} . The angular filter is a raised cosine filter in the angular domain with support ϕ_{BW} and center ϕ_c . However, the precomputed filters mentioned before are location independent. The contextual filtering is actually accomplished at the stage labeled 'selector'. The 'selector' uses the local orientation information to combine the results of the filter bank using appropriate weights for each output. The algorithm also accounts for the curvature of the ridges, something that was overlooked by the previous filtering approaches including gabor filtering. In regions of high curvature, having a fixed angular bandwidth lead to processing artifacts and subsequently spurious minutiae. In the approach proposed by Sherlock et al. the angular bandwidth of the filter is taken as a piece wise linear function of the distance from the singular points such as core and delta. However, this requires that the singular point be estimated accurately. In our algorithm, we instead utilize the angular coherence measure proposed by Rao [73]. This is more robust to errors in the orientation estimation and does

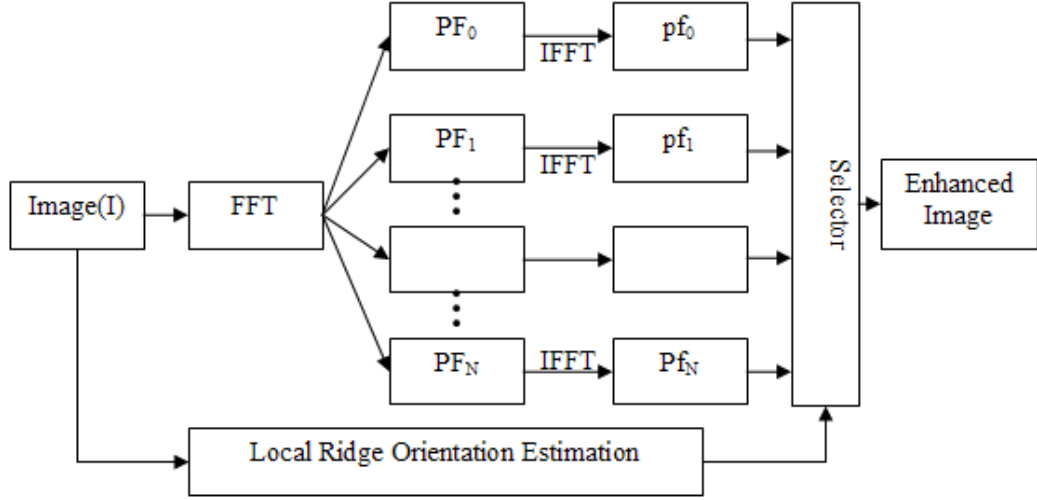


Figure 2.4: **Block diagram of the filtering scheme proposed by Sherlock and Monroe [11]**

not require us to estimate the singular point location. Although the computational complexity is reduced by performing contextual filtering in the last stage of the algorithm, the algorithm has large space complexity since it requires us to compute and retain sixteen prefiltered images ($pf_0 \dots pf_N$). Thus the algorithm is not suitable for embedded applications where memory requirement is at a premium. The results in their paper also indicate that while the algorithm is able to eliminate most of the false minutiae, it also misses more number of genuine minutiae when compared to other existing algorithms.

Watson et al. [92] proposed another approach for performing enhancement in the Fourier domain. This is based on 'root filtering' technique [38]. In this approach the image is divided into overlapping block and in each block, the enhanced image is obtained by

$$I_{enh}(x, y) = FFT^{-1}F(u, v)|F(u, v)|^k \quad (2.8)$$

$$F(u, v) = FFT(I(x, y)) \quad (2.9)$$

An advantage of this approach is that it does not require the computation of intrinsic images for its operation. This has the effect of increasing the dominant spectral components while attenuating

the weak components. This resembles matched filtering [38] very closely. However, in order to preserve the phase, the enhancement also retains the original spectrum $F(u,v)$. Other variations of fourier domain enhancement algorithm may be found in [54].

2.1.3 Intrinsic Images

The *intrinsic images* represent the important properties of the fingerprint image as a pixel map. These include

1. **Orientation Image:** The orientation image \mathbf{O} represents the instantaneous ridge orientation at every point in the fingerprint image. The ridge orientation is not defined in regions where the ridges are not present.
2. **Frequency Image:** The local ridge frequency indicates the average inter ridge distance within a block. Similar to the orientation image, the ridge frequency is not defined for background regions.
3. **Region Mask:** The region mask indicates the parts of the image where ridge structures are present. It is also known as the foreground mask. Some techniques [35] are also able to distinguish between recoverable and unrecoverable regions.

The computation of the intrinsic images forms a very critical step in the feature extraction process. Errors in computing these propagate through all the stages of the algorithm. In particular, errors in estimation of ridge orientation will affect enhancement, feature extraction and as a consequence the accuracy of the recognition. Applications that require a reliable orientation map include enhancement [35, 11, 60, 20], singular point detection [86, 8, 48] and segmentation [57] and most importantly fingerprint classification [16, 15, 47, 74, 39]. The region mask is used to eliminate spurious minutiae [20, 35].

Orientation Image

There have been several approaches to estimate the orientation image of a fingerprint image. These include the use of gradients [35], filter banks [34], template comparison [48], and ridge projection based methods [11]. The orientation estimation obtained by these methods is noisy and have to be smoothed before further use. These are based on vector averaging [46], relaxation methods [11], and mathematical orientation models [10, 90, 32]. Another important property of the orientation image is the ambiguity between 180° and 0° . Unlike vector flows that have a well defined *direction* that can be resolved over $[0^\circ, 360^\circ]$, orientation can be resolved only over $[0^\circ, 180^\circ]$. More has been said about this has been said in [64].

Except in the region of singularities such as core and delta, the ridge orientation varies very slowly across the image. Therefore the orientation image is seldom computed at full-resolution. Instead each non-overlapping block of size $W \times W$ of the image is assigned a single orientation that corresponds to the most probable or *dominant* orientation of the block. The horizontal and vertical gradients $G_x(x, y)$ and $G_y(x, y)$ respectively are computed using simple gradient operators such as a Sobel mask [29]. The block orientation θ is obtained using the following relations

$$G_{xy} = \sum_{u \in W} \sum_{v \in W} 2G_x(u, v)G_y(u, v) \quad (2.10)$$

$$G_{xx} = \sum_{u \in W} \sum_{v \in W} G_x^2(u, v) - G_y^2(u, v) \quad (2.11)$$

$$\theta = \frac{1}{2} \tan^{-1} \frac{G_{yy}}{G_{xx}} \quad (2.12)$$

A rigorous derivation of the above relation is provided in [46]. The dominant orientation so obtained still contains inconsistencies caused by creases and ridge breaks. Utilizing the regularity property of the fingerprint, the orientation image is smoothed. Due to the ambiguity in orientations, simple averaging cannot be utilized. Instead the orientation image is smoothed by vector averaging. Each block orientation is replaced with its neighborhood average according to

$$\theta'(i, j) = \frac{1}{2} \tan^{-1} \left\{ \frac{G(x, y) * \sin(2\theta(i, j))}{G(x, y) * \cos(2\theta(x, y))} \right\} \quad (2.13)$$

Here $G(x, y)$ represents a smoothing kernel such as a Gaussian [29].

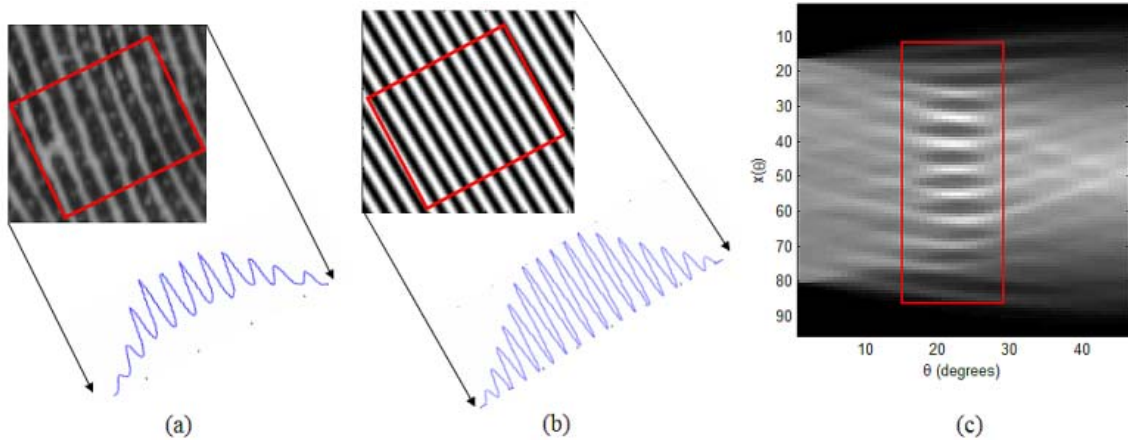


Figure 2.5: **Projection sum obtained for a window oriented along the ridges (a) Sample fingerprint (b) Synthetic image (c)Radon Transform of the fingerprint region**

Ridge Frequency Image

The ridge frequency is another intrinsic property of the fingerprint image. The ridge frequency is also a slowly varying property and hence is computed only once for each non-overlapping block of the image. It is estimated based on the projection sum taken along a line oriented orthogonal to the ridges [35], or based on the variation of gray levels in a window oriented orthogonal to the ridge flow [22]. These methods depend upon the reliable extraction of the local ridge orientation. The projection sum forms a sinusoidal signal and the distance between any two peaks provides the inter-ridge distance. Also, the process of taking the projection is equivalent to computing the radon transform at the angle of the ridge orientation. As figure 2.5 shows, the sinusoidal nature of the projection sum is easily visible. More details may be obtained from [35]. Maio and Maltoni [53] proposed a technique that can be used to compute the ridge spacing without performing peak detection. The frequency image so obtained may be further filtered to remove the outliers.

2.2 Proposed Algorithm: STFT Analysis

We present a new fingerprint image enhancement algorithm based on contextual filtering in the Fourier domain. The proposed algorithm is able to simultaneously estimate the local ridge orientation and ridge frequency information using Short Time Fourier Analysis. The algorithm is also able to successfully segment the fingerprint images. The following are some of the advantages of the proposed approach

1. The proposed approach obviates the need for multiple algorithms to compute the intrinsic images and replaces it with a single unified approach.
2. This is also a more formal approach for analysing the non-stationary fingerprint image than the local/windowed processing found in literature.
3. The algorithm simultaneously computes the orientation image, frequency image and the region mask as a result of the short time Fourier analysis. However, in most of the existing algorithms the frequency image and the region mask depend critically on the accuracy of the orientation estimation.
4. The estimate is probabilistic and does not suffer from outliers unlike most maximal response approaches found in literature.
5. The algorithm utilized complete contextual information including instantaneous frequency, orientation and even orientation coherence/reliability.

2.2.1 Overview

Figure 2.6 illustrates the overview of the proposed approach. During STFT analysis, the image is divided into overlapping windows. It is assumed that the image is stationary within this small window and can be modeled approximately as a surface wave. The fourier spectrum of this small region is analyzed and probabilistic estimates of the ridge frequency and ridge orientation are obtained. The STFT analysis also results in an energy map that may be used as a region mask to

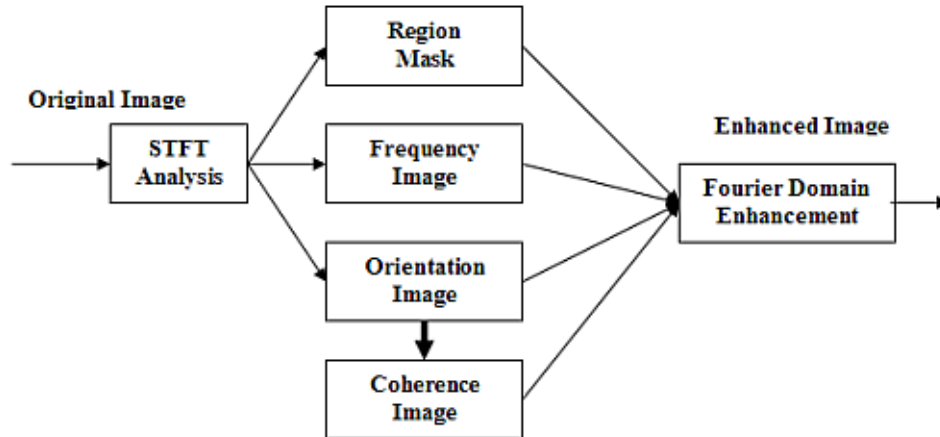


Figure 2.6: Overview of the proposed approach

distinguish between the fingerprint and the background regions. Thus, the STFT analysis results in the simultaneous computation of the ridge orientation image, ridge frequency image and also the region mask. The orientation image is then used to compute the angular coherence [73]. The coherence image is used to adapt the angular bandwidth. The resulting contextual information is used to filter each window in the fourier domain. The enhanced image is obtained by tiling the result of each analysis window.

Short Time Fourier Analysis

The fingerprint image may be thought of as a system of oriented texture with non-stationary properties. Therefore traditional Fourier analysis is not adequate to analyze the image completely. We need to resolve the properties of the image both in space and also in frequency. We can extend the traditional one dimensional time-frequency analysis to two dimensional image signals to perform short (time/space)-frequency analysis. In this section we recapitulate some of the principles of 1D STFT analysis and show how it is extended to 2D for the sake of analyzing the fingerprint.

When analyzing a non-stationary 1D signal $x(t)$ it is assumed that it is approximately stationary in the span of a temporal window $w(t)$ with finite support. The STFT of $x(t)$ is now represented by

time frequency atoms $X(\tau, \omega)$ [33] and is given by

$$X(\tau, \omega) = \int_{-\infty}^{\infty} x(t)\omega^*(t - \tau)e^{-j\omega t} dt \quad (2.14)$$

In the case of 2D signals such as a fingerprint image, the space-frequency atoms is given by

$$X(\tau_1, \tau_2, \omega_1, \omega_2) = \int_{-\infty}^{\infty} \int_{-\infty}^{\infty} I(x, y)W^*(x - \tau_1, y - \tau_2)e^{-j(\omega_1 x + \omega_2 y)} dx dy \quad (2.15)$$

Here τ_1, τ_2 represent the spatial position of the two dimensional window $W(x,y)$. ω_1, ω_2 represents the spatial frequency parameters. Figure 2.7 illustrates how the spectral window is parameterized. At each position of the window, it overlaps OVRLP pixels with the previous position. This preserves the ridge continuity and eliminates 'block' effects common with other block processing image operations. Each such analysis frame yields a single value of the dominant orientation and frequency in the region centered around (τ_1, τ_2) . Unlike regular Fourier transform, the result of the STFT is dependent on the choice of the window $w(t)$. For the sake of analysis any smooth spectral window such as hanning, hamming or even a gaussian [70] window may be utilized. However, since we are also interested in enhancing and reconstructing the fingerprint image directly from the fourier domain, our choice of window is fairly restricted. In order to provide suitable reconstruction during enhancement, we utilize a raised cosine window that tapers smoothly near the border and is unity at the center of the window. The raised cosine spectral window is obtained using

$$W(x, y) = \left\{ \begin{array}{l} 1 \text{ if } (|x|, |y|) < \text{BLKSZ}/2 \\ \frac{1}{2}(1 + \cos(\frac{\pi x}{\text{OVRLP}})) \text{ otherwise} \end{array} \right\} (x, y) \in [-\text{WNDSZ}/2, \text{WNDSZ}/2) \quad (2.16)$$

With the exception of the singularities such as core and delta, any local region in the fingerprint image has a consistent orientation and frequency. Therefore, the local region can be modeled as a surface wave that is characterized completely by its orientation θ and frequency f . It is these parameters that we hope to infer by performing STFT analysis. This approximation model does not account for the presence of local discontinuities but is useful enough for our purpose. A local region of the image can be modeled as a surface wave according to

$$I(x, y) = A \{2\pi f \cos(x \cos(\theta) + y \sin(\theta))\} \quad (2.17)$$

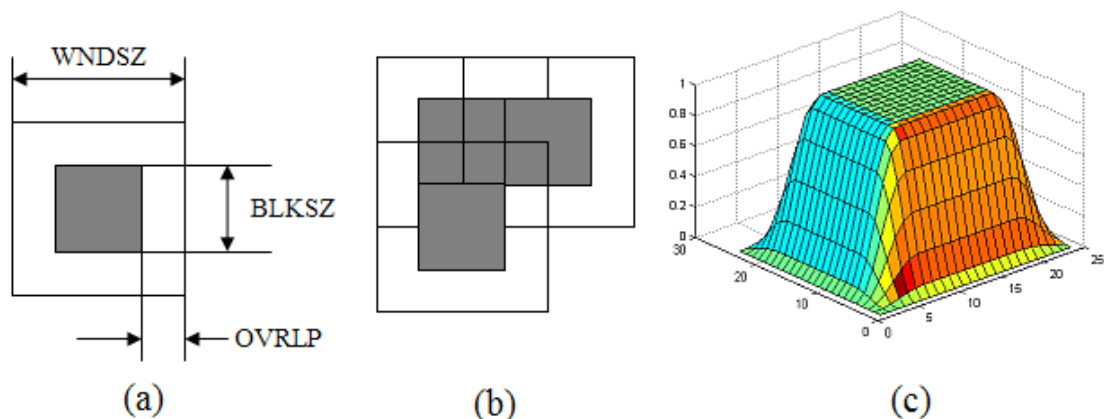


Figure 2.7: (a)Overlapping window parameters used in the STFT analysis (b) Illustration of how analysis windows are moved during analysis (b)Spectral window used during STFT analysis

The parameters of the surface wave (f, θ) may be easily obtained from its Fourier spectrum that consists of two impulses whose distance from the origin indicates the frequency and its angular location indicates the orientation of the wave. However, this straight forward approach is not very useful since the maximum response is prone to errors. Creases running across the fingerprint can easily put off such maximal response estimators. Instead, we propose a probabilistic approximation of the dominant ridge orientation and frequency. It is to be noted that the surface wave model is only an approximation, and the Fourier spectrum of the real fingerprint images is characterized by a distribution of energies across all frequencies and orientations. We can represent the Fourier spectrum in polar form as $F(r, \theta)$. We can define a probability density function $p(r, \theta)$ and the marginal density functions $p(\theta), p(r)$ as

$$p(r, \theta) = \frac{|F(r, \theta)|^2}{\int_r \int_\theta |F(r, \theta)|^2} \quad (2.18)$$

$$p(r) = \int_\theta p(r, \theta) d\theta \quad (2.19)$$

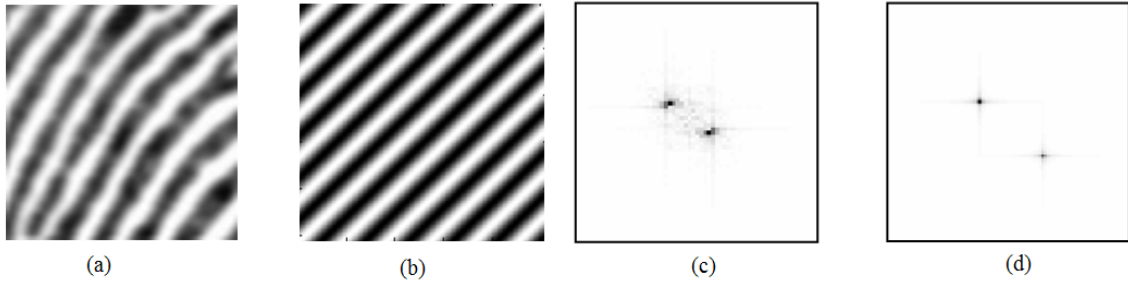


Figure 2.8: **Surface wave approximation: (a) Local region in a fingerprint image (b) Surface wave approximation (c,d) Fourier spectrum of the real fingerprint and the surface wave. The symmetric nature of the Fourier spectrum arrives from the properties of the Fourier transform for real signals [29]**

$$p(\theta) = \int_r p(r, \theta) dr \quad (2.20)$$

2.2.2 Ridge Orientation Image

We assume that the orientation θ is a random variable that has the probability density function $p(\theta)$. The expected value of the orientation may then be obtained by performing a vector averaging according to Equation 2.21. The terms $\sin(2\theta)$ and $\cos(2\theta)$ are used to resolve the orientation ambiguity as mentioned before.

$$E\{\theta\} = \frac{1}{2} \tan^{-1} \left\{ \frac{\int_{\theta} p(\theta) \sin(2\theta) d\theta}{\int_{\theta} p(\theta) \cos(2\theta) d\theta} \right\} \quad (2.21)$$

The estimate is also optimal from a statistical sense as shown in [63]. However, if there is a crease in the fingerprints that spans several analysis frames, the orientation estimation will still be wrong. The estimate will also be inaccurate when the frame consists entirely of unrecoverable regions with poor ridge structure or poor ridge contrast. In such instances, we can estimate the ridge orientation by considering the orientation of its immediate neighborhood. The resulting orientation image $O(x,y)$

is further smoothed using vectorial averaging. The smoothed image $O'(x,y)$ is obtained using

$$O'(x, y) = \frac{1}{2} \left\{ \tan^{-1} \frac{\sin(2O(x, y)) * W(x, y)}{\cos(2O(x, y)) * W(x, y)} \right\} \quad (2.22)$$

Here $W(x,y)$ represent a gaussian smoothing kernel. It has been our experience that a smoothing kernel of size 3x3 applied repeatedly provides a better smoothing result than using a larger kernel of size 5x5 or 7x7.

2.2.3 Ridge Frequency Image

The average ridge frequency is estimated in a manner similar to the ridge orientation. We can assume the ridge frequency to be a random variable with the probability density function $p(r)$ as in 2.19. The expected value of the ridge frequency is given by

$$E\{r\} = \int_r p(r)r dr \quad (2.23)$$

The frequency map so obtained is smoothed by process of isotropic diffusion. Simple smoothing cannot be applied since the ridge frequency is not defined in the background regions. Furthermore the ridge frequency estimation obtained at the boundaries of the fingerprint foreground and the image background is inaccurate in practice. The errors in this region will propagate as a result of the plain smoothing. The smoothed is obtained by the following.

$$F'(x, y) = \frac{\sum_{u=x-1}^{x+1} \sum_{v=y-1}^{y+1} F(u, v)W(u, v)I(u, v)}{\sum_{v=y-1}^{y+1} W(u, v)I(u, v)} \quad (2.24)$$

This is similar to the approach proposed in [35]. Here H, W represent the height and width of the frequency image. $W(x,y)$ represents a gaussian smoothing kernel of size 3x3. The indicator variable $I(x,y)$ ensures that only valid ridge frequencies are considered during the smoothing process. $I(x,y)$ is non zero only if the ridge frequency is within the valid range. It has been observed that the inter-ridge distance varies in the range of 3-25 pixels per ridge [35]. Regions where inter-ridge separation/frequency are estimated to be outside this range are assumed to be invalid.

2.2.4 Region Mask

The fingerprint image may be easily segmented based on the observation that the surface wave model does not hold in regions where ridges do not exist [20]. In the areas of background and noisy regions, there is very little structure and hence very little energy content in the Fourier spectrum. We define an energy image $E(x,y)$, where each value indicates the energy content of the corresponding block. The fingerprint region may be differentiated from the background by thresholding the energy image. We take the logarithm values of the energy to the large dynamic range to a linear scale.

$$E(x, y) = \log \left\{ \int_r \int_\theta |F(r, \theta)|^2 \right\} \quad (2.25)$$

The region mask is obtained by thresholding . We use Otsu's optimal thresholding [61] technique to automatically determine the threshold. The resulting binary image is processed further to retain the largest connected component and binary morphological processing [85].

Coherence Image

Block processing approaches are associated with spurious artifacts caused by discontinuities in the ridge flow at the block boundaries. This is especially problematic in regions of high curvature close to the core and deltas that have more than one dominant direction. These problems are clearly illustrated in [?]. Sherlock and Monro [11] used as piece-wise linear dependence between the angular bandwidth and the distance from the singular point location. However, this requires a reasonable estimation of the singular point location. Most algorithms for singular point location are obtained from the orientation [86, 8] map that is noisy in poor quality images. Instead we rely on the flow-orientation/angular coherence measure [73] that is more robust than singular point detection. The coherence is related to dispersion measure of circular data.

$$C(x_0, y_0) = \frac{\sum_{(i,j) \in W} |\cos(\theta(x_0, y_0) - \theta(x_i, y_i))|}{W \times W} \quad (2.26)$$

The coherence is high when the orientation of the central block $\theta(x_0, y_0)$ is similar to each of its neighbors $\theta(x_i, y_i)$. In a fingerprint image, the coherence is expected to be low close to the points of

the singularity. In our enhancement scheme, we utilize this coherence measure to adapt the angular bandwidth of the directional filter.

2.2.5 Enhancement

The algorithm for enhancement can now be outlined as follows The algorithm consists of two stages.

```

Algorithm: FFTEnhance
Inputs   : Image I(x,y)
Outputs  : Enhanced Image I'(x,y), Ridge Orientation Image O(x,y),
          Ridge Frequency Image F(x,y), Energy Image E(x,y),
          Orientation Coherence Image C(x,y), Region Mask(x,y)
STAGE I: STFT Analysis
1. For each overlapping block B(x,y) in the image
   a. Remove DC content of B, B=B-avg(B)
   b. Multiply by spectral window W
   c. Obtain the FFT of the block, F = FFT(B)
   d. Perform root filtering on F
   e. Perform STFT Analysis. The analysis yields values of
      E(x,y), O(x,y), F(x,y)
   end for
2. Smoothen orientation map O(x,y) by vector averaging to yield O'(x,y)
3. Perform isotropic diffusion on frequency map F(x,y) to yield F'(x,y)
4. Compute coherence image C(x,y) using O'(x,y)
5. Compute region mask R(x,y) by thresholding E(x,y)
STAGE II: Enhancement
6. For each overlapping block B(x,y) in the image
   a. Compute angular filter FA centered around O(x,y) and with
      bandwidth inversely proportional to C(x,y)
   b. Compute radial filter FR centered around frequency F(x,y).
   c. Filter the block in the FFT domain, F= F*FR*FA
   d. Compute the enhanced block B'(x,y) = IFFT(F)
   end for
7. Reconstruct the enhanced image by composing enhanced blocks B'(x,y)

```

Figure 2.9: Outline of the enhancement algorithm

The first stage consists of STFT analysis and the second stages performs the contextual filtering. The STFT stage yields the ridge orientation image, ridge frequency image and the block energy image which is then used to compute the region mask. Therefore the analysis phase simultaneously yields all the intrinsic images that are needed to perform full contextual filtering. The filter itself is

separable in angular and frequency domains and is identical to the filters mentioned in [11].

2.3 Experimental Evaluation

The results of each stage of the STFT analysis and the enhancement is shown in Figure 2.10. It can be seen that the quality of reconstruction is not affected even around the points of high curvature marked by the presence of the singularities. The result of enhancement on several images from FVC database [2] database is shown in Figure 2.11 and 2.12. It can be seen that the enhancement improves the ridge structure even in the areas of high ridge curvature without introducing any artifacts. Figure ?? shows the comparative results for a poor quality fingerprint image. It can be seen from the result that the proposed approach performs better than the root filtering [92] and the Gabor filter based approach. We used Peter Kovesei's implementation [49] of Hong et. al [35] paper for this purpose. The better performance of the proposed approach can be attributed to the simultaneous computation of the intrinsic images using STFT analysis. While in the Gabor filter based approach errors in orientation estimation also propagate to ridge frequency estimation leading to imperfect reconstruction.

While the effect of the enhancement algorithm may be gauged visually, the final objective of the enhancement process is to increase the accuracy of the recognition system. We evaluate the effect of our enhancement on a set of 800 images (100 users, 8 images each) derived from FVC2002 [2] DB3 database. The total number of genuine and impostor comparison are 2800 and 4950 respectively. We used NIST's NFIS2 open source software (<http://fingerprint.nist.gov>) for the sake of feature extraction and matching. The ROC curves before and after enhancement are as shown in the Figure 2.14. The summary of the results is provided in Table 2.1

| DB3 Results | Equal Error Rate |
|---------------------|------------------|
| Without Enhancement | 10.35% |
| With Enhancement | 8.5% |
| Improvement | 17% |

Table 2.1: **Effect on enhancement on the final recognition accuracy**

2.4 Summary

The performance of a fingerprint feature extraction and matching algorithms depend heavily upon the quality of the input fingerprint image. We presented a new fingerprint image enhancement algorithm based on STFT analysis and contextual/non-stationary filtering in the Fourier domain. The algorithm has several advantages over the techniques proposed in literature such as (i) All the intrinsic images(ridge orientation,ridge frequency, region mask) are estimated simultaneously from STFT analysis. This prevents errors in ridge orientation estimation from propagating to other stages. Furthermore the estimation is probabilistic and is therefore more robust.(ii)The enhancement utilizes the full contextual information(orientation,frequency,angular coherence) for enhancement. (iii) The algorithm has reduced space requirements compared to more popular Fourier domain based filtering techniques. We perform an objective evaluation of the enhancement algorithm by considering the improvement in matching accuracy for poor quality prints. We show that it results in 17% relative improvement in recognition rate over a set of 800 images in FVC2002 DB3 [2] database. Our future work includes developing a more robust orientation smoothing algorithm prior to enhancement. The matlab code for the enhancement is available for download at www.cubs.buffalo.edu and at <http://www.mathworks.com/matlabcentral/>.

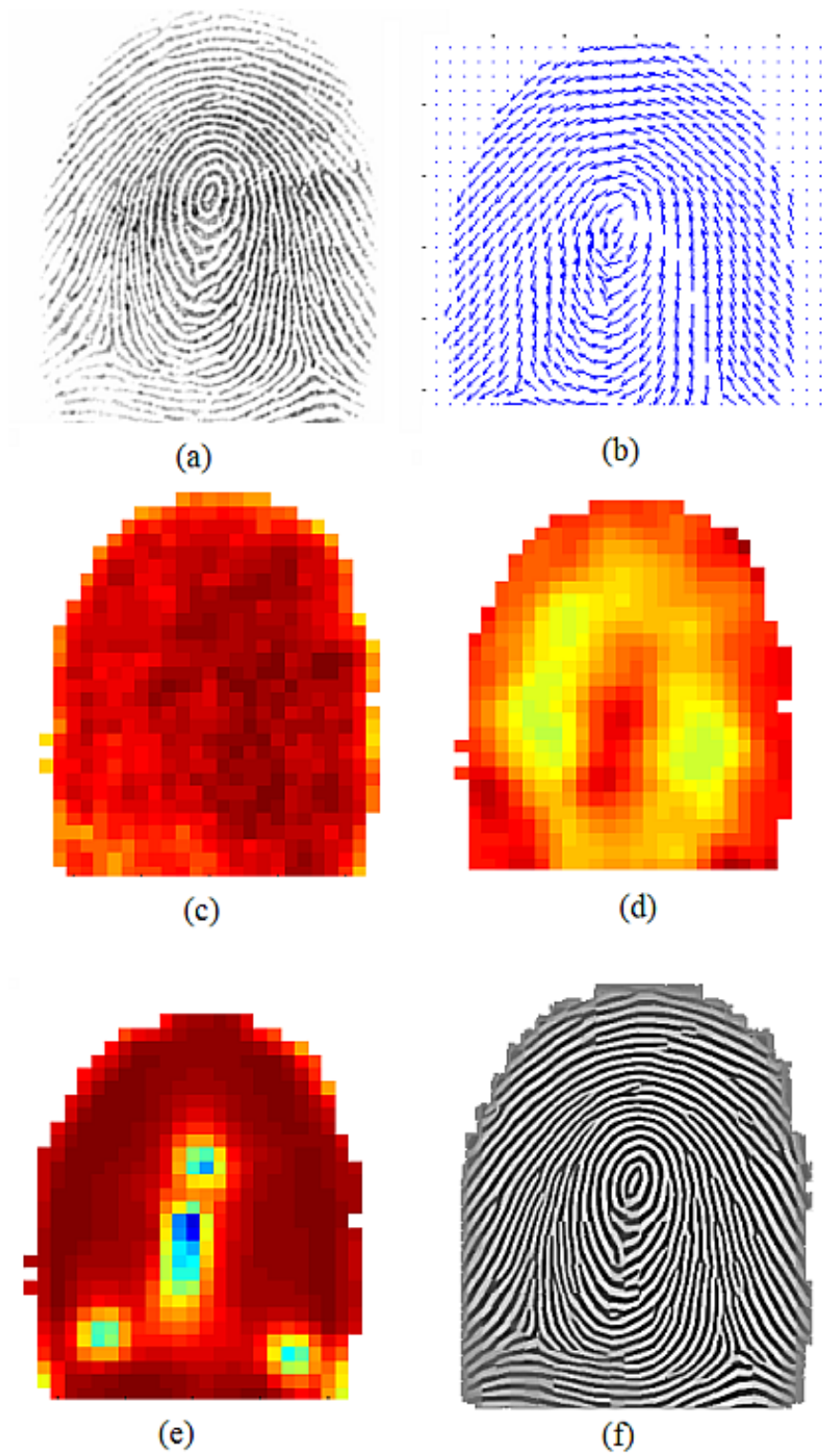


Figure 2.10: Results of the proposed approach: (a)Original Image (b)Orientation Image (c)Energy Image (d)Ridge Frequency Image (e)Angular Coherence Image (f)Enhanced Image

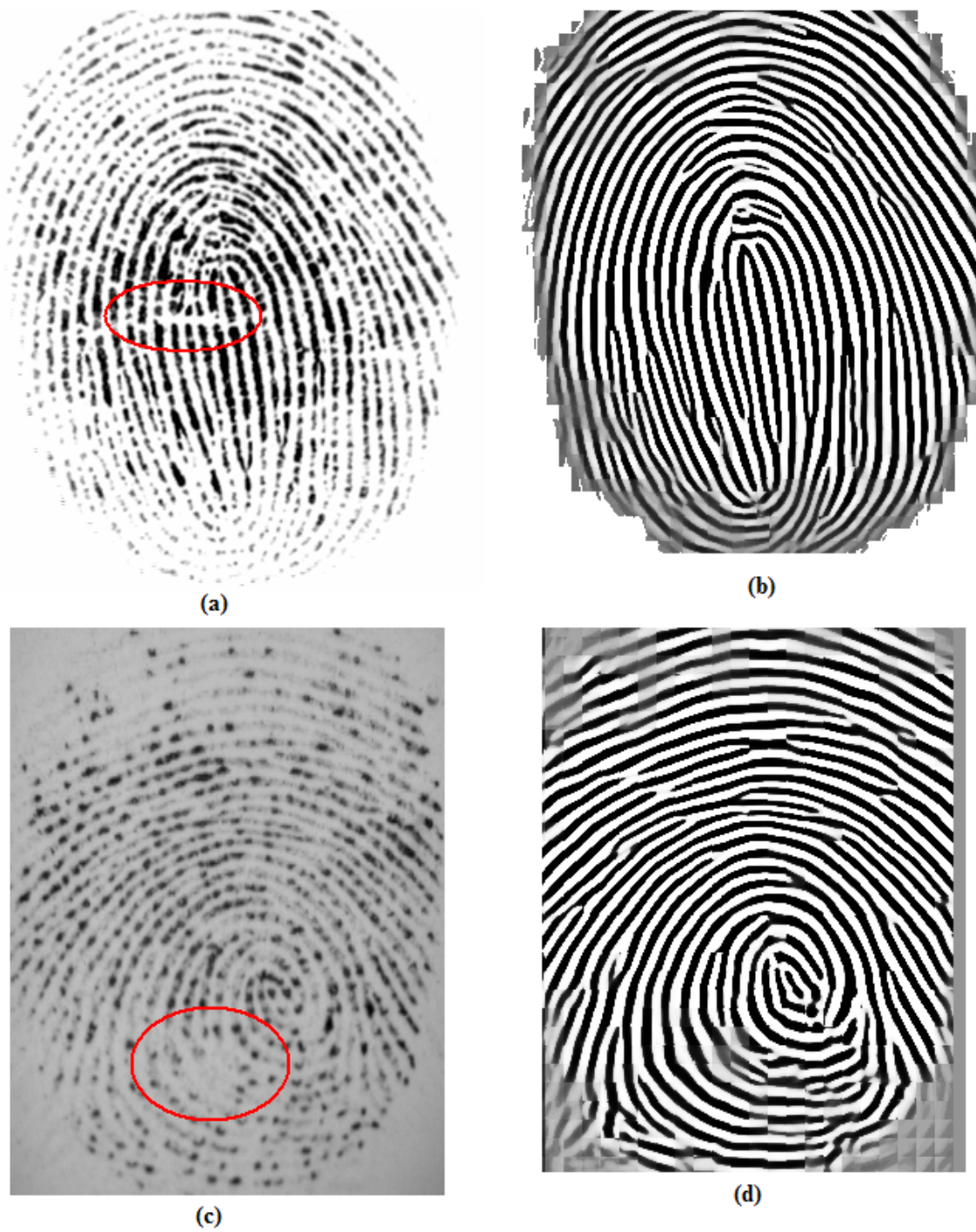


Figure 2.11: Results: (a,b) Original and enhanced image(sample taken from FVC2002 DB1 database)
(c,d) Original and enhanced image(sample taken from FVC2002 DB2 database)



Figure 2.12: Results: (a,b)Original and enhanced image(sample taken from FVC2002 DB3 database)
(c,d) Original and enhanced image(sample taken from FVC2002 DB4database)

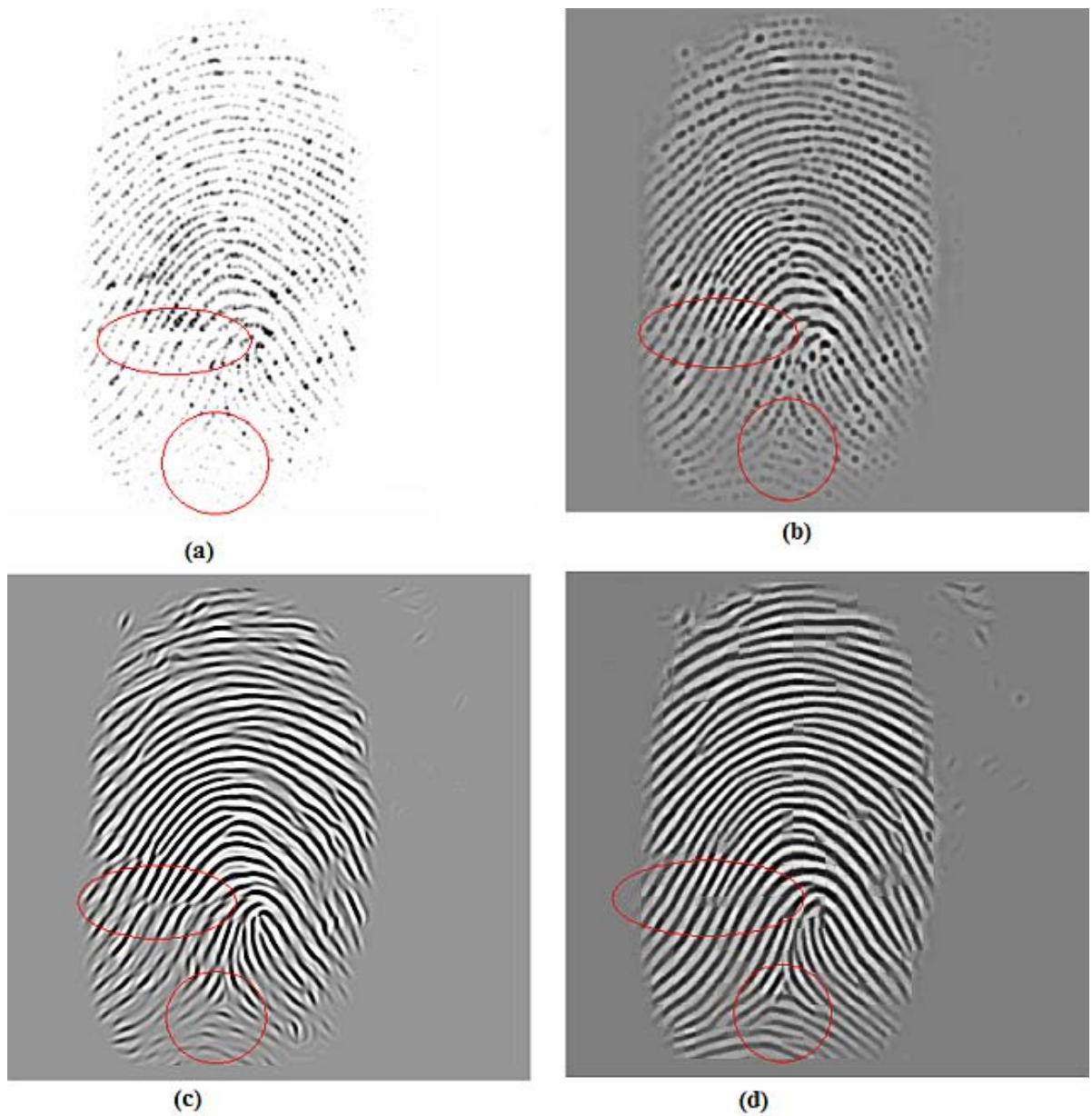
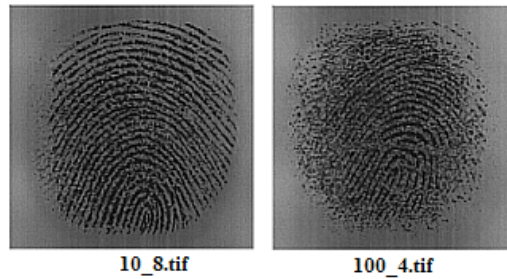
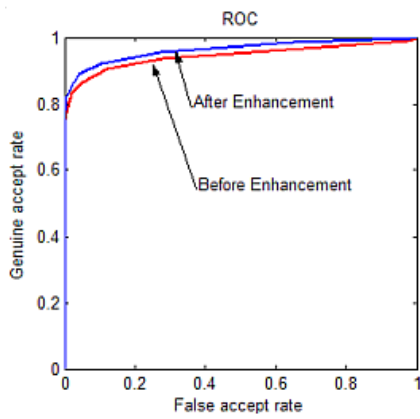


Figure 2.13: Comparative Results: (a)Original image displaying poor contrast and ridge structure (b)Result of root filtering [92]. (c)Result of Gabor filter based enhancement (d) Result using proposed algorithm



| DB3 Results | Equal Error Rate |
|---------------------|------------------|
| Without Enhancement | 10.35% |
| With Enhancement | 8.5% |
| Improvement | 17% |

(a)

(b)

Figure 2.14: Effect on accuracy : (a)ROC curves with and without enhancement (b)Some sample images from DB3 database

Chapter 3

Feature Extraction Using Chain Code

Contours

The representation of the fingerprint feature represents the most important decision during the design of a fingerprint verification system. The representation largely determines the accuracy and scalability of the system. Existing systems rely on minutiae features [37, 76, 9, 54], texture descriptors [40, 41] or raw image representations [91, 78, 79, 7] as discussed in Section 1.4. Minutiae representation is by far, the most widely used method of fingerprint representation.

Minutia or small details mark the regions of local discontinuity within a fingerprint image. These are locations where the the ridge comes to an end(type: ridge ending) or branches into two (type: bifurcation). Other forms of the minutiae includes a very short ridge (type: ridge dot), or a closed loop(type: enclosure). The different types of minutiae are illustrated Figure 3.1 which is repeated here for clarity. There are more than 18 different types of minutiae [54] among which ridge bifurcations and endings are the most widely used. Other minutiae type may simply be expressed as multiple ridge endings of bifurcations. For instance, a ridge dot may be represented by two opposing ridge endings placed at either extremities. Even this simplification is redundant since many matching algorithms do not even distinguish between ridge ending and bifurcations since their types can get flipped during acquisition (see Figure 3.2).

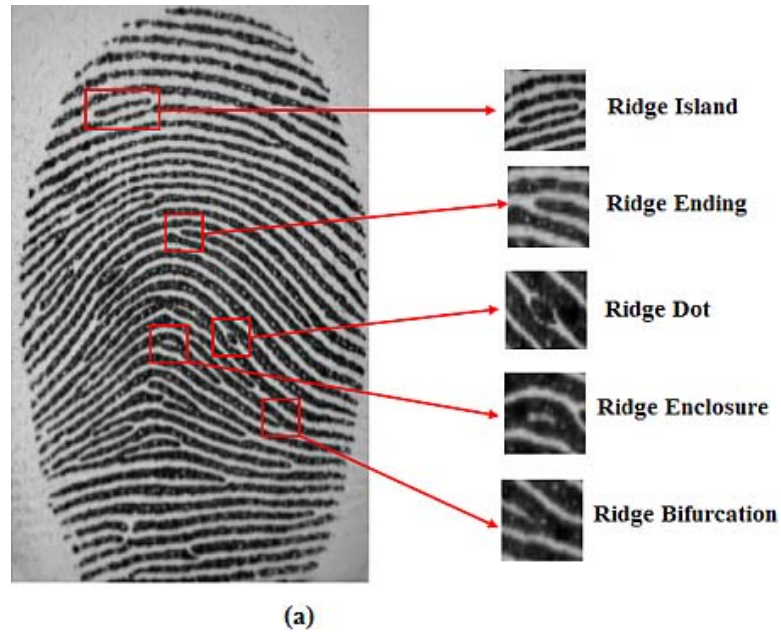


Figure 3.1: **Different types of minutiae details present in a fingerprint image**

The template simply consists of a list of minutiae location and their orientations. The feature extractor takes as input a gray scale image $I(x,y)$ and produces a unordered set of tuples $M = \{m_1, m_2, m_3 \dots m_N\}$. Each tuple m_i corresponds to a single minutia and represents its properties. The properties extracted by most algorithms include its position and orientation. Thus, each tuple m_i is usually represented as a triplet $\{x_i, y_i, \theta_i\}$. However, many systems extract additional information such as minutiae type or the 'quality' of minutiae [28, 17, 67, 68, 22]. Some schemes may also capture the gray scale neighborhood around each minutiae to perform local correlation. [7, 58]. Other minutiae based representation also consider the relative geometry information such as the ridge count to the neighboring minutiae [77], distance to the closes neighbors etc. [43]. However in this thesis we will focus our attention on the simple triplet representation $\{x_i, y_i, \theta_i\}$ for each minutiae. There are several advantages of the minutiae representation as outlined below.

1. Forensic experts also use minutiae representation to establish correspondence between two fingerprints prints.

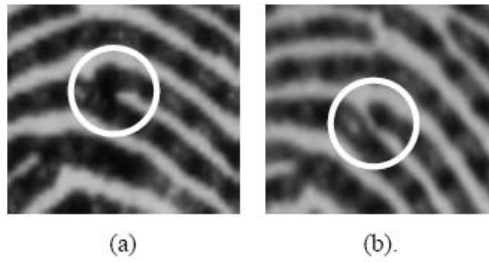


Figure 3.2: **Unreliability of minutiae type: The same minutiae extracted from two different impressions. In (a) it appears as a bifurcation but a ridge ending in (b)**

2. Representation of minutiae information is covered by several standards such as ANSI-NIST [5] and CBEFF [1] making it necessary to use minutiae information if we want interoperability between different recognition algorithms.
3. Minutiae based matching algorithms have accuracy comparable to sophisticated correlation based algorithms [2]. However, while correlation based algorithms have large template sizes, minutiae based representation are very compact, seldom requiring more than 1KB to store the template.
4. Minutiae features have been historically proven to be distinctive between any two individuals [50] and several theoretical models [62, 87] exist that provide a reasonable approximation of its individuality. No such models have been developed for texture based or image based descriptions.
5. Minutia-based representation contain only local information without relying on global information such as singular points or center of mass of fingerprints that are error-prone and difficult to estimate accurately in a poor-quality images.
6. Minutiae features are invariant to displacement and rotations unlike texture and image based features.

3.1 Prior Related Work

Minutiae extraction algorithms presented in literature can be broadly categorized as those based on direct extraction from gray scale images and those based on binarization.

3.1.1 Binarization Approach

In this approach, the gray scale image is converted into a binary image prior to minutiae detection. While algorithms differ in several implementation aspects, they have the following common stages (See Figure 3.3)

1. **Segmentation/Binarization:** In this step, the gray scale image is converted to a binary image through the process of simple thresholding or some form of adaptive binarization. The quality of the binarization output is improved if the gray scale image is enhanced prior to this process. This step is also referred to as segmentation in literature. However, this should not be confused with segmentation of the fingerprint foreground from the background during region mask generation (See 2.1.1).
2. **Thinning:** The resulting binary image is thinned by an iterative morphological process resulting in a single pixel wide ridge map. Some algorithms such as MINDTCT [28] and our proposed approach does not require this stage.
3. **Minutiae Detection:** In cases where thinning is used, the problem of minutiae detection is trivial. The resulting pixel wide map is scanned sequentially and minutiae points are identified based on its neighborhood. Ridge endings are characterized by single neighbor and bifurcations are identified by locating pixels with three or more neighbors. In algorithms where thinning is not present, minutiae detection is done via template matching [28].
4. **Post-processing:** The minutiae extraction process results in two forms of errors. The detection may introduce *spurious* minutiae where they do not exist in the original or may *miss* genuine minutiae. While nothing can be done about the missing minutiae, spurious minutiae

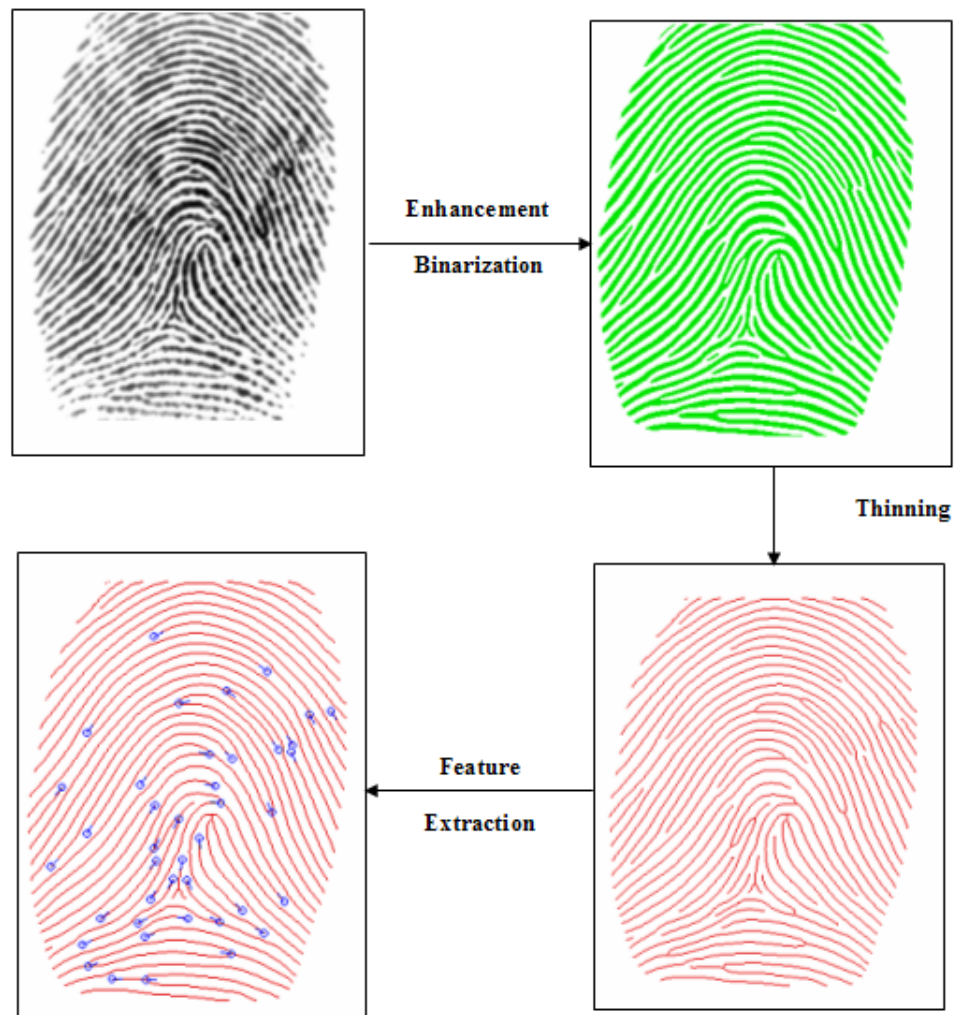


Figure 3.3: Binarization approach: The figure shows the different stages in a typical feature extractor following the binarization approach

can be eliminated by considering their spatial relationships. Several heuristic rules may then be applied to filter out these false positives.

Binarization refers to the process of reducing the bit depth of the gray scale image to just 1 bpp. The straight forward approach for binarization relies on choosing a global threshold T . The

binarization is then done according to

$$I_T(x, y) = \begin{cases} 1 & \text{if } I(x, y) > T \\ 0 & \text{if } I(x, y) \leq T \end{cases} \quad (3.1)$$

This is a very well studied problem in the area of image processing and computer vision. There exist optimal approaches to determine this threshold T based on the statistics of the gray scale distribution within the image [61]. However, due to the non-stationary nature of the fingerprint, such algorithms are not suitable or are sub-optimal at best. The brightness of the image may vary across different regions of the fingerprint image. Therefore an adaptive binarization is often used for this purpose. In such techniques, the threshold T is determined locally considering the properties of the local neighborhood. However, these techniques also fail in poor quality images. The most efficient approaches rely on the structure of the fingerprint ridge structure to perform the segmentation/binarization process.

Coetzee and Botha [19] proposed a binarization technique based on the use of edges extracted using Marr-Hildreth [55] operator. The resulting edge image is used in conjunction with the original gray scale image to obtain the binarized image. This is based on the recursive approach of line following and line thinning [6]. Two adaptive windows, the edge window and the gray-scale window are used in each step of the recursive process. To begin with, the pixel with the lowest gray-scale value is chosen and a window is centered around it. The boundary of the window is then examined to determine the next position of the window. The window is successively positioned to trace the ridge boundary and the recursive process terminates when all the ridge pixels have been followed to their respective ends.

Ratha et al. proposed an adaptive flow orientation based segmentation or binarization algorithm [75]. In this approach the orientation field is computed to obtain the ridge directions at each point in the image (See section 2.1.3). To segment the ridges, a 16x16 window oriented along the ridge direction is considered around each pixel. The projection sum along the ridge direction is computed. The centers of the ridges appear as peak points in the projection (See Figure 2.5). The ridge skeleton thus obtained is smoothed by morphological operation. Finally minutiae are detected by locating

the end points and bifurcations in the thinned binary image.

A more rigorous approach for binarization was proposed by Domeniconi et al [24]. In this technique, the gray scale image is smoothed using a process of anisotropic diffusion [65, 82]. The intensity image can be expressed as a surface $S(x,y,z)$ with level $z = I(x, y)$ (Figure 3.4). From a mathematical perspective, the ridge peaks correspond to the points of local maxima(stationary point) along the principal curvature of the ridge. A straight-forward way of determining stationary points is by finding the second derivatives along the principle directions. They compute the Hessian matrix

$$H = \begin{bmatrix} \frac{\partial^2 I}{\partial x^2} & \frac{\partial^2 I}{\partial x \partial y} \\ \frac{\partial^2 I}{\partial x \partial y} & \frac{\partial^2 I}{\partial y^2} \end{bmatrix} \quad (3.2)$$

Let λ_1 and λ_2 be the Eigen values of the Hessian H , such that $|\lambda_1| > |\lambda_2|$. Since the eigenvalue with the maximum absolute value corresponds to the direction along which intensities have maximum change, a point p is on the ridge if and only if

$$\lambda_1 < \lambda_2 = 0 \quad (3.3)$$

In reality we also have to consider the possibility of the ridge being a saddle point. Therefore an additional condition is also added

$$\lambda_1 \lambda_2 < 0 \text{ with } \lambda_1 < 0, \lambda_2 > 0 \quad (3.4)$$

Other approaches based on binarization may be found in [83, 88, 60, 11]. The binarized image obtained using any one of the above mentioned techniques is usually noisy with spurious objects, holes and irregular ridge boundaries. Several regularization techniques have been discussed in literature to clean up the binary image prior to the thinning operation. These region filling approaches by Coetzee and Botha [19], directional morphology approach by Ratha et al. [75] etc.

3.1.2 Direct Gray-Scale Approaches

Approaches working with gray level images are mostly based on ridge following. Maio and Maltoni [53] proposed a feature extraction algorithm that directly operates on gray scale image. This

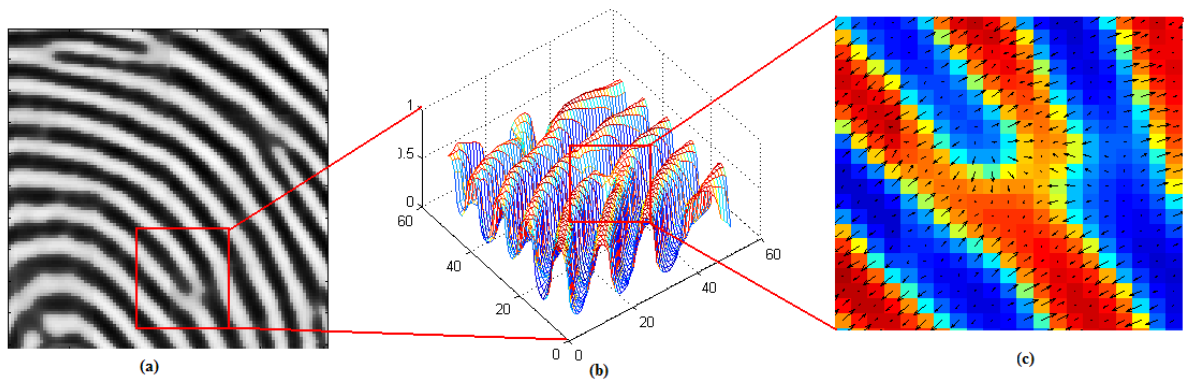


Figure 3.4: **Binarization scheme proposed by Domeniconi et al [24]: (a)A section of a fingerprint image (b)Ridges and valleys visualized as a 3D surface (c)Surface gradients. Notice that the gradients are zero on the ridges and valleys**

algorithm is based on tracking the ridges by following the location of the local maxima along the flow direction. The ridge line algorithm attempts to locate at each step, the local maxima relative to a section perpendicular to the local ridge direction. Given a starting point (x_0, y_0) and a direction θ_0 , the algorithm computes the next ridge point by moving μ pixels in the direction θ_0 . Since the position (x_1, y_1) is only approximate, the algorithm computes the ridge position by finding the peak along a line orthogonal to θ_0 . The algorithm then computes the next point by moving μ pixels in the new direction θ_1 . The algorithm avoid revisiting the same ridge by keeping track of the points traced so far. They also compared their method to binarization and thinning approaches and concluded that ridge following significantly reduces computation time. Other variations of the algorithm also exist such as [44].

Unlike Ratha's [75] approach which is a point wise operation, Maio and Maltoni's approach is based on ridge pursuit where each ridge is sequentially traced along its full length. With this approach, the local maxima cannot be reliably located in poor quality images and therefore, false positives are still introduced. However, grayscale approaches have several advantages over binarization approaches such as

Chain codes is translation invariant and can be made rotation invariant if we use relative directions. This is one of the primary reasons why it is used for object recognition applications in machine vision. However, we are interested in this representation since it provides us with a loss-less representation of ridge contours at the same time yielding a wide range of information about the contour such as curvature, direction, length etc [89]. The chain code representation has several advantages mentioned below

1. By directly processing the contour we obviate the need for thinning the binary image. This reduces the computational complexity of the feature extraction process.
2. Several post processing steps previously used to eliminate spurious features can now be integrated into the contour processing stage. For instance, holes within the ridges can be filled by considering only exterior contours. Also small artifacts can be easily removed by neglecting contours whose length is beneath a pre-defined threshold.
3. Detecting minutiae becomes very straight forward as will be seen in the ensuing sections.

Binarization

Clearly, the contour extraction process works only after the image has been binarized. Our adaptive binarization approach is based on the directional binarization technique used by MINDTCT [28]. In this approach, each pixel is successively examined and assigned white or black value. If a pixel lies in the region of low ridge flow (one of the intrinsic images computed by MINDTCT that indicates the quality of ridges in each part of the image), it is assigned white. However, if a pixel lies in a region where the ridge flow is well defined, then it is assigned white if it lies on the valley and black if it lies on the ridge. To determine if the pixel lies on the ridge or valley, an oriented window with column width set to 7 pixels and row height set to 9 pixels is considered. The window is rotated such that its rows align with the local ridge direction and is centered around the pixel to be binarized. The size is chosen so that it corresponds roughly to one ridge and one valley. If a pixel is on the ridge, then the row sum is less than the average row sum of the entire window and is therefore assigned

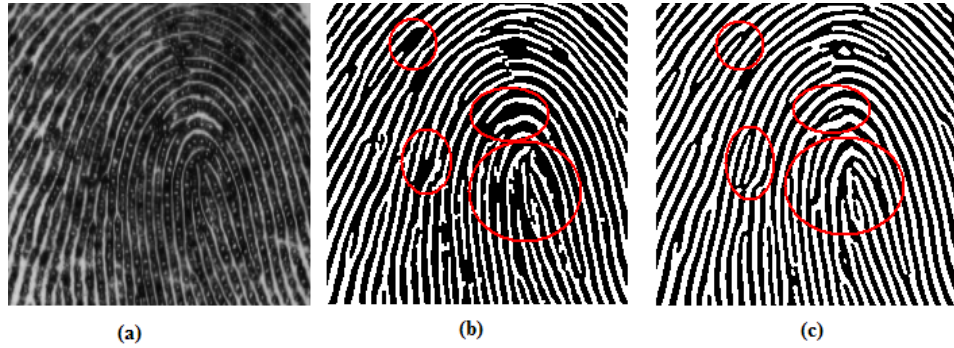


Figure 3.6: Adaptive binarization: (a)Original Image(b)Binary image obtained by MINDTCT(c) Binary image obtained by our approach

black. If its row sum is greater than the average row sum, then it means that the pixel lies on the valley and is assigned white.

However, unlike MINDTCT that uses, we utilize the contextual information obtained through STFT analysis (See section 2.2). We adapt the size of the window based on the ridge frequency map such that it always cover exactly one ridge cycle. This allows us to preserve the ridge structure in regions where the inter-ridge spacing is very low or very high. (See Figure 3.6). This is of particular importance, since the binarization step is very critical to the process of minutiae detection. Errors in this stage gets propagated into subsequent phases of feature extraction. Therefore, the binarization process has to be robust and resilient to the quality of the input image.

Minutiae Detection

As the contour of the ridges is traced consistently in a counter-clockwise direction, the minutiae points are encountered as locations where the contour has a *significant* turn. Specifically, the ridge end occurs as significant left turn and the bifurcation as a significant right turn in the contour. (See Figure 3.7). Analytically the turning direction may be determined by considering the sign of the cross product of the incoming and outgoing vectors at each point, represented by \vec{P}_{IN} and \vec{P}_{OUT}

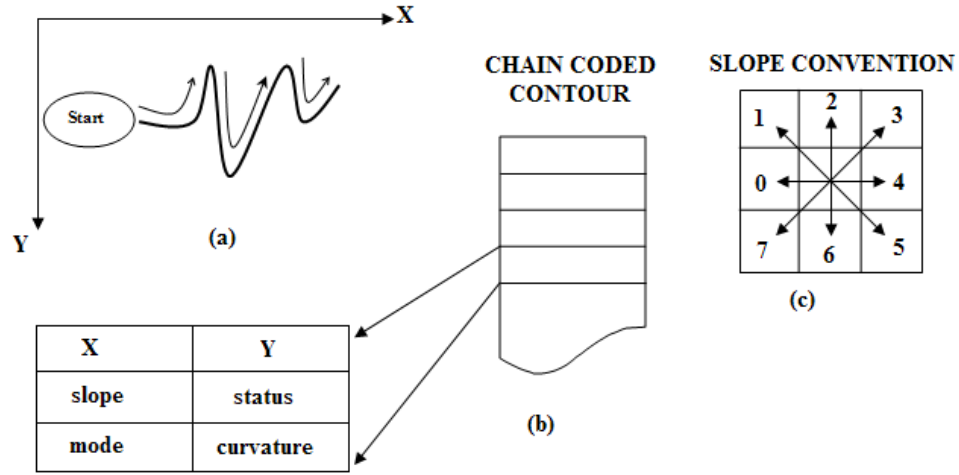


Figure 3.7: Chain code contour representation: (a)The contour is extracted by tracing the ridge boundaries in a counter clockwise direction. Each contour element along with its co-ordinates, curvature slope and other information is stored in a list (b) The slope convention

respectively. The product is right handed if

$$\text{sign}(\vec{P}_{IN} \times \vec{P}_{OUT}) > 0 \quad (3.5)$$

and left handed if

$$\text{sign}(\vec{P}_{IN} \times \vec{P}_{OUT}) < 0 \quad (3.6)$$

The turn is termed significant only if the angle between the vectors is greater than some pre-determine threshold value T_θ . The angle can be determined by using the well known dot product relation

$$\cos(\theta) = \frac{\vec{P}_{IN} \cdot \vec{P}_{OUT}}{|\vec{P}_{IN}| |\vec{P}_{OUT}|} \quad (3.7)$$

In practice, a group of points along the turn satisfy this condition. We define the minutia point as the center of this group. The orientation of the minutiae is determine by considering the orientation of the vector P that is given by

$$\vec{P} = \frac{-\vec{P}_{IN} + \vec{P}_{OUT}}{2} \quad (3.8)$$

Post-processing

The feature extraction process is inexact and results in the two forms of errors outlined below.

1. **Missing minutiae:** The feature extraction algorithm fails to detect existing minutia when the minutiae is obscured by surrounding noise or poor ridge structures.
2. **Spurious minutia:** The feature extraction algorithm falsely identifies a noisy ridge structure such as a crease, ridge break or gaps as minutiae.

The causes for the spurious minutiae are very particular to the feature extraction process. When the feature extraction is performed using binarization and thinning, spurs, bridges, opposing minutiae, triangles, ladders are some of the structures leading to false minutiae detection [54]. Gray level based feature extraction methods such as the ridge following approach proposed by Maio and Maltoni [53] can eliminate many of the sources of error that are caused by binarization and thinning. However, in poor contrast or poor quality images where the local maxima of the ridges cannot be reliably located, false positives are still introduced. In our approach, spurious minutiae are generated mostly by irregular or discontinuous contours. Therefore, minutiae extraction is usually followed by a post-processing step that tries to eliminate false positives. It has been shown that this refinement can result in considerable improvement in the accuracy of a minutia based matching algorithm [68]. These approaches can be broadly classified into (i) Structural post processing and (ii) Gray level image based filtering.

Structural post processing methods prune spurious minutia based on heuristics rules or ad-hoc steps specific to the feature extraction algorithm. Xiao and Raafat [94] provided taxonomy of structures resulting from thinning that lead to spurious minutia and proposed heuristic rules to eliminate them. Hung [36] proposed a graph-based algorithm that exploits the duality of the ridges and bifurcation. The binarization and thinning is carried on positive and negative gray level images resulting in ridge skeleton and its complementary valley skeleton. Only the features with a corresponding counterpart are retained while eliminating the false positives. Gray scale based techniques use the gray scale values in the immediate neighborhood to verify the presence of a real minutia. Prabhakar

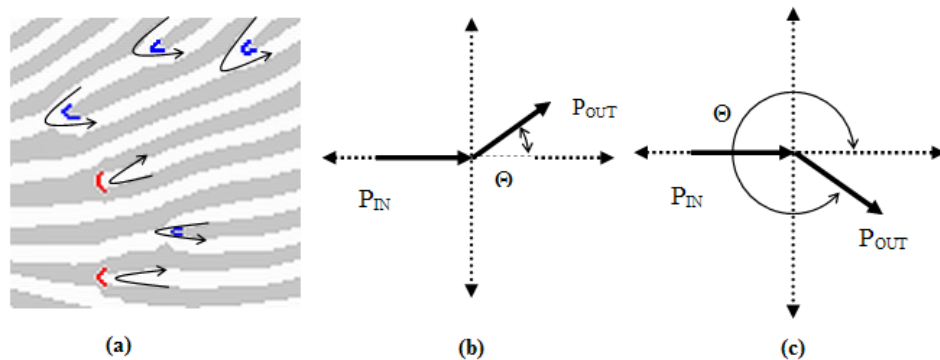


Figure 3.8: (a) Minutiae marked by significant turn in the contour (b) Left turn (c) Right turn

et al [67] proposed a gray scale image based approach to eliminate false minutiae. A 64x64 block surrounding a minutia is taken and is normalized with respect to orientation, brightness and variance. The block is then filtered using horizontally oriented Gabor filter. The central 32x32 pixels are taken as features and the resulting 1024 dimensional vectors is used to train a supervised classifier based on Learning Vector Quantization. Maio and Maltoni [22] also proposed a neural network based approach for minutiae filtering relying on gray scale features. The minutia and non-minutia neighborhoods are normalized with respect to orientation and are passed to a multi-layer shared weights neural network that classifies them as ridge ending, bifurcation or non-minutia

We use a set of simple heuristic rules to eliminate false minutiae (See Figure 3.10)

1. We merge the minutiae that are within a certain distance of each other and have similar angles. This is to merge the false positives that arise out of discontinuities along the significant turn of the contour.
2. If the direction of the minutiae is not consistent with the local ridge orientation, then it is discarded. This removes minutiae that arise out of noise in the contour.
3. We discard all minutiae that are within a distance of the border of the fingerprint area. The border is determined based on the energy map. This rule removes spurious minutiae that

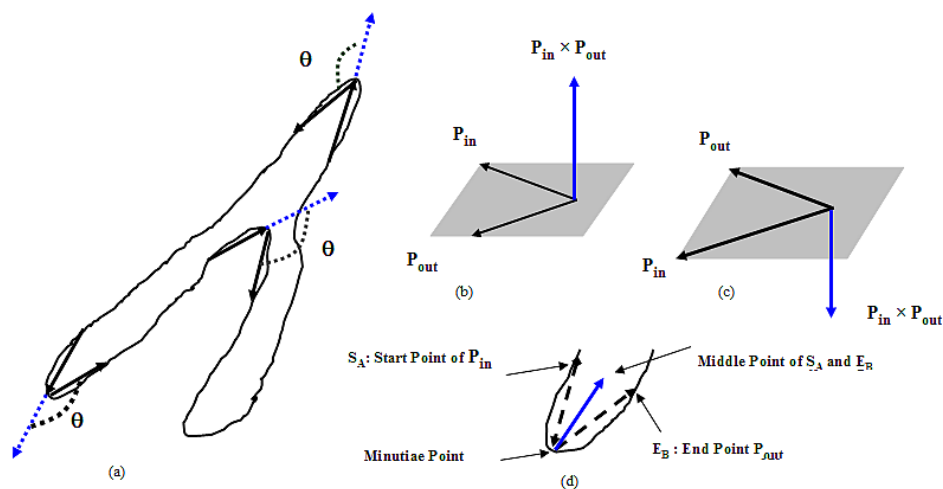


Figure 3.9: Minutiae Detection (a) Detection of turning points, (b) and (c) Vector cross product for determining the turning type, (d) Determining minutiae direction

occur along the border of the fingerprint image

4. We remove the pair of opposing minutiae that are within a certain distance of each other. This rule removes the minutiae that occur at either ends of a ridge break.

3.3 Experimental Evaluation

We measure two quantities namely *Sensitivity* and *Specificity* to objectively evaluate the algorithm [11]. The sensitivity and specificity indicates the ability of the algorithm to detect the true minutiae and reject false minutiae respectively and are given by

$$\text{Sensitivity} = 1 - \frac{\text{Missed minutiae}}{\text{Ground truth number of minutiae}} \quad (3.9)$$

$$\text{Specificity} = 1 - \frac{\text{False minutiae}}{\text{Ground truth number of minutiae}} \quad (3.10)$$

In addition we also consider the number of minutiae whose type (ridge ending/bifurcation) were flipped during the process of minutiae detection. In order to measure the objective performance, 150

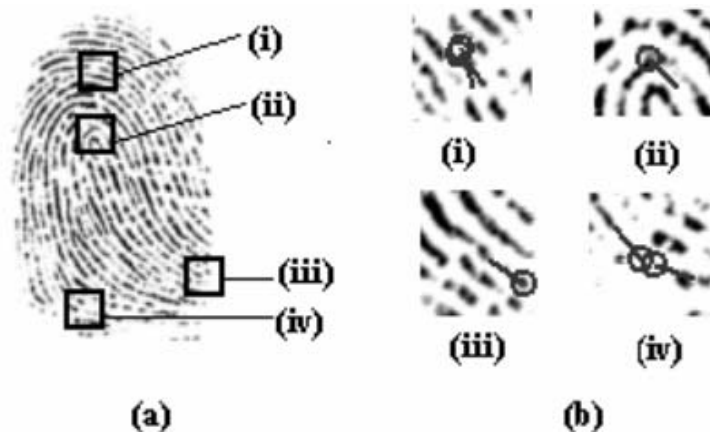


Figure 3.10: Heuristic post processing rules: (a) Fingerprint image with locations of spurious minutiae marked (b) Types of spurious minutiae removed by applying heuristic rules (i-iv)

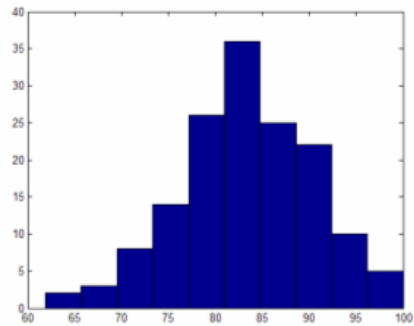
fingerprint images were randomly selected from the FVC2002 DB1 database (FVC2002) for evaluation. The ground truth minutiae for these images were marked using a semi-automated truthing tool (www.cubs.buffalo.edu). The minutiae features were then detected using our feature extraction algorithm and the sensitivity and specificity were measured over the entire database. We compared our performance with the NIST open source feature extractor MINDTCT [28]. The algorithm was executed on a PC with AMD Athlon 1.1GHz processor running Windows XP. It took an average of 0.98s over the test images. We found that the number of true positives due to the proposed methods exceeds the number of true positives found by the NIST approach in 110 of the 150 test images. Furthermore, the number of minutiae that whose type were flipped during feature extraction is less in 110 of the 150 test images when compared to the NIST method. See Figure 3.12 for summary results of the objective evaluation.

3.4 Summary

The performance of a fingerprint recognition algorithm relies upon the efficiency of its feature extraction stage. We presented a new feature extraction algorithm based on chain code contour pro-

| File Name | NIST | | | | | Proposed method | | | |
|-----------|--------|----|----|----|----|-----------------|----|---|----|
| | Actual | TP | FP | M | F | TP | FP | M | F |
| 10_8.tif | 18 | 16 | 8 | 2 | 1 | 17 | 0 | 1 | 1 |
| 11_6.tif | 50 | 40 | 4 | 10 | 2 | 41 | 4 | 9 | 4 |
| 12_8.tif | 29 | 22 | 5 | 7 | 3 | 22 | 3 | 7 | 1 |
| 13_6.tif | 35 | 28 | 10 | 7 | 4 | 28 | 10 | 7 | 2 |
| 14_6.tif | 44 | 34 | 12 | 10 | 6 | 37 | 13 | 7 | 5 |
| 15_7.tif | 38 | 37 | 7 | 1 | 5 | 37 | 3 | 1 | 0 |
| 16_7.tif | 41 | 35 | 12 | 6 | 5 | 36 | 8 | 5 | 8 |
| 17_6.tif | 43 | 35 | 16 | 8 | 11 | 36 | 7 | 8 | 11 |
| 18_8.tif | 34 | 31 | 7 | 3 | 4 | 32 | 6 | 2 | 1 |
| 19_7.tif | 35 | 26 | 8 | 9 | 3 | 31 | 6 | 4 | 5 |

Figure 3.11: Examples of features extracted from FVC2002 database.



(a)

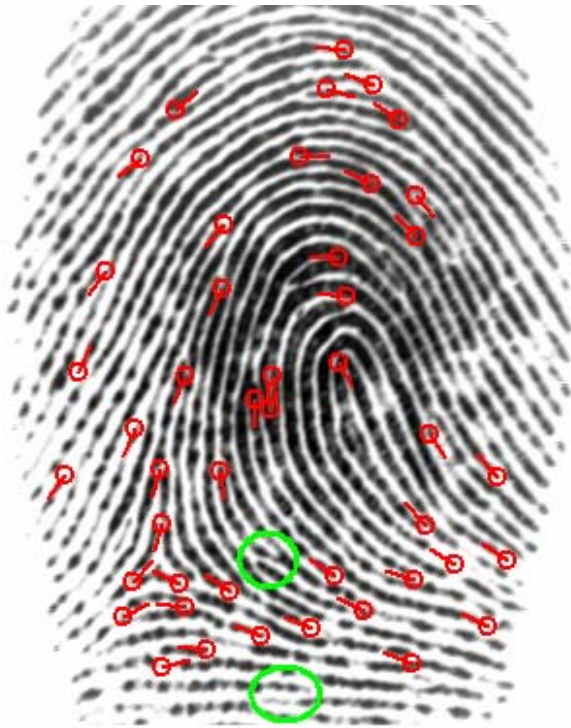
| Metric | NIST | Proposed |
|----------------|------|----------|
| Sensitivity(%) | 82.8 | 83.5 |
| Specificity(%) | 77.2 | 76.8 |
| Flipped(%) | 12.0 | 10.9 |

(b)

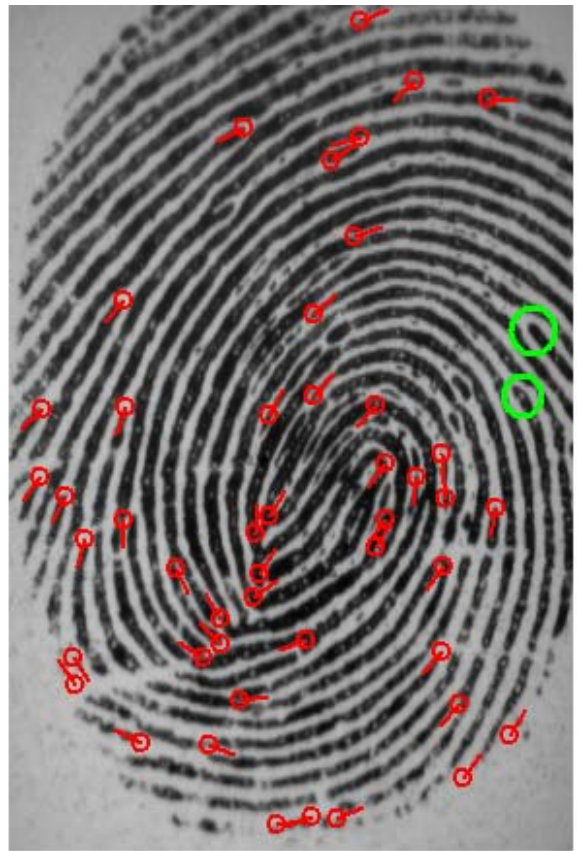
Figure 3.12: Summary results: (a)Sensitivity Distribution (b) Overall Statistics

cessing. The algorithm has several advantages over the techniques proposed in literature such as (i) The contour processing obviates the need for a thinning stage, thus increasing the computational efficiency of the algorithm. (ii) The adaptive directional binarization process utilizes full contextual information, thus reducing artifacts generated by other binarization processes. We presented

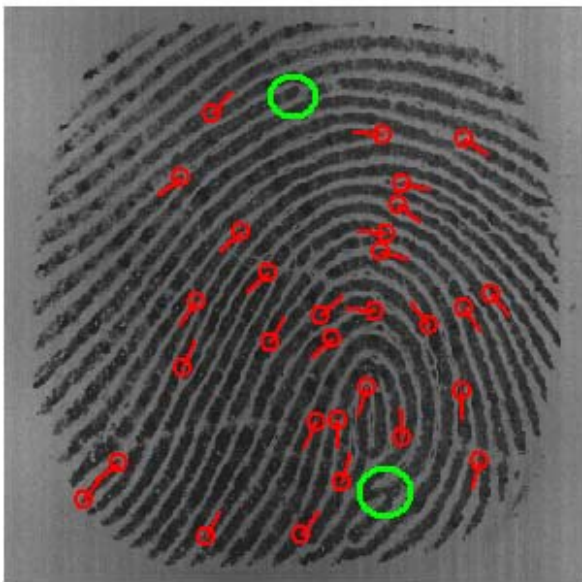
an objective evaluation of the feature extraction algorithm by measuring the *sensitivity* and *specificity* parameters and show that it compares favorably with the NIST MINDTCT algorithm. The matlab code for the feature extraction is available for download at www.cubs.buffalo.edu and at <http://www.mathworks.com/matlabcentral/>.



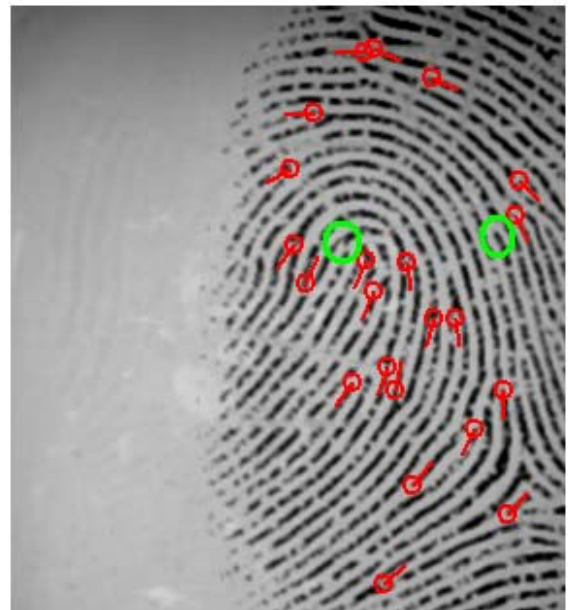
(a)



(b)



(c)



(d)

72
Figure 3.13: Some results of feature extraction. Images a-d are taken from FVC2002 DB1-DB4 databases respectively. The minutiae missed by the algorithm are highlighted in green

Chapter 4

Fingerprint Matching

Clearly the most important stage of a fingerprint verification system is the matching process. The matching algorithm takes template representations (T, I) of two different fingerprints and returns a similarity score $S(T, I)$. The representation T and I may either be image, texture descriptors or minutiae information as outlined in Section 1. In this thesis, our primary focus will be on the minutiae representation.

Despite decades of research on fingerprint verification, reliably matching fingerprints is still a challenging problem due to the following reasons

1. **Poor quality images:** Sweat, excessively dry fingers, creases, bruises obscure the ridge structure leading to generation of spurious minutiae and leading to absence of genuine ones. Furthermore, Intrinsic images cannot be reliably extracted from poor quality images resulting in further errors during feature extraction and matching phases. It was shown in FVC2000 that 80% of the errors were caused by 20% of the fingerprints [54]. These can be corrected to an extent by proper enhancement algorithm.
2. **Representational limitation:** Human experts utilize visual and contextual information present in the image itself in addition to minutiae information while performing the matching. None of the algorithms or representations capture this information and utilize it in the process of

matching. Minutiae based representation completely avoid using the textural and visual information present in the image. While the texture based matching approaches [?] do not utilize the positional properties of the minutiae. The correlation based approaches utilize the global ridge structure of the image, but do not explicitly represent or utilize textural or minutiae information. Thus all algorithms mentioned in literature rely on incomplete information . It is not known as to how much discriminatory information actually exists in each of the fingerprint representations or in the image itself [62, 54].

3. **Sensor size:** Most of the commercial sensors are governed by economy of production than by accuracy requirements. Many commercial solid state sensors have area less than 1 square inch. Thus the area of the sensor is less than the surface area of the fingerprint. It has shown that the accuracy of the matcher relates directly to the sensor area [42]. The partial prints so obtained do not have sufficient discriminatory information leading to increased error rates during recognition. In effect, **the small solid state sensors are undermining public opinion about reliability of fingerprints that the forensic community has worked so hard to establish over the last century.**
4. **Non-linear distortion:** The fingerprint image is obtained by capturing the three dimensional ridge pattern on the surface of the finger to a two-dimensional image. Therefore apart from skew and rotation assumed under most distortion models, there is also considerable stretching. Most matching algorithms assumed the prints to be rigidly transformed (strictly rotation and displacement) between different instances and therefore perform poorly under such situations. (See Figure 4.2).
5. **Intra user variation:** Due to the limited sensor size, there is a large variation between fingerprints of the same user acquired at different instances of time (See Figure 4.1).

Here we recapitulate some information from Section 1 for the sake of clarity. Each minutiae may be described by a number of attributes such as its position (x,y) , its orientation θ , its quality etc. However, most algorithms consider only its position and orientation information. Given a pair of



Figure 4.1: An illustration of the large intra-class variation between images of the same user

fingerprints and their corresponding minutiae features to be matched, features may be represented as an unordered set given by

$$I_1 = \{m_1, m_2, \dots, m_M\} \text{ where } m_i = (x_i, y_i, \theta_i) \quad (4.1)$$

$$I_2 = \{m'_1, m'_2, \dots, m'_N\} \text{ where } m'_i = (x'_i, y'_i, \theta'_i) \quad (4.2)$$

Here the objective is to find a point m'_j in I_2 that exclusively corresponds to each point m_i in I_1 . Usually points in I_2 is related to points in I_1 through a geometric transformation $T()$. Therefore, the technique used by most minutiae matching algorithms is to recover the transformation function $T()$ that maps the two point sets as shown in (Figure 1.15). The resulting point set I'_2 is given by

$$I'_2 = T(I_1) = \{m''_1, m''_2, m''_3, \dots, m''_M\} \quad (4.3)$$

$$m''_1 = T(m'_1) \quad (4.4)$$

$$\vdots \quad (4.5)$$

$$m''_N = T(m'_N) \quad (4.6)$$

$$(4.7)$$

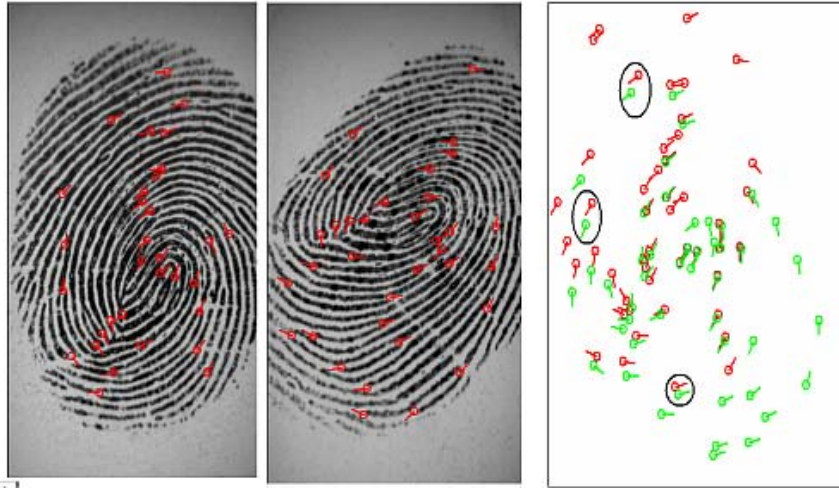


Figure 4.2: An illustration of the non-linear distortion

The minutiae pair m_i and m''_j are considered to be a match only if

$$\sqrt{(x_i - x''_j)^2 + (y_i - y''_j)^2} \leq r_0 \quad (4.8)$$

$$\min(|\theta_i - \theta''_j|, 360 - |\theta_i - \theta''_j|) < \theta_0 \quad (4.9)$$

Here r_0 and θ_0 denote the tolerance window.

The matcher can make on of the following assumptions on the nature of the transformation T

1. **Rigid Transformation:** Here it is assumed that one point set is rotated and shifted version of the other.
2. **Affine Transformation:** Affine transformations are generalization of Euclidean transform. Shape and angle are not preserved during transformation.
3. **Non-linear Transformation:** Here the transformation may be due to any arbitrary and complex transformation function T(x,y).

4.1 Prior Related Work

A large number of recognition algorithms have been proposed in literature to date. In this thesis we will include a survey of some minutiae based matching algorithms since these are by far the most widely approach for fingerprint recognition. The algorithms can be broadly classified as follows

1. **Global Matching:** In this approach, the matching process tries to simultaneously align all points at once. In other words, the transformation function is assumed to be identical at all points in the print. However, this is only an approximation since two instances of the fingerprint belonging to the same individual are often related by a non-linear transformation [54]. The global matching approach can be further categorized into
 - *Implicit Alignment* Most point pattern matching problem belong to this class. Here the process of finding the point correspondences and finding the optimal alignment are performed simultaneously.
 - *Explicit Alignment* In this approach, the optimal transformation is obtained after explicitly aligning one or more corresponding points.
2. **Local Matching:** In this approach, the matching tries to match points occurring within a small local neighborhood. The reliability of matching all the points is obtained by combining these local matches. Local matching algorithms are more robust to non-linear distortion and partial overlaps when compared to global approaches.

4.1.1 Global Matching

Implicit Alignment

The problem of matching minutiae can be treated as an instance of generalized *point pattern matching* problem. In its most general form, point pattern matching consists of matching two **unordered** set of points of possibly different cardinalities and each point . It is assumed that the two points

sets are related by some geometrical relationship. In most situations, some of the point correspondences are already known (e.g. control points in an image registration problem [31, 30, 4, 13]) and the problem reduces to finding the most optimal geometrical transformation that relates these two sets. However, in fingerprints, the point correspondences themselves are unknown and therefore the points have to be matched with no prior assumption making it a very challenging combinatorial problem. There have been several prior approaches where general point pattern techniques have been applied. Some of these have been discussed here.

Ranade and Rosenfield [72] proposed an iterative approach for obtaining point correspondences. In this approach, for each point pair m_i, m'_j they assign p_{ij} , the likelihood of the point correspondence and $c(i, j, h, k)$, a cost function that captures the correspondence of other pairs (m_h, m'_k) as a result of matching m_i with m_j . In each iteration p_{ij} is incremented if it increases the compatibility of other points and is decremented if it does not. At the point of convergence, each point m_i is assigned to the point $argmax_k(p_{ik})$. While this is a fairly accurate approach and is robust to non-linearities, the iterative nature of the algorithm makes it unsuitable for most applications.

The hough transform [25] approach or the transformation clustering approach reduces the problem of point pattern matching to detecting the most probable transformation in a transformation search space. Ratha et al [76] proposed a fingerprint matching algorithm based on this approach. In this technique, the search space consists of all the possible parameter under the assumed distortion model. For instance, if we assume a rigid transformation, then the search space consists of all possible combinations of all translations $(\Delta x, \Delta y)$, scales s and rotations and θ . However, to avoid computation complexity the search space is usually discretized into small cells. Therefore the possible transformations form a finite set with

$$\Delta x \in \{\Delta_1 x, \Delta_2 x \dots \Delta_I x\} \quad (4.10)$$

$$\Delta y \in \{\Delta_1 y, \Delta_2 y \dots \Delta_J y\} \quad (4.11)$$

$$\theta \in \{\theta_1, \theta_2 \dots \theta_K\} \quad (4.12)$$

$$s \in \{s_1, s_2 \dots s_L\} \quad (4.13)$$

A four dimensional accumulator of size $(I \times J \times K \times L)$ is maintained. Each cell $A(i, j, k, l)$ indicates the likelihood of the transformation parameters $(\Delta_i x, \Delta_j y, \theta_k, s_l)$. To determine the optimal transformation, every possible transformation is tried on each pair of points. The algorithm used in [?] is summarized below

1. for each point m_i in fingerprint T
2. for each point m'_j in fingerprint I
 - a for each $\theta_k \in \{\theta_1, \theta_2 \dots \theta_K\}$
 - b for each $s_l \in \{s_1, s_2 \dots s_L\}$
 - c compute the translations $\Delta x, \Delta y$

$$\begin{bmatrix} \Delta x \\ \Delta y \end{bmatrix} = \begin{bmatrix} \Delta x_i \\ \Delta y_i \end{bmatrix} - s_l \begin{bmatrix} \cos(\theta_k) & -\sin(\theta_k) \\ \sin(\theta_k) & \cos(\theta_k) \end{bmatrix} \begin{bmatrix} x'_j \\ y'_j \end{bmatrix} \quad (4.14)$$

- d Let $(\Delta_i x, \Delta_j y)$ be the quantized versions of $(\Delta x, \Delta y)$ respectively.
- e If $T\{m_i\}$ matches with m'_j increase the evidence for the cell $A[\Delta_i x, \Delta_j y, \theta_k, s_l]$

$$A[\Delta_i x, \Delta_j y, \theta_k, s_l] = A[\Delta_i x, \Delta_j y, \theta_k, s_l] + 1 \quad (4.15)$$

3. The optimal transformation parameters are obtained using

$$(\Delta^* x, \Delta^* y, \theta^*, s^*) = \underset{(i,j,k,l)}{\operatorname{argmax}} A[\Delta_i x, \Delta_j y, \theta_k, s_l] \quad (4.16)$$

A FPGA hardware implementation was also proposed by Ratha [76] for large scale databases.

Explicit Alignment

In this approach, the two fingerprints are explicitly aligned with each other prior to obtaining the rest of the point correspondences. The alignment may be absolute (based on singular point such as core and delta) or relative (based on a minutiae pair). Absolute alignment approaches are not very

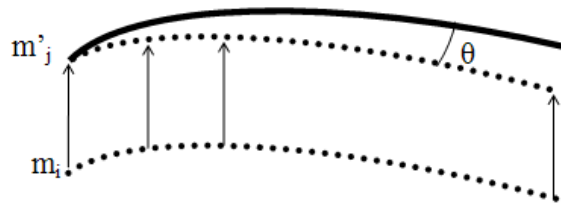


Figure 4.3: **Explicit alignment:** An illustration of the relative alignment using ridges associated with minutiae m_i and m'_j .

accurate since singular point location in poor quality prints is unreliable. In fact, there have been a very vast quantity of research dedicated to this problem [86, 8, 59, 71].

Jain et al [37] proposed a relative alignment approach based on alignment of ridges. In this technique, apart from storing the location of each minutiae, they also record a section of the ridge attached to the minutiae in the form of a planar curve(See figure 4.3). The best point of correspondence between the point sets is obtained after matching all possible pairs of ridge curves. Once the alignment is done, they match the two fingerprints by treating it as a string matching problem [21].

4.1.2 Local Matching

In local matching approaches, the fingerprint is matched by accumulating evidence from matching local neighborhood structure. Each local neighborhood is associated with structural properties that are invariant under translation and rotation. However, local neighborhood do not sufficiently capture the global structural relationships making false accepts very common. Therefore in practice, matching algorithms that rely on local neighborhood information are implemented in two stages

1. **Local structure matching:** In this step, local structures are compared to derive candidate matches for each structure in the reference print.
2. **Consolidation:** In this step, the candidate matches are validated based on how it agrees to the global match and a score is generated by consolidating all the valid matches.

The various local structure based algorithms mentioned in literature can be differentiated in the following respect

1. **Local features/representation chosen:** Hreichak and McHugh associate an eight dimensional vector $\{v_1, v_2 \dots v_8\}$ to each minutiae encoding the local neighborhood information. where each dimension represents the number of minutiae of a given type occuring in the local neighborhood. The minutiae type considered are dots, ridge endings, bifurcation, island etc. Jian and Yau [45] propose a eleven dimensional feature vector (See Figure 4.4) constructed by considering two nearest neighbors (m_j, m_k) of each minutiae m_i . The feature vector $[d_{ij}, d_{ik}, \theta_{ij}, \theta_{ik}, \phi_{ij}, \phi_{ik}, n_{ij}, n_{ik}, t_i, t_j, t_k]$. Here d_{ab} represents the Euclidean distance between minutiae m_a and m_b . n_{ab} represents the ridge count between the minutiae m_a and m_b . θ_{ab} represents the relative orientation of minutia m_b w.r.t minutia m_a . ϕ_{ab} represents the orientation of the edge connecting m_a to m_b measured relative to θ_i . Jea and Govindaraju [43] simplify this representation to include only minutiae information. They reduce the feature vector to a five dimensional one retaining only $[d_{ij}, d_{ik}, \theta_{ij}, \theta_{ik}, \phi_{ij} - \phi_{ik}]$ without considerable loss in accuracy. Ratha et al. [77] represent the local structure (*star*) in the form of a minutiae adjacency graph (MAG). The graph represented by $G(V, E)$ consists of a center vertex v_i representing m_i and all vertices v_j such that the Euclidean distance $d_{ij} < Th_d$ where Th_d is some threshold. Each edge $e_{ij} \in E$ is labelled with five features $(i, j, d_{ij}, n_{ij}, \phi_{ij})$ with the elements having the same meaning as mentioned before.
2. **Criterion for matching local neighborhoods:** In Jian and Yau's approach [45] the neighborhoods are matched considering a weighted distance between the vectors. A similar approach is followed in Jea and Govindaraju [43]. Ratha et al. [77] match each *star* by considering minutiae in increasing angles of ϕ . The local matching process results in a set of candidate *star* pairs.
3. **Consolidation process:** In Jian and Yau's approach, the pair of best correspondence is obtain by considering the pair that has the least weighted distance. This pair is then used to register

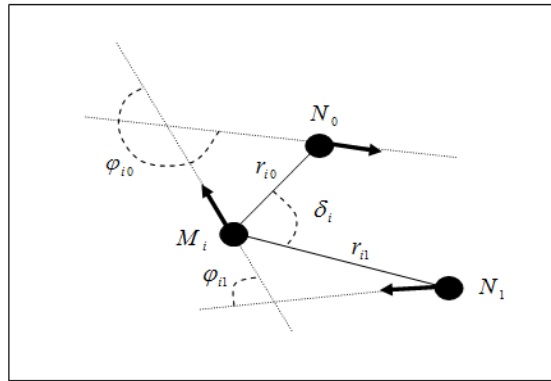


Figure 4.4: Illustration of the local secondary features used by [45, 43]

the two point sets with each other. In the consolidation process, the weighted distance of all the aligned pairs are considered to determine the final match score. It is to be noted that there is an explicit alignment/registration stage involved in this process. In Ratha's approach each candidate *star* pair is checked for consistency in the second stage. A *star* pair is said to be consistent if a certain fraction of the *stars* centered at each vertex of the matching pair is also consistent. Jea and Govindaraju adopt a different approach for consolidation of the local matches. In their approach, after the candidate secondary feature pairs have been obtained, a histogram of the global rotation parameter is constructed. The peak of the histogram will correspond to the optimal rotation angle. The secondary features pairs are then pruned by checking their local rotation parameter with the global optimum. The centers of the secondary feature pair with the minimum cost of misalignment is chosen as the reference point for alignment. The minutiae points are then converted to polar co-ordinates and matched using a bipartite graph matching algorithm. More details are provided in [43]

4.2 Proposed Approach: Graph Based Matching

We propose a novel graph based algorithm for robust fingerprint recognition. We define a new representation called *K-plet* to represent local neighborhood of a minutiae that is invariant under translation and rotation. We also define a directed graph $G(V,E)$ that represents this local relations in a formal manner. The local neighborhoods are matched using a dynamic programming based algorithm. The consolidation of the local matches is done by a novel *Coupled Breadth First Search* algorithm that propagates the local matches simultaneously in both the fingerprints. This is very similar to the way a human expert matches fingerprints where each successive match is considered in the immediate neighborhood of previously matched minutia. A important advantage of this algorithm is that, no explicit alignment of the minutiae sets is required at any stage of the matching process. Furthermore, the proposed algorithm provides a very generic but formal framework of consolidating the local matches during fingerprint recognition. In the following section, we describe our approach using the following three aspects

- Representation
- Local Matching
- Consolidation

4.2.1 Representation: K-plet

We define a representation to capture the local structural information in fingerprints called the *K-plet*. The K-plet representation is invariant under translation and rotation since it defines its own local co-ordinate system. The K-plet consists of a central minutiae m_k and K other minutiae $\{m_1, m_2 \dots m_K\}$ chosen from its local neighborhood. Each neighborhood minutiae is defined in terms of its local radial co-ordinates $(\phi_{ij}, \theta_{ij}, r_{ij})$ (See Table 4.1) where r_{ab} represents the Euclidean distance between minutiae m_a and m_b . θ_{ij} is the relative orientation of minutia m_j w.r.t the central minutiae m_i . ϕ_{ij} represents the direction of the edge connecting the two minutia. The angle

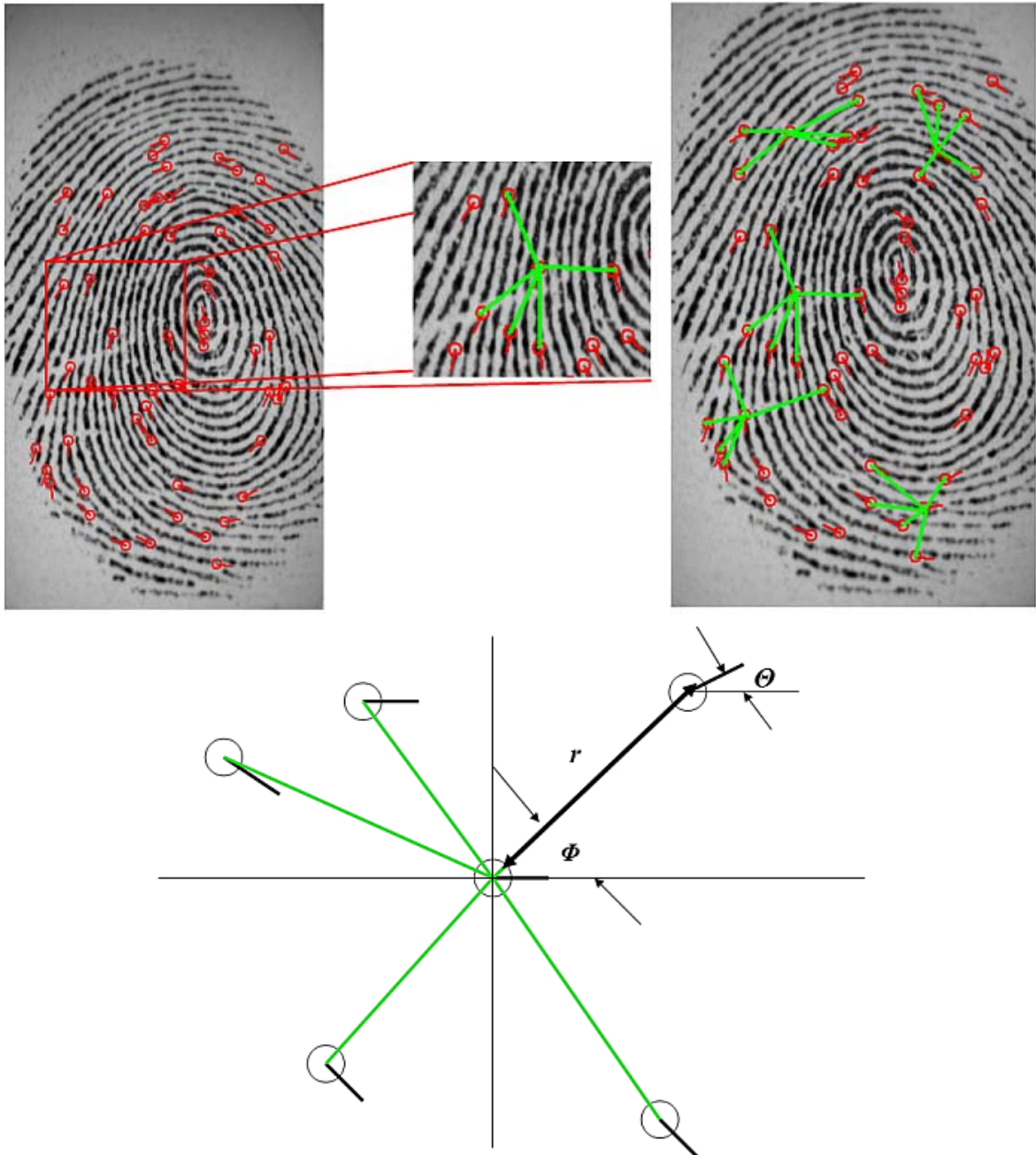


Table 4.1: Top:An illustration of K-plets defined in a fingerprint, bottom:Local co-ordinate system of the K-plet

measurement is made w.r.t the X-axis which is now aligned with the minutia direction of m_i . It is to be noted that this representation is a more general form of the *star* representation used by Ratha et al [77]. Unlike the *star* representation, the K-plet does not specify how the K neighbors are chosen. We outline two different approaches of doing this.

1. In the first approach we construct the K-plet by considering the K-nearest neighbors of each minutia. While this is a fairly simple representation, it is not very effective if the minutia are clustered since it cannot propagate matches globally.
2. To maintain high connectivity between different parts of the fingerprint, we also chose K neighboring minutia such that a nearest neighbor is chosen in each of the four quadrant sequentially. The resulting K neighbors need no necessarily be the K closest neighbors.

This is not meant to be an exhaustive enumeration of ways to construct the K-plet.

4.2.2 Graphical View

We encode the local structural relationship of the K-plet formally in the form of a graph $G(V, E)$. Each minutiae is represented by a vertex v and each neighboring minutiae is represented by a directed edge (u, v) (See Figure 4.5). Each vertex u is colored with attributes $(x_u, y_u, \theta_u, t_u)$ that represents the co-ordinate, orientation and type of minutiae(ridge ending or bifurcation). Each directed edge (u, v) is labelled with the corresponding K-plet co-ordinates $(r_{uv}, \phi_{uv}, \theta_{uv})$

4.2.3 Local Matching: Dynamic Programming

Our matching algorithm is based on matching a local neighborhood and propagating the match to the K-plet of all the minutiae in this neighborhood successively. The accuracy of the algorithm therefore depends critically on how this local matching is performed. It is particularly important to match all neighbors simultaneously since a greedy approach of matching the closest or the best matching neighbor is sub-optimal as illustrated in Figure 4.6. We convert the unordered neighbors of each

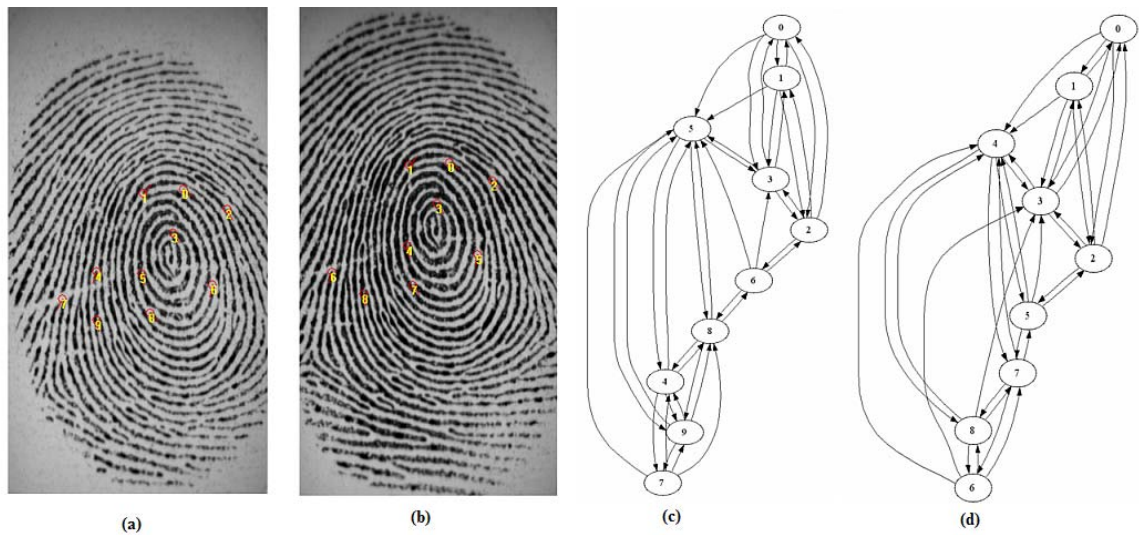


Figure 4.5: Illustration of two fingerprints of the same user with marked minutiae and the corresponding adjacency graph based on the K-plet representation. In this particular example each minutia is connected to its $K=4$ nearest neighbors. It is also to be noted that the topologies of the graphs are different due to an extra unmatched minutiae in the left print

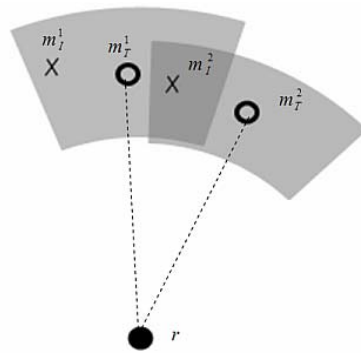


Figure 4.6: Illustration showing that greedy approaches of performing minutiae pairing is sub-optimal. Minutiae marked with O are from the reference fingerprint and those marked with X are from the test fingerprint. The figure illustrates wrong assignment of one minutia m_I^1 with m_T^2 .

K-plet into an ordered sequence by arranging them in the increasing order of the radial distance r_{kj} . The problem now reduces to matching two ordered sequences $S\{s_1, s_2 \dots s_M\}$ $T\{t_1, t_2 \dots t_N\}$. Note that the sequences S and T need not necessarily be of the same length. However, in our case it usually is since we choose each K-plet to have a fixed number of minutia neighbors. We utilize a dynamic programming approach based on string alignment algorithm [21]. The approach can also be treated as a dynamic time warping(DTW) [27] problem. used in speech processing. However, in DTW each element in one sequence can be assigned to more than one element in another sequence.

Formally, the problem of string alignment can be stated as follows: Given two strings or sequences S and T, the problem is two determine two auxiliary strings S' and T' such that

1. S' is derived by inserting spaces (-) in S
2. T' is derived by inserting spaces in T
3. $|S'| = |T'|$
4. The cost $\sum_{i=1}^{|S'|} \sigma(s'_i, t'_i)$ is maximized.

For instance, the resulting of aligning the sequences $S = \{acbcd\}$ and $T = \{cadbd\}$ is given by

$$S' = ac_bcd \quad (4.17)$$

$$T' = _cadb_d \quad (4.18)$$

A trivial solution would be to list all possible sequences S' and T' and select the pair with the least/most alignment cost. However, this would require exponential time. Instead we can solve this using dynamic programming in $O(MN)$ time as follows. We define $D[i,j](i \in \{0, 1 \dots M\}, j \in \{0, 1 \dots N\})$ as the cost of aligning substrings $S(1..i)$ and $T(1..j)$. The cost of aligning S and T is therefore given by $D[M,N]$. Dynamic programming uses a recurrence relation between $D[i,j]$ and already computed values to reduce the run-time substantially. It is assumed ofcourse that $D[k,l]$ is optimal $\forall k < i, l < j$. Given that the previous sub-problems have been optimally defined, we can match s_i and t_j in three ways

1. the elements $s[i]$ and $t[j]$ match with cost $\sigma(s[i], t[j])$,

2. a gap is introduced in t (s[i] is matched with a gap) with cost $\sigma(s[i], _)$
3. a gap is introduced in s (t[j] is matched with a gap) with cost $\sigma(_, t[j])$

Therefore, the recurrence relation to compute $D[i,j]$ is given by

$$D[i, j] = \max \left\{ \begin{array}{l} D[i-1, j-1] + \sigma(s[j], t[i]) \\ D[i-1, j] + \sigma(s[i], _) \\ D[i, j-1] + \sigma(_, t[j]) \end{array} \right\} \quad (4.19)$$

The base conditions are given as follows

$$D[0, 0] = 0 \quad (4.20)$$

$$D[0, j] = D[0, j-1] + \sigma(_, t[j]) \quad (4.21)$$

$$D[i, 0] = D[i-1, 0] + \sigma(s[i], _) \quad (4.22)$$

While this process produces the cost of optimally aligning the two sequences, determining the subsequence takes additional steps of keeping track of our choices in each step of the process. After the $D[M,N]$ has been determined, the aligned sequence can be generated in $O(|S|)$ time.

4.2.4 Consolidation: Coupled Breadth First Search

The third contribution and perhaps the most important aspect of the new matching algorithm is a formal approach for consolidating all the local matches between the two fingerprints without requiring explicit alignment. We propose a new algorithm called *Coupled BFS algorithm*(CBFS) for this purpose. CBFS is a modification of the regular breadth first algorithm [21] except for two special modifications

1. The graph traversal occurs in two directed graphs G and H corresponding to reference and test fingerprints simultaneously. (The graphs are constructed as mentioned in Section 4.2.2)
2. While the regular BFS algorithm visits each vertex v in the adjacency list of G , CBFS visits only the vertices $v_G \in V$ and $v_H \in H$ such that v_G and v_H are locally matched vertices.

The overview of the CBFS algorithm is given in Figure 4.7

```

Algorithm: CBFS
Inputs   : Graphs G(V,E) and H(V,E) corresponding to reference and
           test fingerprints
           i: source node in graph G
           j: source node in graph H
Outputs  : No. of vertices that can be matched from the given sources

1. Let G(V,E) and H(V,E) represent the graphs corresponding to the two
   prints
2. Let GQ and HQ represent a FIFO queue
3. Let M represent a set of matched vertex pairs <g,h>
4. Initialize
   a. For each vertex g in G(V,E) and h in H(V,E)
       i. color[g] = WHITE //unvisited node
       ii. color[h] = WHITE
   b. color[i] = GRAY
   c. color[j] = GRAY
   d. M = M + <g[i],h[j]>
   e. ENQUEUE (GQ,g[i])
   f. ENQUEUE (HQ,h[j])
5. While (GQ is not empty and HQ is not empty)
   a. gu = DEQUEUE (GQ)
   b. hu = DEQUEUE (HQ)
   c. Find matching neighbors of gu,hu using dynamic programming
   d. For each matching neighbor gv (of gu) and hv (of hv)
       e. If (color[gv] == WHITE and color[hv] == WHITE)
           i. M = M + <gv,hv>
           ii. ENQUEUE (GQ,gv)
           iii. ENQUEUE (HQ,hv)
6. Return M (the size of M gives the match count)

```

Figure 4.7: An overview of the CBFS algorithm

Example of CBFS matching

Here we describe an example of the algorithm run on a fingerprints with just a few minutiae. Let us assume that the fingerprints on the left and right (See Figure 4.5) are referred to by graphs G and H respectively. Figures 4.8 and 4.9 are used to describe each stage of the algorithm.

1. To begin with vertex 3 (colored yellow) is considered as the source nodes in both the graphs. The CBFS algorithm visits each neighbor in the K-plet successively and enques it (each enqueued node is colored gray). Vertex 3 is now dequeued (colored black) since it does not have any more neighbors to traverse. The matched neighbors are added to the list of matched vertex pairs M.
2. Vertices $g[0],g[1],g[2]$ of G and H have no valid neighbors to match (the end of path is shown by a circle drawn around it) and is therefore subsequently dequeued (colored black). However vertex $g[5]$ of G and $h[4]$ of H have valid neighbors that are examined in the step III.

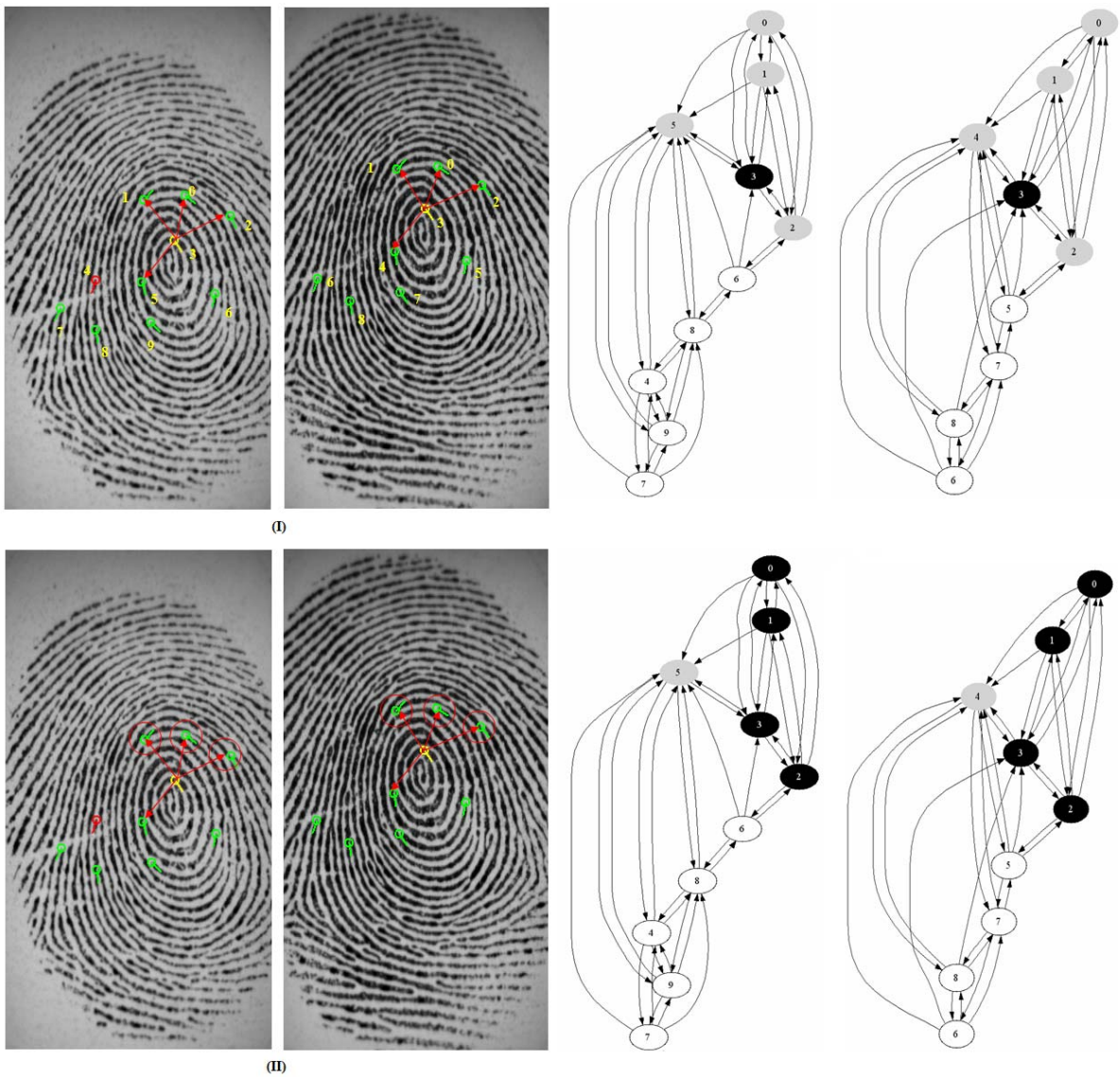


Figure 4.8: Steps I,II of the example

3. The CBFS algorithm adds $g[5]$ and $h[4]$ to the matched list and visits each neighbor vertex $g[9]$ and $g[7]$ respectively.
4. The CBFS matches the vertices $g[6], g[8], g[9]$ to $h[5], h[8], h[7]$ respectively and adds them to the matched pairs. $g[6], g[9], h[5], h[7]$ have no more neighbors to traverse. The CBFS



Figure 4.9: Steps III-VI of the example

algorithm removes them from the queue. However $g[8]$ and $h[8]$ have valid neighbors.

5. CBFS matches $g[7]$ to $h[6]$ and examines their neighbors.

6. Both $g[7]$ and $h[6]$ have no unvisited neighbors and therefore the algorithm finally terminates

with a total of 9 pairs in the matched list.

4.2.5 Matching Algorithm

It is to be noted that the CBFS algorithm requires us to specify two vertices as the source nodes from which to begin the traversal. Since the point correspondences are not known apriori, we execute the CBFS algorithm for all possible correspondence pairs $g[i], h[j]$. We finally consider the maximum number of matches return to compute the matching score. The score is generated by using a very popular approach [9]

$$s = \frac{m^2}{M_R M_T} \quad (4.23)$$

Here m represents the number of matched minutiae and M_R and M_T represent the number of minutiae in the reference and template prints respectively.

4.3 Experimental Evaluation

In order to measure the objective performance, we run the matching algorithm on images from FVC2002 DB1 database. The database consists of 800 images (100 distinct fingers, 8 instances each). In order to obtain the performance characteristics such as EER (Equal Error Rate) we perform a total of 2800 genuine (each instance of a finger is compared with the rest of the instances resulting in $(8 \times 7)/2$ tests per finger) comparison and 4950 impostor comparisons (the first instance of each finger is compared against the first instance of all other fingers resulting in a total of $(100 \times 99)/2$ tests for the entire database). We present the comparative results in Table 4.4. The improvement in the ROC characteristic can be seen from Figure 4.10.

4.4 Summary

We presented a new fingerprint matching algorithm based on graph matching principles. We defined a new representation called K-plet to encode the local neighborhood of each minutiae. We also

| Database | NIST MINDTCT/BOZORTH3 | | Proposed Approach | |
|-------------|-----------------------|--------|-------------------|--------|
| | EER | FMR100 | EER | FMR100 |
| FVC2002 DB1 | 3.6% | 5.0% | 1.5% | 1.65% |

Table 4.2: A summary of the comparative results

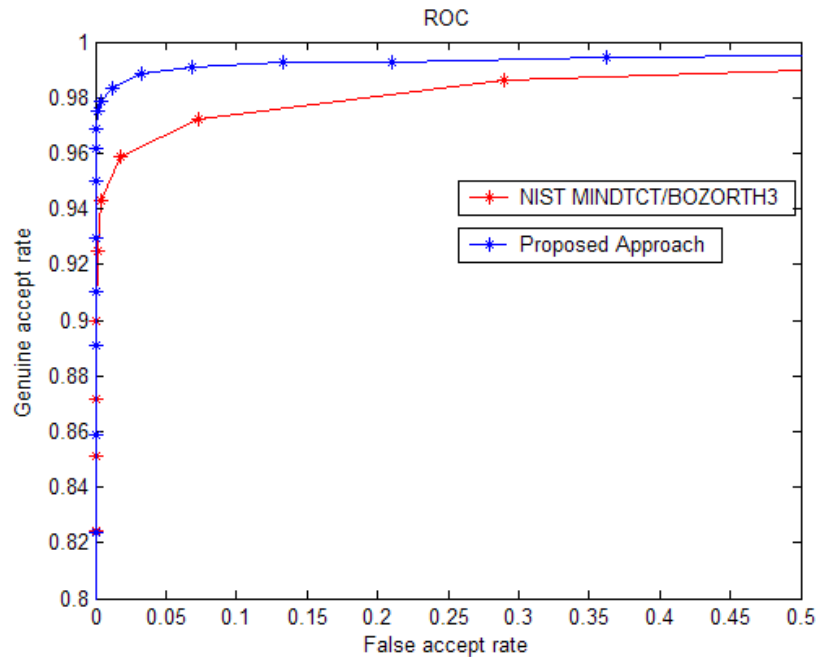


Figure 4.10: A comparison of ROC curves for FVC2002 DB1 database

presented an dynamic programming approach for matching each local neighborhood in an optimal fashion. Further, we presented CBFS (Coupled BFS), a new dual graph traversal algorithm for consolidating all the local neighborhood matches and analyzed its computational complexity. The unique advantages of the proposed algorithm are as follows:(i)The proposed algorithm is robust to non-linearities since only local neighborhoods are matched at each stage. (ii)Ambiguities in minutiae pairings are solved by employing an optimization approach. Local matches are made using a dynamic programming based algorithm. (iii) The coupled BFS algorithm provides a very

generic way of consolidating the local matches. The K-plet construction is entirely arbitrary and can be constructed in several ways such as K-nearest neighbors, all neighbors within a given circular radius (similar to Ratha et. al's star). (iv) No explicit alignment is required during the entire matching process. We also presented an experimental evaluation of the proposed approach and showed that it exceeds the performance of the NIST BOZORTH3 [28] matching algorithm.

Chapter 5

Conclusion

Here we recapitulate the ideas proposed in this thesis. The contribution of this thesis is threefold

1. We introduced a new approach for fingerprint image enhancement based on Short Time Fourier Transform(STFT) Analysis. The proposed analysis and enhancement algorithm simultaneously estimates several intrinsic properties of the fingerprint such as the foreground region mask, local ridge orientation and local frequency. The algorithm has reduced space requirements compared to more popular Fourier domain based filtering techniques.
2. We presented a new feature extraction algorithm based on chain code countour processing. The algorithm has several advantages over the techniques proposed in literature such as (i) The contour processing obviates the need for a thinning stage, thus increasing the computational efficiency of the algorithm. (ii) The adaptive directional binarization process utilizes full contextual information, thus reducing artifacts generated by other binarization processes. We also presented an objective evaluation of the feature extraction algorithm and showed that it performs better than the existing approaches such as NIST MINDTCT algorithm.
3. Finally we presented a novel minutia based fingerprint recognition algorithm that incorporates three new ideas. Firstly, we defined a new representation called K-plet to encode the local neighborhood of each minutia. Secondly, we also presented a dynamic programming

approach for matching each local neighborhood in an optimal fashion. Lastly, we proposed CBFS (Coupled Breadth First Search), a new dual graph traversal algorithm for consolidating all the local neighborhood matches and analyze its computational complexity. We presented an experimental evaluation of the proposed approach and showed that it exceeds the performance of the popular NIST BOZORTH3 matching algorithm.

5.1 Software

The software for the enhancement and matching may be obtained from on the following site

- <http://www.cubs.buffalo.edu>
- <http://www.mathworks.com/matlabcentral/>

Bibliography

- [1] Common biometric exchange file format (<http://www.itl.nist.gov/div895/isis/bc/cbeff/>).
- [2] Fingerprint verification competition. <http://bias.csr.unibo.it/fvc2002/>.
- [3] Nist fingerprint vendor technology evaluation (<http://fpvte.nist.gov/>).
- [4] Registration of images with geometric distortions. *Transactions on Geoscience and Remote Sensing*, 26(1), 1988.
- [5] New York American National Standards Institute. American national standard for information systems, data format for the interchange of fingerprint information, 1993. ANSI/NIST-CSL 1-1993.
- [6] Orit Baruch. Line thinning by line following. *Pattern Recognition Letters*, 8:271–276, 1988.
- [7] A. M. Baze, G. T. B Verwaaijen, S. H. Gerez, L. P. J. Veelunturf, and B. J. van der Zwaag. A correlation-based fingerprint verification system. In *ProRISC2000 Workshops on Circuits, Systems and Signal Processing*, Nov 2000.
- [8] A. M. Bazen and S.H. Gerez. Extraction of singular points from directional fields of fingerprints. February 2001.
- [9] Asker M. Bazen and Sabih H. Gerez. Fingerprint matching by thin-plate spline modeling of elastic deformations. *Pattern Recognition*, 36:1859–1867, 2003.

- [10] B.G.Sherlock and D.M.Monro. A model for interpreting fingerprint topology. *Pattern Recognition*, 26(7):1047–1055, 1993.
- [11] B.G.Sherlock, D.M.Monro, and K.Millard. Fingerprint enhancement by directional fourier filtering. In *Visual Image Signal Processing*, volume 141, pages 87–94, 1994.
- [12] Ruud Bolle, J. H. Connell, S. Pankanti, N. K. Ratha, and A. W. Senior. *Guide to Biometrics*. Springer Verlag, 2003.
- [13] L. Brown. A survey of image registration techniques. *ACM Computing Surveys*, 1992.
- [14] Oriented Texture Completion by AM-FM Reaction-Diffusion. *IEEE Transactions on Image Processing*, 10(6), 2001.
- [15] G. T. Candela, P. J. Grother, C. I. Watson, R. A. Wilkinson, and C. L. Wilson. Pcasys - a pattern-level classification automation system for fingerprints, April 1995.
- [16] R. Cappelli, A. Lumini, D. Maio, and D. Maltoni. Fingerprint classification by directional image partitioning. *IEEE Transactions on Pattern Analysis and Machine Intelligence*, 21(5), 1999.
- [17] S. Chikkerur, S. Pankanti, N. K. Ratha, R. Bolle, and V. Govindaraju. Novel approaches for minutiae verification in fingerprint images. In *IEEE WACV*, 2005.
- [18] A. M. Choudhary and A. A. S. Awwal. Optical pattern recognition of fingerprints using distortion-invariant phase-only filter. In *SPIE, Photonic devices and algorithms for computer*, volume 3805, pages 162–170, October 1999.
- [19] L. Coetzee and E. C. Botha. Fingerprint recognition in low quality images. *Pattern Recognition*, 26(10), 1993.
- [20] J. Connell, N. K. Ratha, and R. M. Bolle. Fingerprint image enhancement using weak models. In *IEEE International Conference on Image Processing*, 2002.

- [21] Thomas H. Cormen, Charles E. Leiserson, and Ronald L. Rivest. *Introduction to algorithms*. McGraw-Hill Book Company, 1998.
- [22] Maio D. and Maltoni D. Neural network based minutiae filtering in fingerprint images. In *14th International Conference on Pattern Recognition*, pages 1654–1658, 1998.
- [23] J. Daugman. Complete discrete 2d gabor transform by neural networks for image analysis and compression. *Transactions on Acoustics, Speech and Signal Processing*, 36:1169–1179, 1988.
- [24] C. Domeniconi, S. Tari, and P. Liang. Direct gray scale ridge reconstruction in fingerprint images. In *ICASSP*, 1998.
- [25] R. O. Duda and P. E. Hart. Use of the hough transformation to detect lines and curves in pictures. *Communications of the ACM*, 15(1), 1972.
- [26] W. Freeman and E. Aldeman. The design and use of steerable filters. *Transactions on PAMI*, 13(9):891–906, 1991.
- [27] S. Furui. Cepstral analysis technique for automatic speaker verification. 29(2):254–272, 1981.
- [28] M. D. Garris, C. I. Watson, R. M. McCabe, and C. L. Wilson. Users guide to nist fingerprint image software (nfi). Technical Report NISTIR 6813, National Institute of Standards and Technology, 2002.
- [29] Gonzalez, Woods, and Eddins. *Digital Image Processing*. Prentice Hall, 2004.
- [30] Ardeshir Goshtasby. Piecewise linear mapping functions for image registration. *Pattern Recognition*, 19(6), 1986.
- [31] Ardeshir Goshtasby. Piecewise cubic mapping functions for image registration. *Pattern Recognition*, 20(5):525–533, 1987.
- [32] Jinwei Gu and Jie Zhou. A novel model for orientation field of fingerprints. In *IEEE Computer Society Conference On Computer Vision and Pattern Recognition*, 2003.

- [33] S. Haykin and B. V. Veen. *Signals and Systems*. John Wiley and Sons, 1999.
- [34] L. Hong, A. K. Jain, S. Pankanti, and R. Bolle. Fingerprint enhancement. In *IEEE WACV*, pages 202–207, 1996.
- [35] L. Hong, Y. Wang, and A. K. Jain. Fingerprint image enhancement: Algorithm and performance evaluation. *Transactions on PAMI*, 21(4):777–789, August 1998.
- [36] D. C. Hung. Enhancement and feature purification of fingerprint images. *Pattern Recognition*, 26(11):1661–1671, 1993.
- [37] A. Jain, L. Hong, and R. Bolle. On-line fingerprint verification. In *Pattern Analysis and Machine Intelligence*, volume 19, pages 302–313, 1997.
- [38] A. K. Jain. *Fundamentals of digital image processing*. Prentice Hall International, 1989.
- [39] A. K. Jain, S. Prabhakar, and L. Hong. A multichannel approach to fingerprint classification. *IEEE Transactions on Pattern Analysis and Machine Intelligence*, 21(4):348–359, 1999.
- [40] Anil Jain, Salil Prabhakar, Lin Hong, and Sharath Pankanti. Filterbank-based fingerprint matching. In *Transactions on Image Processing*, volume 9, pages 846–859, May 2000.
- [41] Anil Jain, Arun Ross, and Salil Prabhakar. Fingerprint matching using minutiae texture features. In *International Conference on Image Processing*, pages 282–285, october 2001.
- [42] T. Jea, V. K. Chavan, V. Govindaraju, and J. K. Schneider. Security and matching of partial fingerprint recognition systems. In *Proceeding of SPIE*, number 5404, pages 39–50, 2004.
- [43] Tsai-Yang Jea and Venu Govindaraju. A minutia-based partial fingerprint recognition system. *Submitted to Pattern Recognition*, 2004.
- [44] Jiang, Yau, and Ser. *Pattern Recognition*, 34(5):999–1013, 2001.
- [45] Xudong Jiang and Wei-Yun Yau. Fingerprint minutiae matching based on the local and global structures. In *International Conference on Pattern Recognition*, pages 1038–1041, 2000.

- [46] M. Kaas and A. Witkin. Analyzing oriented patterns. *Computer Vision Graphics Image Processing*, 37(4):362–385, 1987.
- [47] K. Karu and A.K. Jain. Fingerprint classification, 1996.
- [48] Kawagoe and Tojo. Fingerprint pattern classification. *Pattern Recognition*, 17(3):295–303, 1987.
- [49] P. D. Kovesi. Matlab functions for computer vision and image analysis. <http://www.csse.uwa.edu.au/simpk/research/matlabfns>.
- [50] H. C. Lee and R. E. Gaennslen. *Advances in Fingerprint Technology*. Elsevier, 2001.
- [51] S. H. Lee, S. Y. Yi, and E. S. Kim. Fingerprint identification by use of volume holographic optical correlator. In *SPIE Optical pattern recognition*, volume 3715, pages 321–325, march 1999.
- [52] Tai Sing Lee. Image representation using 2d gabor wavelets. *Transactions on PAMI*, 18(10):959–971, 1996.
- [53] D. Maio and D. Maltoni. Direct gray scale minutia detection in fingerprints. *Transactions on PAMI*, 19(1), 1997.
- [54] D. Maio, D. Maltoni, A. K. Jain, and S. Prabhakar. *Handbook of Fingerprint Recognition*. Springer Verlag, 2003.
- [55] D. Marr and E. C. Hilderith. Theory of edge detection. *Proceedings of the Royal Society*, pages 187–217.
- [56] T. Matsumoto, H. Matsumoto, K. Yamada, and S. Hoshino. Impact of artificial gummy fingers on fingerprint systems. In *Proceedings of SPIE, Optical Security and Counterfeit Deterrence Techniques IV*, volume 8577, 2002.

- [57] B. M. Mehtre, N. N. Murthy, S. Kapoor, and B. Chatterjee. Segmentation of fingerprint images using the directional image. *Pattern Recognition*, 20:429–425, 1987.
- [58] K. Nandakumar and A. K. Jain. Local correlation-based fingerprint matching. In *Indian Conference on Computer Vision, Graphics and Image Processing*, pages 503–508, 2004.
- [59] K. Nilsson and J. Bigun. Localization of corresponding points in fingerprints by complex filtering. *Pattern Recognition Letters*, 24, 2003.
- [60] L. O’Gormann and J.V.Nickerson. An approach to fingerprint filter design. *Pattern Recognition*, 22(1):29–38, 1989.
- [61] N. Otsu. A threshold selection method from gray level histograms. *IEEE Transactions on Systems, Man and Cybernetics*, 9:62–66, 1979.
- [62] S. Pankanti, S. Prabhakar, and A. K. Jain. On the individuality of fingerprints. *Transactions on PAMI*, 24(8):1010–1025, 2002.
- [63] Papoulis and Pillai. *Probability, Random Variables and Stochastic processes*. Mc Graw Hill, 2002. 4th edition.
- [64] P. Perona. Orientation diffusion. *Transactions on Image Processing*, 1999.
- [65] P. Perona and J. Malik. Scale-space and edge detection using anisotropic diffusion. *IEEE Transaction on PAMI*, 12(7):629–639, 1990.
- [66] S. Prabhakar, S. Pankanti, and A. K. Jain. Biometric recognition: Security and privacy concerns. *IEEE Security and Privacy Magazine*, 1(2):33–42, 2003.
- [67] Salil Prabhakar, Anil Jain, and Sharath Pankanti. Learning fingerprint minutiae location and type. Number 8, pages 1847–1857, 2003.
- [68] Salil Prabhakar, Anil Jain, J. Wang, Sharath Pankanti, and Ruud Bolle. Minutiae verification and classification for fingerprint matching. In *International Conference on Pattern Recognition*, volume 1, pages 25–29, 2000.

- [69] Shie Qian and Dapang Chen. *Joint Time-Frequency Analysis, Methods and Applications*. Prentice Hall, 1996.
- [70] Rabiner and Schafer. *Digital Processing of Speech Signals*. Prentice Hall International, 1978.
- [71] P. Ramo, M. Tico, V. Onnia, and J. Saarinen. Optimized singular point detection algorithm for fingerprint images. *IEEE Transactions on Image Processing*, 3:242–245, 2001.
- [72] A. Ranade and A. Rosenfeld. Point pattern matching by relaxation. *Pattern Recognition*, 12(2):269–275, 1993.
- [73] A. Ravishankar Rao. *A Taxonomy of Texture Descriptions*. Springer Verlag.
- [74] K. Rao and K. Balck. Type classification of fingerprints: A syntactic approach. *IEEE Transactions on Pattern Analysis and Machine Intelligence*, 2(3):223–231, 1980.
- [75] N. Ratha, S. Chen, and A. K. Jain. Adaptive flow orientation based feature extraction in fingerprint images. *Pattern Recognition*, 28:1657–1672, 1995.
- [76] N. K. Ratha, K. Karu, S. Chen, and A. K. Jain. A real-time matching system for large fingerprint databases. *Transactions on Pattern Analysis and Machine Intelligence*, 18(8):799–813, 1996.
- [77] N. K. Ratha, V. D. Pandit, R. M. Bolle, and V. Vaish. Robust fingerprint authentication using local structure similarity. In *Workshop on applications of Computer Vision*, pages 29–34, 2000.
- [78] D. Roberge, C. Soutar, and B. V. K. Kumar. Optimal trade-off filter for the correlation of fingerprints. *Optical Engineering*, 38(1):108–113, 1999.
- [79] Danny Rodberg, Colin Soutar, and B. V. K. Vijaya Kumar. High-speed fingerprint verification using an optical correlator. In *Optical Pattern Recognition IX*, volume 3386, pages 123–133, 1998.

- [80] Greenberg S., Aladjem M., Kogan D., and Dimitrov I. Fingerprint image enhancement using filtering techniques. In *International Conference on Pattern Recognition*, volume 3, pages 326–329, 2000.
- [81] B. Schneier. Inside risks: The uses and abuses of biometrics. *Communications of the ACM*, 42:136, 1999.
- [82] J. Shah. Common framework for curve evolution, segmentation and anisotropic diffusion. In *Conference on Computer Vision and Pattern Recognition (CVPR '96)*. IEEE, 1996.
- [83] A. Sherstinsky and R. W. Picard. Restoration and enhancement of fingerprint images using m-lattice, 1994.
- [84] E. P. Simoncelli and H. Farid. Steerable wedge filters for local orientation analysis. *Transactions on Image Processing*, 5(9), 1996.
- [85] Sonka, Hlavac, and Boyle. *Image Processing, Analysis and Machine Vision, second edition*. Thomson Asia, 2004.
- [86] V. S. Srinivasan and N. N. Murthy. Detection of singular points in fingerprint images. *Pattern Recognition*, 25(2):139–153, 1992.
- [87] D. A. Stoney and J. I. Thornton. A critical analysis of quantitative fingerprint individuality models. *Journal of Forensic Sciences*, 31(4):1187–1216, October 1986.
- [88] M. Tico and P. Kuosmanen. A topographic method for fingerprint segmentation. In *Internal Conference on Image Processing*, pages 36–40, 1999.
- [89] V. Govindaraju V., Z. Shi, and J. Schneider. Feature extraction using a chaincoded contour representation. In *International Conference on Audio and Video Based Biometric Person Authentication*, 2003.
- [90] Viscaya and Gerhardt. A nonlinear orientation model for global description of fingerprints. *Pattern Recognition*, 29(7):1221–1231, 1996.

- [91] Watson, Grother, and Caessant. Distortion tolerant filter for elastic-distorted fingerprint. Technical Report NIST IR 6489, National Institute of Standards and Technology, 2000.
- [92] C. I. Watson, G. T. Candela, and P. J. Grother. Comparison of fft fingerprint filtering methods for neural network classification. *NISTIR*, 5493, 1994.
- [93] Che-Yen Wen and Chiu-Chung Yu. Fingerprint enhancement using am-fm reaction diffusion systems. *Journal of Forensic Science*, 48(5), 2003.
- [94] Q. Xiao and H. Raafat. *Combining Statistical and Structural Information for Fingerprint Image Processing Classification and Identification*, pages 335–354. World Scientific, NJ, 1991.
- [95] G. Z. Yang, P. Burger, D. N. Firmin, and S. R. Underwood. Structure adaptive anisotropic image filtering. *Image and Vision Computing*, 14:135–145, 1996.